Advances in Meteorology

Monitoring and Modeling Terrestrial Ecosystems' Response to Climate Change 2016

Guest Editors: Dong Jiang, Gang Liu, and Yongping Wei

Monitoring and Modeling Terrestrial Ecosystems' Response to Climate Change 2016

Advances in Meteorology

Monitoring and Modeling Terrestrial Ecosystems' Response to Climate Change 2016

Guest Editors: Dong Jiang, Gang Liu, and Yongping Wei

Editorial Board

Contents

Hindawi Publishing Corporation
Advances in Meteorology
Volume 2016, Article ID 5984595, 2 pages
http://dx.doi.org/10.1155/2016/5984595

Editorial

Monitoring and Modeling Terrestrial Ecosystems' Response to Climate Change 2016

Dong Jiang,[1] Gang Liu,[2] and Yongping Wei[3]

[1]*Key Laboratory for Resources Use and Environmental Remediation, Institute of Geographical Sciences and Natural Resources Research, Chinese Academy of Sciences, Beijing, China*
[2]*University of Southern Denmark, Odense, Denmark*
[3]*University of Queensland, Brisbane, QLD, Australia*

Correspondence should be addressed to Dong Jiang; jiangd@igsnrr.ac.cn

Received 23 October 2016; Accepted 23 October 2016

Nowadays great attention has been paid to the impact of global climate change on the terrestrial ecosystem and their adaption as well. Dataset and in-deep insights on the spatial and temporal dynamics of ecosystems' response to climate change are of great significance for global change related studies. This special issue, which consists of 6 articles, aims to present the typical recent advances in these areas.

Conservation services are key indices for measuring the terrestrial ecosystems' response to climate change. J. Zhai et al. provided a method for evaluating the water conservation service together with ecosystem conservation service based on multisource satellite imagery and in situ observation data. In their case study in the national key ecological function zones in China, spatial and temporal features of conservation services were analyzed from 2000 to 2014. Another useful index is the phenological calendar, which is a specialized calendar recording the sequence of phenological events. It is regarded as the fingerprints of climate change and has been widely used for assessing the impacts of climate change on the terrestrial ecosystems. F. Zheng et al. compiled the phenological calendars of 3 phenological observation stations in East China for the periods 1987–1996 and 2003–2012. It could be derived from those data that the beginning date of spring and summer in East China advanced, while the beginning date of autumn and winter delayed mainly because of the increasing of temperature. Another novel and interesting paper by Y. Liu et al. revealed that phenology could serve as an efficient methodology for monitoring and assessing the impact of climate change on plant-based tourist activities, such as fruit-picking.

Climate change has resulted in significant impacts on terrestrial water cycle. Z. Yang et al. analyzed the changes in evapotranspiration (ET) over the Loess Plateau in China based on the Global Land Data Assimilation System (GLDAS) data. It was proved that the Loess Plateau showed an increasing trend in potential ET compared to the decreasing trend in most other parts of the globe. Y. Zhou et al. proposed a regional water balance model based factor analysis method to identify the major factors that contribute to the variation of groundwater depth in Beijing Plain. The results indicated that the increasing domestic and environmental water use contributed greatly to the groundwater depletion.

Global change may lead to more frequent occurrence of meteorological hazards. B. Hou et al. tried to investigate whether earthquakes and rainstorm flood were correlated through a series of statistical analysis. The results revealed that some flood events might relate to earthquake events from a statistical perspective, which is especially true when the earthquake events happened in the vapor transmission zone where rainstorm events lead to abundant water vapors. In this regard, earthquake events are more likely to cause big rainstorm flood events.

This special issue presented the most recent findings and case studies in monitoring and modeling terrestrial ecosystems' response to climate change.

Acknowledgments

We would like to thank all the authors and reviewers who contributed to this special issue.

Dong Jiang
Gang Liu
Yongping Wei

Hindawi Publishing Corporation
Advances in Meteorology
Volume 2016, Article ID 9783646, 11 pages
http://dx.doi.org/10.1155/2016/9783646

Research Article

Climate Change and Fruit-Picking Tourism: Impact and Adaptation

Jun Liu,[1] Fan Chen,[1] Quansheng Ge,[2] and Yunyun Li[1]

[1] *School of Tourism, Sichuan University, Chengdu 610064, China*
[2] *Institute of Geographic Sciences and Natural Resources Research, Chinese Academy of Sciences, A11 Datun Road, Chaoyang District, Beijing 100101, China*

Correspondence should be addressed to Yunyun Li; arina_scdxlyy@126.com

Received 17 March 2016; Accepted 3 October 2016

Academic Editor: Herminia García Mozo

The purpose of this work is to present phenology as a valid indicator and methodology for monitoring and assessing the impact of climate change on plant-based tourist activities. Fruit-picking has become a popular rural tourism activity worldwide. However, fruit maturity dates (FMD) have been affected by climate change (CC), which has in turn profoundly affected fruit-picking tourism activities (FPTA). In this paper, phenological data on the FMD for 45 types of plants in 1980–2012, dates for more than 200 fruit-picking festivals, and data on monthly average air temperature in 1980–2013 were used to assess the impact of CC on FPTA by wavelet and correlation analyses. The findings indicated that the study area had been significantly affected by CC. Prevailing temperatures at one or three months prior have a decisive influence on FMD. Among the 11 plants directly related to FPTA, the FMD of four were significantly advanced, while 6-7 were significantly delayed owning to increased temperature. Of the 11 FPTA, only two had realized the impact of CC and had adjusted festival opening dates based on dynamic changes. However, a considerable number of festival activities remained fixed or scheduled on the weekends.

1. Introduction

The phenophases of plants (such as flowering and changes in leaf coloration) have important ecological and economic significance. In the past, people would celebrate seasons when plants blossom and bear fruits by holding festivals and carrying out related events and activities. These forms of leisure and tourism activities have always been very popular. Examples include the cherry blossom festivals held in Japan and the United States (US), tulip festival in Netherlands, and narcissus festival in Austria. Nowadays, viewing the flowering and leaf coloration changes of ornamental plants and fruit-picking have become attractive tourism activities. These aspects of the agritourism industry are valued at trillions of dollars. Every spring, the National Cherry Blossom Festival in Washington attracts 700,000 visitors [1], while daily visitors viewing the cherry blossoms in Ueno Park of Tokyo, Japan, amount to hundreds of thousands. Likewise, the National Cherry Festival held from November to December in the town of Young in New South Wales, Australia, every year attracts thousands of visitors. In China, viewing peach blossoms is a tradition that has lasted more than a thousand years. Each year, the Peach Blossom Festival held in Longquanyi District, Chengdu, attracts more than four million visitors.

In recent years, an important activity of rural tourism in China is fruit-picking during seasons when fruits ripen. During these periods, previous bases for fruit cultivation have now become important places for fruit-picking. It is also a popular recreation and tourism activity worldwide for individuals to pick fruits from fruit-producing bases personally and then savoring them fresh. Such activities in China attract the participation of large numbers of tourists. These include the annual loquat harvesting festival in spring, watermelon, and grape picking festivals in summer and citrus festival in fall. Tourism revenue derived from fruit-picking activities has gradually become an important component of local farmers' incomes.

The Strawberry Festival of Tongzhou District, Beijing, was officially opened on March 22, 2013. The event brought more than 20,000 visitors to the district and its surrounding

towns and villages daily, generating daily incomes that amounted to 1.3 million *renminbi* (RMB). The first Grape Festival of Daxing District, Beijing, held in 2015 welcomed thousands of tourists on the opening day. In the fall of 2014, Beiwu Town, located in the Shunyi District of Beijing, promoted fruit-picking tours within an integrated green and ecological zone occupying 3,000 mu (Chinese acre), attracting large numbers of tourists.

The Shanghai Citrus Festival is organized on Changxing Island and draws more than 100,000 tourists annually. That number comprises half of the island's total tourist arrivals per year. The mulberry-producing base in Chongming County, Shanghai, which hosts the annual fruit-picking of mulberry festival, has a cultivated area of 7,148 mu, annual output capacity up to 8,500 tons, and annual output value amounting to one hundred million RMB. The 2015 Grape Cultural Festival of Pancheng New Street, Nanjing, lasted half a month and received more than 130,000 visitors. The cumulative weight of grapes sold was 8.75 million kilograms, translating to sales revenue of 109 million RMB. The Lvshun Cherry Festival welcomed 220,000 visitors in 2011, reaping nine million RMB in ticket sales. In addition, 20,000 tons of sweet cherries were sold, generating total revenue of 280 million RMB.

Phenological studies indicate that plants are more sensitive to temperatures during the phenophases (flowering and fruiting dates) [2–4]. There is already existing literature [5] that made use of phenological observation data on the flowering and leaf coloration changes of plants to examine the impact of climate change (CC) on plants' phenophases and related tourism activities, such as viewing floral blossoms in spring [6–8] and red foliage of trees in fall [9]. Aono and Kazui [10] pointed out that the average full flowering date of Kyoto's cherry blossoms in 1971–2000 had been advanced by seven days compared to 1,200 years ago. As an adaptation strategy to CC and the induced effect of the flowering date being advanced, Japan set up a dedicated website which was set up in Japan to provide visitors with accurate forecasts for the durations of and locations for viewing cherry blossoms. On the other hand, existing literature does not contain studies in which phenological data on fruit maturation are used to study possible impacts of CC on fruit-picking tourism activities (FPTA), nor have any adaptive measures been made.

In this context, this paper used phenological observation data on fruit maturation and defined characteristics of CC within the study area as the basis to analyze the sensitivity of maturity dates to air temperature. In so doing, the aim was to determine the types of plants whose FMD are being affected by CC. Next, the relationship between air temperature and the various fruit-picking festivals' opening date was analyzed. We also examined whether FMD and fruit-picking festivals were aligned with trends in temperature fluctuations.

These findings were used as the basis to determine the possible impact that CC has on fruit-picking tourism, as well as to propose strategies that can help related operators adapt to CC. The study subject was fruit-picking festival, while Chongqing Municipality was selected as the study area because there is a wide variety of FPTA held there. This meant that the impact will be felt there greater and that the comprehensive tourism effect will be more prominently. We hope that the study will alert researchers to the economic significance of phenology.

These findings can provide a preliminary insight into the adaptability of tourism activities to CC and serve as an important scientific basis to understand the temporal and regional variations in seasonal plant-related tourism activities. Furthermore, they can also guide the adaptation of tourism activities to CC and improve the accuracy and risk estimates of the economic impact that CC has on the tourism industry, and help tourism policy makers formulate strategies that will help tourism activities adapt to CC.

2. Study Area

Chongqing, the largest city in southwest China, is located between longitude 105°17′–110°11′ east and latitude 28°10′–32°13′ north. It is an important tourism center along the upper reaches of the Yangtze River (Figure 1). In 2014, it hosted a total of 349 million tourists and tourism revenue was more than 200 billion RMB. Among that, rural tourism comprised 80 million visitors and business income of 15 billion RMB. The industry generated related jobs for more than 600,000 people and helped 180,000 farmers out of poverty.

The scale of FPTA in Chongqing has enlarged in recent years and its development has reached a more mature stage. Consequently, the comprehensive benefits of 11 FPTA have become more significant. Such activities have gradually become an important source of rural tourism revenue, with related tourism incomes having exceeded one billion RMB since 2013. At the 2010 Grape Tourism and Culture Festival of Bishan District, there were 120,000 visitors on the opening day alone and the tourism revenue reached 5.2 million RMB. For the Loquat Tourism Cultural Festival of Dazu District, visitor arrivals for both 2012 and 2013 exceeded 300,000 per year.

3. Materials and Methods

3.1. Data Sources

3.1.1. Data on FMD. Data on FMD for 45 plant species at Chongqing's Beibei Station for the two time periods of 1980–1996 and 2003–2012 were obtained from the Chinese Phenological Observation Network (CPON). The network was established upon the advocation of Mr. Zhu Kezhen and now it has more than 30 stations. It has the largest number of field observation stations within China, most abundant observed species, and uninterrupted plant phenophase data over the longest period (Table 1).

3.1.2. Data on Fruit-Picking Festivals and Activities. Extensive searches were made on authoritative newspapers (including *Chongqing Daily*, *Chongqing Evening News*, and *Chongqing Economic Times*) and web sites (including *People's Daily Online* and Tencent's *Dayu Online*) for the periods October–December 2014 and January-February 2016. The purpose was to collate from these sources the opening dates for the various fruit-picking festivals. This resulted in more than 200 records. Next, the opening dates for each festival as documented by

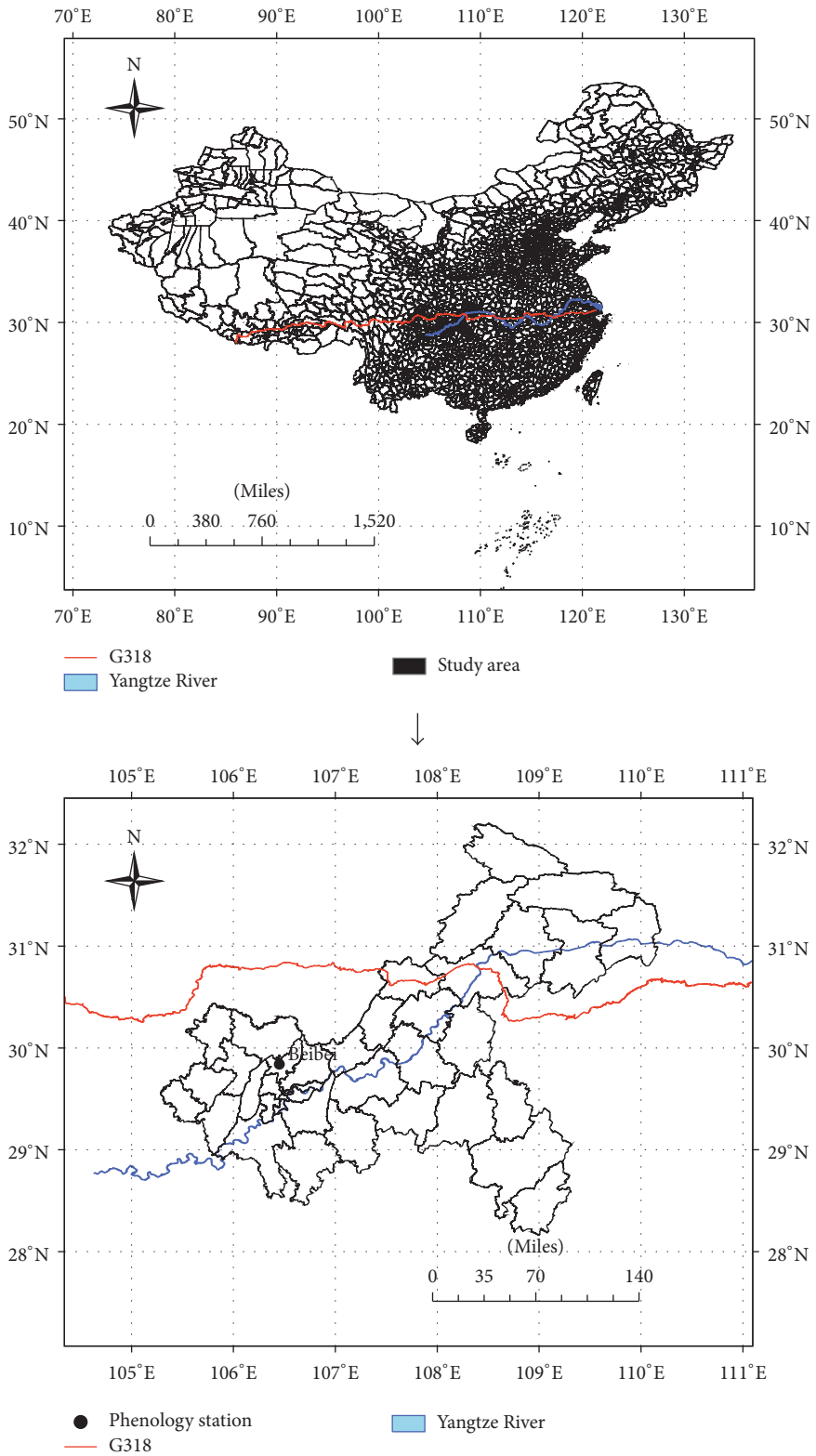

Figure 1: The spatial distribution of study area.

Table 1: Summary of phenological data from the 45 species in Beibei during 1980–1996 and 2003–2012.

Number	Species	Family	*N*	FMD
B1	*Michelia alba DC. (white Michelia flower)*	Michelia	5	8/24
B2	*Cupressus funebris (Kashiwagi)*	Cupressaceae	12	9/2
B3	*Platycladus orientalis (Platycladus orientalis)*	Platycladus	16	9/4
B4	*Salix babylonica (Willow)*	Salix	11	4/22
B5	*Robinia pseudoacacia (Locust)*	Robinia	23	7/3
B6	*Ligustrum compactum Ait (Ligustrum)*	Ligustrum	21	11/2
B7	*Citrus sinensis (Goose Orange)*	Citrus	12	11/13
B8	*Pterocarya stenoptera (Chinese Wingnut)*	Pterocarya	10	8/1
B9	*Broussonetia papyrifera (Paper Mulberry)*	Broussonetia	18	7/25
B10	*Pittosporum tobira (Pittosporum)*	Pittosporum	15	11/4
B11	*Camptotheca acuminata Decne (Camptotheca acuminata)*	Camptotheca	12	11/2
B12	*Albizia julibrissin Durazz (Albizzia)*	Albizzia	8	8/2
B13	*Lindera megaphylla Hemsl (Lindera megaphylla)*	Lindera	6	8/13
B14	*Juglans regia (Persian Walnut)*	Juglandaceae	11	9/10
B15	*Sophora japonica (Chinese scholar tree)*	Sophora	19	11/11
B16	*Platycodon grandiflorus (Bellflower)*	Campanulaceae	13	10/22
B17	*Chimononthus praecox (Winter Sweet)*	Chimononthus	4	5/28
B18	*Ulmus parvifolia (Chinese Elm)*	Ulmus	16	10/29
B19	*Prunus salicina (Plum)*	Prunus	12	6/18
B20	*Podocarpus macrophyllus (Yacca)*	Podocarpus	14	7/6
B21	*Spiraea salicifolia (Spiraea)*	Rosaceae	15	5/4
B22	*Paulownia fortunei (Paulownia)*	paulownia	8	9/27
B23	*Herba Ainsliaeae Lancifoliae (All-grass of Lanceleaf Ainsliaea)*	Asteraceae	5	9/22
B24	*Malus pumila (Apple)*	Malus	13	8/4
B25	*Vitis vinifera (Grapes)*	Vitaceae	21	7/16
B26	*Acer buergerianum (Triangle Maple)*	Acer	6	8/11
B27	*Morus alba (Mulberry)*	Morus	21	4/27
B28	*Amygdalus davidiana (Mountain Peach)*	Rosaceae	11	6/18
B29	*Punica granatum (Pomegranate)*	Punica	19	9/27
B30	*Amygdalus persica (Peach)*	Rosaceae	15	6/17
B31	*Firmiana platanifolia (Chinese parasol (tree))*	Firmiana	17	9/4
B32	*Cinnamomum camphora (Camphor tree)*	Cinnamomum	23	10/13
B33	*Ligustrum quihoui (Purpus Privet)*	Ligustrum	12	10/9
B34	*Platanus acerifolia (Planetree)*	Platanus	11	9/6
B35	*Fontanesia fortunei (Fontanesia)*	Fontanesia	14	10/5
B36	*Cerasus pseudocerasus (Cherry)*	Cerasus	9	4/13
B37	*Vernicia fordii (Tung tree)*	Vernicia	12	10/27
B38	*Firmiana simple (Phoenix tree)*	Firmiana	9	8/11
B39	*Cercis chinensis (Chinese redbud)*	Cercis	21	8/24
B40	*Wisteria sinensis (Wisteria)*	Leguminosae	10	7/21
B41	*Lagerstroemia indica (Crape myrtle)*	Lagerstroemia	18	10/16
B42	*Eriobotrya japonica (Loquat)*	Rosaceae	20	5/12
B43	*Citrus maxima (Shaddock)*	Citrus	18	10/8
B44	*Koelreuteria paniculata (Goldenrain tree)*	Koelreuteria	21	10/18
B45	*Melia azedarach (Chinaberry)*	Melia	25	11/8

B1–B45 were species from Beibei. *N*, number of observation years; FMD denote timing of fruit maturity date.

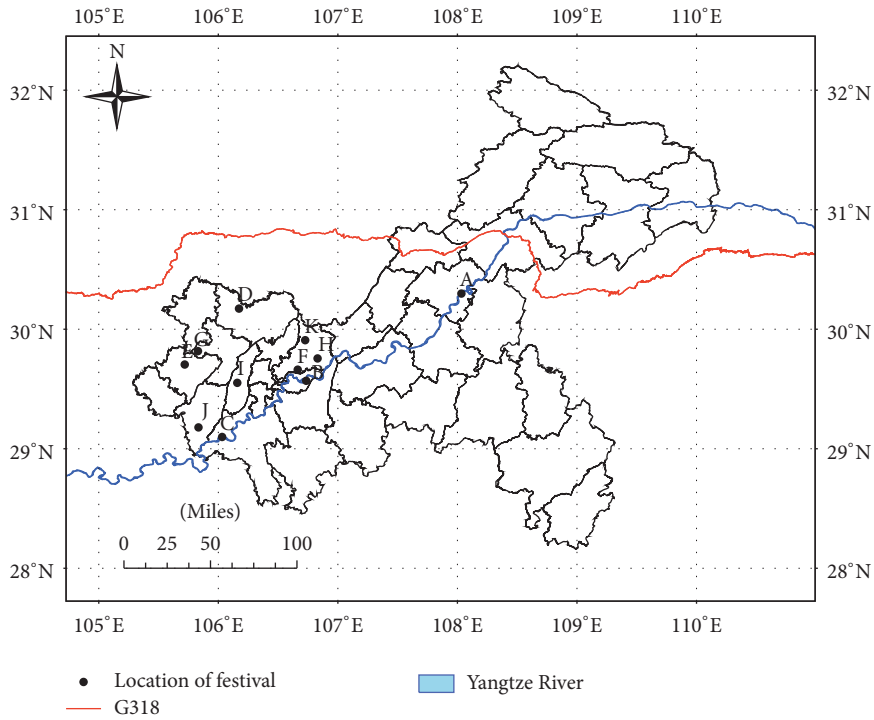

Figure 2: Location of fruit-picking tourism festival in Chongqing (A, Citrus Cultural Festival of Zhong County; B, Loquat Festival of Jiangnan District, C, Rural Tourism and Late Maturing Citrus Fruit-Picking Festival of Shimen Town, Jiangjin District, D, Loquat Fruit-Picking Festival of Gulou Town, E, Loquat Tourism Cultural Festival of Dazu District, F, Cherry Festival of Yufengshan Town, G, Cherry Festival of Shuangshan Town, H, Grape Festival of Sichuan Town, I, Grape Tourism and Culture Festival of Bishan District, J, Watermelon Tourism and Cultural Festival of Yongchuan District, and K, Waxberry Cultural Festival of Xinglong Town).

the different media were verified individually. Eventually, the sequences of dates for 11 types of FPTA were established (Figure 2).

3.1.3. Meteorological Data. Data on monthly average air temperature recorded at seven meteorological stations in Chongqing between 1980 and 2013 were acquired from *Chinese Meteorological Data Online* (http://data.cma.gov.cn/site/index.html). The seven stations were Fengjie, Liangping, Wanzhou, Shapingba, Fuling, Youyang, and Beibei. The data were used to analyze the climatic trends in the study area. Separately, data on monthly average air temperature recorded at the Shapingba, Dazu, Hechuan, and Jiangjin Meteorological Stations between 2007 and 2015 were used to conduct correlation analysis with the opening dates of the various festivals.

3.2. Methodology

3.2.1. Analyzing Sensitivity of FMD and FPTA to Air Temperature Changes. Correlation analyses were made on a yearly basis between (i) the temperature sequence data at the Beibei Meteorological Station and (ii) phenological observation data on FMD for 45 plants. The purpose was to determine the degree of sensitivity of FMD to CC within the study area. Correlation analyses were also made between the opening dates of the various fruit-picking festivals and air temperature at the corresponding meteorological stations. This was to ascertain whether the operators of fruit-picking festivals had taken CC into consideration.

3.2.2. Analyzing Patterns of Cyclical Changes in Air Temperature. Since CC contains regional variations, it was necessary to confirm whether the study area had experienced CC. Wavelet analysis has the advantage of being able to determine the magnitude and timing of change for a time series and hence is widely used in climate diagnostics [11, 12]. Considering that air temperature is the most important factor affecting plant phenology, this paper applied the Morlet wavelet analysis [13] to study the patterns of cyclical changes in the air temperature for Chongqing.

4. Results

4.1. Significant Changes in CC in the Study Area. There had been significant cyclical changes in the annual average air temperature of the study area between 1980 and 2013. For the real-part isolines and norm time-frequency of the wavelet transform coefficients, the positive and negative centers represent air temperature on the high and low sides, respectively.

Overall, isolines for the annual average wavelet coefficients are relatively dense around the 4–7a, 8–16a, and 26–32a temporal scales. Among these, the density for the 4–7 a temporal scale was the most prominent over the entire

Table 2: Fitting equation of fruit maturity date and air temperature ($T1$) in Beibei.

Number	Species	Family	Phases	Air temperature	Fitting equation	Adj. R^2
B4	*Salix babylonica (Willow)*	Salix	FMD	$T1$	$y = 3.21x + 58.24$	0.5962^{***}
B5	*Robinia pseudoacacia (Locust)*	Robinia	FMD	$T1$	$y = 9.00x - 37.79$	0.5484^{***}
B6	*Ligustrum compactum Ait (Ligustrum)*	Ligustrum	FMD	$T1$	$y = -3.66x + 385.72$	0.6523^{***}
B7	*Citrus sinensis (Goose Orange)*	Citrus	FMD	$T1$	$y = -3.62x + 385.69$	0.8517^{***}
B8	*Pterocarya stenoptera (Chinese Wingnut)*	Pterocarya	FMD	$T1$	$y = 10.26x - 48.06$	0.8536^{***}
B9	*Broussonetia papyrifera (Paper Mulberry)*	Broussonetia	FMD	$T1$	$y = 9.13x - 31.59$	0.3658^{***}
B10	*Pittosporum tobira (Pittosporum)*	Pittosporum	FMD	$T1$	$y = -4.76x + 400.89$	0.6913^{***}
B11	*Camptotheca acuminata Decne (Camptotheca acuminata)*	Camptotheca	FMD	$T1$	$y = -3.66x + 375.38$	0.5007^{***}
B12	*Albizia julibrissin Durazz (Albizzia)*	Albizzia	FMD	$T1$	$y = 13.10x - 126.28$	0.7522^{***}
B13	*Lindera megaphylla Hemsl (Lindera megaphylla)*	Lindera	FMD	$T1$	$y = -5.34x + 383.92$	0.7311^{**}
B14	*Juglans regia (Persian Walnut)*	Juglandaceae	FMD	$T1$	$y = -4.44x + 377.57$	0.5319^{***}
B15	*Sophora japonica (Chinese scholar tree)*	Sophora	FMD	$T1$	$y = -0.13x + 58.58$	0.7604^{***}
B16	*Platycodon grandiflorus (Bellflower)*	Campanulaceae	FMD	$T1$	$y = -1.08x + 316.45$	0.3586^{**}
B17	*Chimononthus praecox (Winter Sweet)*	Chimononthus	FMD	$T1$	$y = 3.44x + 81.07$	0.7409^{*}
B18	*Ulmus parvifolia (Chinese Elm)*	Ulmus	FMD	$T1$	$y = -3.39x + 377.82$	0.4593^{***}
B19	*Prunus salicina (Plum)*	Prunus	FMD	$T1$	$y = 5.11x + 59.53$	0.63^{***}
B20	*Podocarpus macrophyllus (Yacca)*	Podocarpus	FMD	$T1$	$y = 9.38x - 40.89$	0.6622^{***}
B21	*Spiraea salicifolia (Spiraea)*	Rosaceae	FMD	$T1$	$y = 3.32x + 67.83$	0.7254^{***}
B22	*Paulownia fortunei (Paulownia)*	paulownia	FMD	$T1$	$y = -2.32x + 325.95$	0.4433^{*}
B23	*Herba Ainsliaeae Lancifoliae (All-grass of Lanceleaf Ainsliaea)*	Asteraceae	FMD	$T1$	$y = -7.46x + 462.35$	0.6613^{**}
B24	*Malus pumila (Apple)*	Malus	FMD	$T1$	$y = 6.64x + 37.85$	0.7617^{***}
B25	*Vitis vinifera (Grapes)*	Vitaceae	FMD	$T1$	$y = 3.43x + 109.13$	0.4004^{***}
B26	*Acer buergerianum (Triangle Maple)*	Acer	FMD	$T1$	$y = 10.53x - 77.23$	0.6898^{**}
B27	*Morus alba (Mulberry)*	Morus	FMD	$T1$	$y = 5.85x + 23.36$	0.7597^{***}
B29	*Punica granatum (Pomegranate)*	Punica	FMD	$T1$	$y = -3.19x + 355.93$	0.4633^{***}
B30	*Amygdalus persica (Peach)*	Rosaceae	FMD	$T1$	$y = 2.06x + 120.69$	0.2968^{**}
B32	*Cinnamomum camphora (Camphor tree)*	Cinnamomum	FMD	$T1$	$y = -4.12x + 395.32$	0.6648^{***}
B33	*Ligustrum quihoui (Purpus Privet)*	Ligustrum	FMD	$T1$	$y = -19.07x + 623.30$	0.8315^{***}
B35	*Fontanesia fortunei (Fontanesia)*	Fontanesia	FMD	$T1$	$y = -5.52x + 418.43$	0.8808^{***}
B37	*Vernicia fordii (Tung tree)*	Vernicia	FMD	$T1$	$y = -1.18x + 328.35$	0.244^{*}
B38	*Firmiana simple (Phoenix tree)*	Firmiana	FMD	$T1$	$y = 9.54x - 35.38$	0.6006^{***}
B39	*Cercis chinensis (Chinese redbud)*	Cercis	FMD	$T1$	$y = 5.84x + 76.47$	0.2019^{**}
B8	*Wisteria sinensis (Wisteria)*	Leguminosae	FMD	$T1$	$y = 6.37x + 27.93$	0.7724^{***}
B41	*Lagerstroemia indica (Crape myrtle)*	Lagerstroemia	FMD	$T1$	$y = -3.64x + 373.20$	0.4625^{***}
B42	*Eriobotrya japonica (Loquat)*	Rosaceae	FMD	$T1$	$y = 4.59x + 52.31$	0.4512^{***}
B43	*Citrus maxima (Shaddock)*	Citrus	FMD	$T1$	$y = -5.84x + 429.37$	0.5341^{***}

Table 2: Continued.

Number	Species	Family	Phases	Air temperature	Fitting equation	Adj. R^2
B44	*Koelreuteria paniculata (Goldenrain tree)*	Koelreuteria	FMD	$T1$	$y = -4.96x + 405.65$	0.8599^{***}
B45	*Melia azedarach (Chinaberry)*	Melia	FMD	$T1$	$y = -6.84x + 443.52$	0.8608^{***}

$T1$ denotes the average air temperature one month prior to fruit maturity date, where $*$, $**$, and $***$ denote 10%, 5%, and 1% significance levels, respectively.

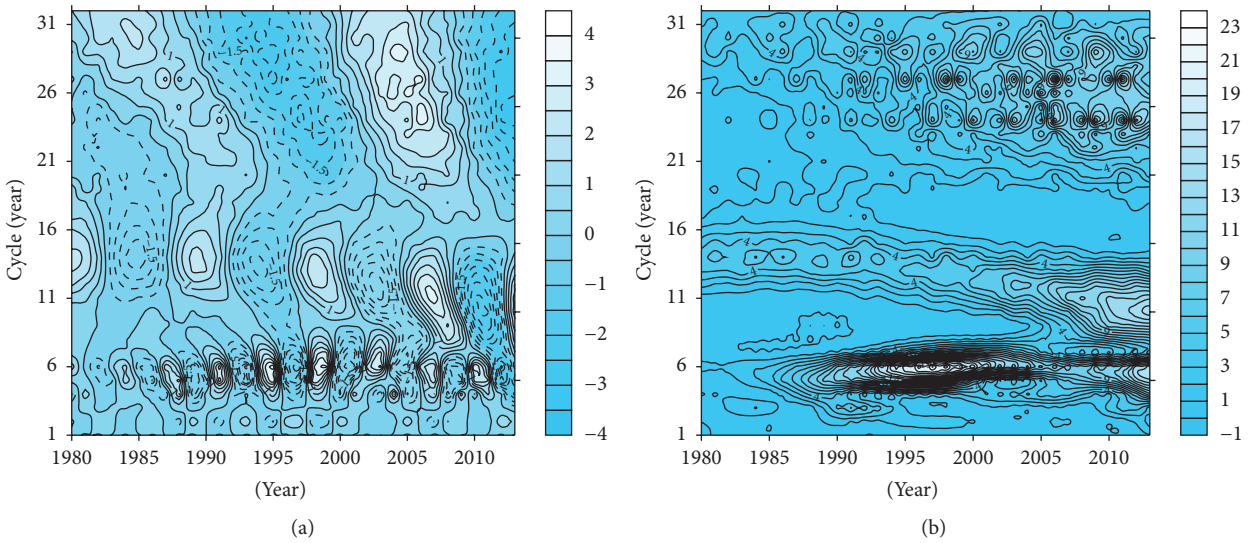

Figure 3: The isoline of the real part of wavelet coefficients, the norm time-frequency of wavelet coefficients of annual average air temperature.

study period (1980–2013). Its center temporal scale was approximately 6 a, during which temperatures underwent 8.5 alternating cycles of low → high → low → high. Next was the 8–16 a temporal scale, during which density was quite high. Its center temporal scale was approximately 6 a, during which temperatures underwent 3.5 alternating cycles of low → high → low → high. Last was the 26–32a temporal scale, with its center at 29 a (Figure 3(a)).

The norm time-frequency diagram of wavelet transform coefficients indicates that, among the three temporal scales, the cyclical oscillation during 4–7a was the strongest and had the widest coverage. These mainly occurred in 1981–2006, with the oscillation center at approximately 1998. The other cyclical oscillations were relatively weak (Figure 3(b)).

4.2. FMD Are Highly-Sensitive to Air Temperature Changes. Temperature changes have significant impact on FMD, with different species having varying degrees of sensitivities. Of the 45 types of plants, 37 were sensitive to prevailing temperatures for the previous month (Table 2). Among these, the FMD of 20 plants were advanced due to rising temperatures, with the sensitivity range being 0.13–19.71 d/°C. For the four plants specifically related to fruit-picking, the sensitivity range was 3.19–5.84 d/°C. Pomegranate was the most sensitive, while shaddock was the least. On the other hand, the FMD of 17 plants were delayed due to rising temperatures, with the sensitivity range being 2.06–13.10 d/°C. The sensitivity range for the six plants related to fruit-picking was 2.06–6.64 d/°C, with apple and peach being the most and least sensitive, respectively.

Prevailing temperatures for the previous three months affected 38 plants (Table 3). Among these, the FMD of 16 plants were advanced. The overall sensitivity range and that for the four plants directly related to fruit-picking were 1.56–9.97 d/°C and 4.18–7.23 d/°C, respectively. Pomegranate and cherry were the most and least sensitive, respectively. The FMD of the remaining 22 plants were delayed due to rising temperatures. The sensitivity range was 2.06–10.26 d/°C. Of these, the seven plants related to fruit-picking had a sensitivity range of 2.06–7.39 d/°C, with mulberry being the most sensitive and Mountain Peach the least.

4.3. Adaptation of FPTA to CC. Correlation analysis was made between 11 FPTA and monthly average air temperature one month prior to the respective opening dates of those activities. Only two fruit-picking festivals were significantly consistent with trends in temperature variations ($P < 0.05$): (i) Cherry Festival of Shuangshan Town (Figure 4(b)) and (ii) Citrus Cultural Festival of Zhong County (Figure 4(d)). Of the remaining nine festivals, the opening dates for three were related to the previous month's temperatures ($P < 0.1$). These were the Loquat Tourism Cultural Festival of Dazu District (Figure 4(a)), Waxberry Cultural Festival of Xinglong Town (Figure 4(c)), and Grape Tourism and Cultural Festival of Bishan District (Figure 4(e)).

Specifically, rising temperatures led to the advance of the Cherry Festival of Shuangshan Town's opening date by 3.14 d/°C (Figure 4(b)). The opening dates of the remaining four festivals were all delayed due to temperature increases,

Table 3: Fitting equation of fruit maturity date and air temperature ($T3$) in Beibei.

Number	Species	Family	Phases	Air temperature	Fitting equation	Adj. R^2
B1	*Michelia alba DC. (white Michelia flower)*	Michelia	FMD	$T3$	$y = 5.85x + 77.21$	0.7999^{**}
B2	*Cupressus funebris (Kashiwagi)*	Cupressaceae	FMD	$T3$	$y = 7.22x + 54.42$	0.616^{***}
B3	*Platycladus orientalis (Platycladus orientalis)*	Platycladus	FMD	$T3$	$y = 4.18x + 132.68$	0.385^{***}
B4	*Salix babylonica (Willow)*	Salix	FMD	$T3$	$y = 4.49x + 55.94$	0.5543^{***}
B5	*Robinia pseudoacacia (Locust)*	Robinia	FMD	$T3$	$y = 9.90x - 30.50$	0.773^{***}
B6	*Ligustrum compactum Ait (Ligustrum)*	Ligustrum	FMD	$T3$	$y = -4.15x + 411.48$	0.5648^{***}
B7	*Citrus sinensis (Goose Orange)*	Citrus	FMD	$T3$	$y = -4.72x + 429.36$	0.6295^{***}
B8	*Pterocarya stenoptera (Chinese Wingnut)*	Pterocarya	FMD	$T3$	$y = 7.95x + 32.44$	0.9769^{***}
B9	*Broussonetia papyrifera (Paper Mulberry)*	Broussonetia	FMD	$T3$	$y = 10.07x - 26.19$	0.7062^{***}
B10	*Pittosporum tobira (Pittosporum)*	Pittosporum	FMD	$T3$	$y = -6.72x + 470.03$	0.6289^{***}
B12	*Albizia julibrissin Durazz (Albizzia)*	Albizzia	FMD	$T3$	$y = 9.38x - 7.98$	0.9041^{***}
B15	*Sophora japonica (Chinese scholar tree)*	Sophora	FMD	$T3$	$y = -7.20x + 480.48$	0.5147^{***}
B16	*Platycodon grandiflorus (Bellflower)*	Campanulaceae	FMD	$T3$	$y = -1.56x + 332.90$	0.3994^{**}
B18	*Ulmus parvifolia (Chinese Elm)*	Ulmus	FMD	$T3$	$y = -4.38x + 411.30$	0.4636^{***}
B19	*Prunus salicina (Plum)*	Prunus	FMD	$T3$	$y = 5.97x + 68.11$	0.6569^{***}
B20	*Podocarpus macrophyllus (Yacca)*	Podocarpus	FMD	$T3$	$y = 8.46x + 12.90$	0.8613^{***}
B21	*Spiraea salicifolia (Spiraea)*	Rosaceae	FMD	$T3$	$y = 4.54x + 66.98$	0.7922^{***}
B24	*Malus pumila (Apple)*	Malus	FMD	$T3$	$y = 7.08x + 45.99$	0.752^{***}
B25	*Vitis vinifera (Grapes)*	Vitaceae	FMD	$T3$	$y = 2.30x + 133.95$	0.3858^{***}
B26	*Acer buergerianum (Triangle Maple)*	Acer	FMD	$T3$	$y = 8.66x - 0.14$	0.8935^{***}
B27	*Morus alba (Mulberry)*	Morus	FMD	$T3$	$y = 7.39x + 29.03$	0.6055^{***}
B28	*Amygdalus davidiana (Mountain Peach)*	Rosaceae	FMD	$T3$	$y = 2.06x + 129.26$	0.4054^{**}
B29	*Punica granatum (Pomegranate)*	Punica	FMD	$T3$	$y = -7.23x + 465.29$	0.3348^{***}
B30	*Amygdalus persica (Peach)*	Rosaceae	FMD	$T3$	$y = 2.19x + 126.46$	0.4828^{***}
B31	*Firmiana platanifolia (Chinese parasol (tree))*	Firmiana	FMD	$T3$	$y = 8.01x + 36.85$	0.4245^{***}
B32	*Cinnamomum camphora (Camphor tree)*	Cinnamomum	FMD	$T3$	$y = -7.57x + 475.66$	0.3458^{***}
B34	*Platanus acerifolia (Planetree)*	Platanus	FMD	$T3$	$y = -1.61x + 295.34$	0.2766^{*}
B35	*Fontanesia fortunei (Fontanesia)*	Fontanesia	FMD	$T3$	$y = -9.59x + 526.56$	0.6768^{***}
B36	*Cerasus pseudocerasus (Cherry)*	Cerasus	FMD	$T3$	$y = -4.18x + 148.02$	0.7584^{***}
B37	*Vernicia fordii (Tung tree)*	Vernicia	FMD	$T3$	$y = -1.61x + 343.40$	0.2597^{*}
B38	*Firmiana simple (Phoenix tree)*	Firmiana	FMD	$T3$	$y = 10.26x - 31.01$	0.7707^{***}
B39	*Cercis chinensis (Chinese redbud)*	Cercis	FMD	$T3$	$y = 9.13x + 2.45$	0.7293^{***}
B40	*Wisteria sinensis (Wisteria)*	Leguminosae	FMD	$T3$	$y = 5.22x + 74.80$	0.7649^{***}
B41	*Lagerstroemia indica (Crape myrtle)*	Lagerstroemia	FMD	$T3$	$y = -4.37x + 402.51$	0.2792^{**}
B42	*Eriobotrya japonica (Loquat)*	Rosaceae	FMD	$T3$	$y = 5.96x + 54.64$	0.3813^{***}
B43	*Citrus maxima (Shaddock)*	Citrus	FMD	$T3$	$y = -5.54x + 422.98$	0.3158^{**}

Table 3: Continued.

Number	Species	Family	Phases	Air temperature	Fitting equation	Adj. R^2
B44	*Koelreuteria paniculata (Goldenrain tree)*	Koelreuteria	FMD	$T3$	$y = -6.53x + 462.33$	0.6029^{***}
B45	*Melia azedarach (Chinaberry)*	Melia	FMD	$T3$	$y = -9.97x + 533.49$	0.6324^{***}

$T3$ denotes the average air temperature three months prior to fruit maturity date, where $*$, $**$, and $***$ denote 10%, 5%, and 1% significance levels, respectively.

with the rates being 5.30 d/°C (Figure 4(a)), 3.96 d/°C (Figure 4(c)), 1.10 d/°C (Figure 4(d)), and 3.35 d/°C (Figure 4(e)), respectively.

The opening dates for the Loquat Tourism Cultural Festival of Dazu District, Cherry Festival of Shuangshan Town, and Grape Tourism and Cultural Festival of Bishan District were found to be consistent with the trends in temperature variations. The dates were also aligned with the changing trends of FMD for the observed species (loquat, cherry, and grape, resp.) resulting from temperature changes. For the Jiangnan Loquat Festival (one of the other six festivals), half of its opening dates over the years remained scheduled on the weekends.

These findings indicate that most organizers of fruit-picking festivals did not take into account the effects of temperature changes when planning those events and that only a few activities were arranged to comply with changing phonological patterns of the related species. Most festival organizers have yet to consider the impact of CC on festival activities or have not paid adequate attention to the impact of temperature changes. Instead, they tended to simply schedule festival activities on the weekends.

5. Conclusion and Discussion

FPTA are essentially dependent on FMD. Although there has gradually been a consensus over the fact that CC affects plant phenology, the responses of different species to air temperature changes vary significantly. Some may even exhibit reactions opposite to regular patterns. In this study, 11 species that are directly related to FPTA were examined. Among them, the FMD for four species were advanced significantly, while the remaining 6-7 were significantly delayed. Specifically, pomegranate, apple, and mulberry were the most sensitive to temperature changes, while shaddock, peach, and cherry were the least sensitive. The implication is that the complexity of FPTA adaptation measures to CC has increased greatly. There is a need for researchers to examine each species individually to determine the trend and degree of sensitivity for each species' FMD in response to CC. In addition, even for the same species, the degree of phenological sensitivity to CC may vary significantly in different regions. Therefore, more comprehensive comparative analysis of case studies must be done to confirm the extent of CC's impact.

In recent years, more members of the public have gained a better understanding of CC and its impacts. It was found that prevailing temperatures for one or three months prior have a decisive influence on FMD. In order to adapt to CC, relevant management departments that operate FPTA should adjust the dates and durations of festival activities promptly based on changes in FMD or temperatures. However, this study found that very few festival organizers were aware of the impact of CC, nor have they adjusted festival opening dates according to dynamic temperature changes. A considerable number of festivals continue to fix the schedule of festival activities on the weekends. This will result in tourists missing out on the optimal fruit-picking season. The key to the further development of fruit-picking tourism is the provision of timely and accurate information on FMD to both tour operators and tourists.

There is a rich variety of FPTA around the world, most of which are vulnerable to CC's impact. However, there is a lack of existing phenological observations on species directly related to FPTA. Hence, it is necessary to increase the existing database of observations to include those species. The optimal season to carry out FPTA is between the time when fruits are beginning to ripen and that when they fall off the plants. The duration that each species' fruit maturity is sustained determines the period over which FPTA can be carried out. Existing phenological observation data contain more records on the timing when fruits begin to ripen, but there is a relative lack of records on the timing when fruits fall. This has in turn affected the accuracy of assessment studies on the impact of CC on FPTA.

In terms of the adaptability of fruit-picking tourism to CC, there is a need to establish phenological observation stations over a greater geographical distribution and a public platform for real-time dissemination of information. Presently, there are less than 40 observation stations in the whole of China. This is clearly insufficient to meet the needs of seasonal tourism activities. However, there is a lack of funds to establish large number of observation stations. In this regard, China can draw upon the experience of other countries by cultivating volunteers who make phenological observations and encouraging large-scale public participation through the setting up of a real-time phenology reporting mechanism. In addition, it is noted that China has yet to adopt a flexible vacation system. Even if festival organizers were to make real-time adjustments to event dates based on FMD and CC, visitors may not be able to participate due to the lack of leave. Thus the implementation of a flexible salaried vacation system which includes paid leave will be an important policy that will strengthen the adaptability of fruit-picking tourism to CC and ensure the sustainable development of the industry.

Appendix

See Tables 1, 2, and 3.

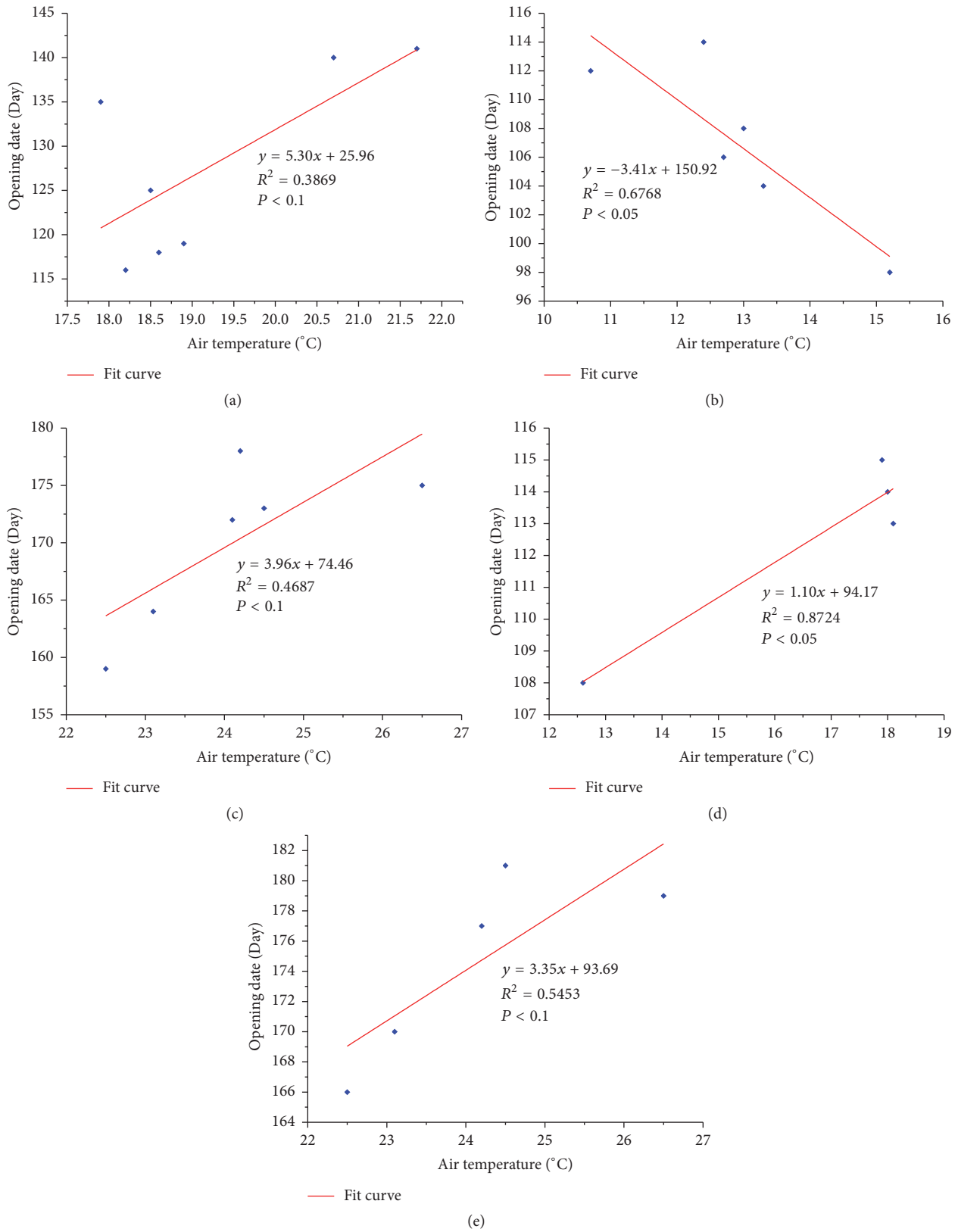

Figure 4: Response relationship between picking tourism festival open date and air temperature in Chongqing.

Competing Interests

The authors have declared that no conflict of interests exists.

Acknowledgments

This study was supported by the National Major Scientific Instruments and Equipments Development Project (Grant no. 41427805), the Ministry of Education of Humanities and Social Science Project (Grant no. 16YJC790060), Social Science Planning Annual Project of Sichuan, China (Grant no. SC15B046), Soft Science Research Project of Sichuan, China (Grant no. 2015ZR0225), and the Fundamental Research Funds for the Central Universities (Grant no. skqy201639).

References

[1] P. P. Mohanan, "Cardiology blooms at ACC 2014 at Washington DC but no cherry blossoms," *Indian Heart Journal*, vol. 66, no. 2, pp. 253–254, 2014.

[2] L. Wang, H. Chen, Q. Li, and W. Yu, "Research advances in plant phenology and climate," *Acta Ecologica Sinica*, vol. 30, no. 2, pp. 447–454, 2010.

[3] X. Yunjia, D. Junhu, W. Huanjiong et al., "Variations of main phenophases of natural calendar and analysis of responses to climate change in Harbin in 1985–2012," *Geographical Research*, vol. 34, no. 9, pp. 1662–1674, 2015.

[4] B. Jie, G. Quansheng, and D. Junhu, "Response of woody plant phenophases to climate change for recent 30 years in Guiyang," *Geographical Research*, vol. 28, no. 6, pp. 1606–1614, 2009.

[5] C. M. Hall, "Tourism and biodiversity: more significant than climate change?" *Journal of Heritage Tourism*, vol. 5, no. 4, pp. 253–266, 2010.

[6] M. Li and F. Xiuqi, "Effect of global warming on seasonal tourism for the last 20 years in Beijing: a case study on the peach flower stanza of Beijing Botanical Garden," *Advance in Earth Science*, vol. 21, no. 3, pp. 313–319, 2006.

[7] R. Sakurai, S. K. Jacobson, H. Kobori et al., "Culture and climate change: Japanese cherry blossom festivals and stakeholders' knowledge and attitudes about global climate change," *Biological Conservation*, vol. 144, no. 1, pp. 654–658, 2011.

[8] L. Jun, L. Yunyun, L. Haolong et al., "Climate change and peach blossom viewing: impact and adaptation," *Geographical Research*, vol. 35, no. 3, pp. 504–512, 2016.

[9] Q. Ge, J. Dai, J. Liu, S. Zhong, and H. Liu, "The effect of climate change on the fall foliage vacation in China," *Tourism Management*, vol. 38, pp. 80–84, 2013.

[10] Y. Aono and K. Kazui, "Phenological data series of cherry tree flowering in Kyoto, Japan, and its application to reconstruction of springtime temperatures since the 9th century," *International Journal of Climatology*, vol. 28, no. 7, pp. 905–914, 2008.

[11] W. He, R. Bu, Z. Xiong, and Y. Hu, "Characteristics of temperature and precipitation in Northeastern China from 1961 to 2005," *Acta Ecologica Sinica*, vol. 33, no. 2, pp. 519–531, 2013.

[12] L. Guangsheng, W. Genxu, H. Hongchang et al., "Climate change characteristics in the source regions of the Yangtze River and Yellow River over the past 45 years," *Resources Science* , vol. 32, no. 8, pp. 1486–1492, 2010.

[13] C. Torrence and G. P. Compo, "A practical guide to wavelet analysis," *Bulletin of the American Meteorological Society*, vol. 79, no. 1, pp. 61–78, 1998.

Hindawi Publishing Corporation
Advances in Meteorology
Volume 2016, Article ID 5194091, 11 pages
http://dx.doi.org/10.1155/2016/5194091

Research Article

Water Conservation Service Assessment and Its Spatiotemporal Features in National Key Ecological Function Zones

Jun Zhai,[1] Yuping Liu,[1] Peng Hou,[1] Tong Xiao,[1] and Guangzhen Cao[2]

[1]*State Environmental Protection Key Laboratory of Satellite Remote Sensing, Satellite Environment Center, Ministry of Environmental Protection of the People's Republic of China, Beijing 100094, China*
[2]*Key Laboratory of Radiometric Calibration and Validation for Environmental Satellites, China Meteorological Administration, National Satellite Meteorological Center, Beijing 100081, China*

Correspondence should be addressed to Peng Hou; houpcy@163.com and Guangzhen Cao; caogz@cma.gov.cn

Received 8 March 2016; Revised 11 July 2016; Accepted 1 August 2016

Academic Editor: Dong Jiang

In order to improve ecosystem service and protect nation ecology security, the government had designated lots of important ecosystem service protection areas, named national key ecological function zones (NKEFZ) in China. Water conservation service had been assessed with the help of multisource remote sensing data, and spatiotemporal features were analyzed from 2000 to 2014 in these ecological services zones. By assuming precipitation scenario as the constant, contribution for water conservation from human activities and climate change was analyzed, and result shows that, because of vegetation restoration by human activities, evapotranspiration increased obviously with the increase of the vegetation coverage. This could reduce the water conservation. However, actual annual increase of water conservation mainly comes from the increase of precipitation. Our analysis revealed that the choice of evaluation model played a decisive role in the reason analysis, which would affect the development of ecological policy.

1. Introduction

Water conservation service, as one of the most important terrestrial ecosystem services, is a comprehensive feature of ecological function by water, soil, and vegetation interactions. Vegetation is the main source of water conservation service in terrestrial ecosystem. The vegetation growth and change characteristics could reflect water conservation ability. At present, small watershed research about water conservation is relatively mature. The main research methods include field observation, statistical analysis, and watershed simulation models [1–3]. However, the assessment methods extrapolation from watershed scale to regional scale of ecosystem water conservation service is still facing great challenges. The main reason is that traditional hydrological models could not quantify the water conservation effects of ecosystem changes, especially in region with complex underlying surface, such as the land management planning or ecological protection project regions [4, 5]. In addition, less study cases quantitatively decompose the influence of ecosystems and ecological services from human activities and climate. This limits us to devise targeted management measures and implement differentiated protection projects in different ecological regions.

National key ecological function zone (NKEFZ) is the important region of ecosystem service and national ecological security. The purpose of this policy is to restore and improve the regional ecological function of water conservation, soil and water conservation, windbreak and sand fixation, and biodiversity maintenance [6, 7]. NKEFZ planning had been considered in the natural ecosystem service factors and social economic factors and had formed regional function index and regionalization scheme [8]. Therefore these zones are also the demonstration area of harmonious coexistence of human and nature. NKEFZ is an important basis of regional ecological compensation, transfer payment, and delineation of ecological protection redline regions [6, 9]. At present, related research mainly focuses on ecological service assessment in a single zone [10, 11]. Cases about dynamic assessment in temporal and spatial variation and the

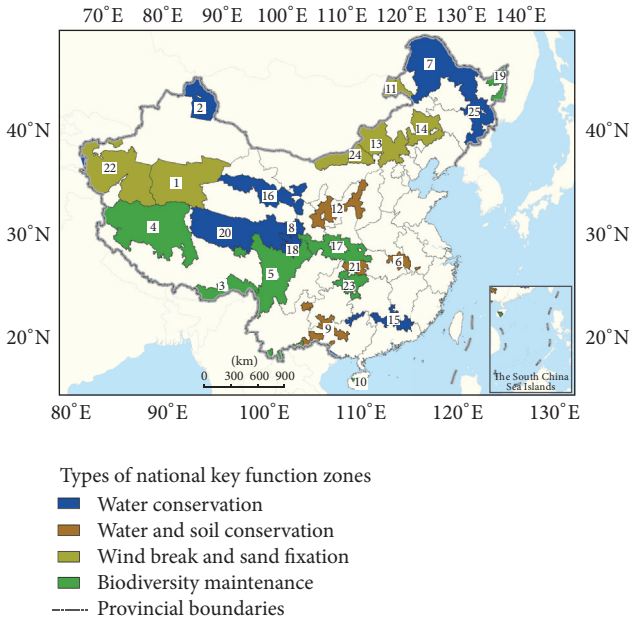

Figure 1: Distribution and location of national key ecological function zones: 1: grassland desertification control region in Arkin (GA); 2: mountain forest steppe region in Altai (MA); 3: forest region in the edge of southeastern Tibet (FT); 4: desert region of Qiangtong Plateau in the northwestern Tibet (DT); 5: forest and biodiversity in Sichuan and Yunnan (FY); 6: soil and water conservation region in Dabie Mountain (SM); 7: forest region in greater and lesser Hinggan Mountains (FM); 8: important water supply region of the Yellow River in Gannan (IG); 9: karst rocky desertification region in Guangxi, Guizhou, and Yunnan (KY); 10: tropical rainforest region of central Hainan Island (TI); 11: grassland meadow region in Hulun Buir (GB); 12: hilly and gully region of Loess Plateau (HP); 13: Hunshandake desertification region (HD); 14: grassland desert region of Horqin (GH); 15: forest and biodiversity region in Nanling Mountain (FNM); 16: glacier and water conservation region in Qilian Mountain (GM); 17: biodiversity region in Qinba (BQ); 18: grassland wetland region of Ruoergai (GR); 19: wetland region of Sanjiang plain (WS); 20: grassland meadow wetland region in Sanjiangyuan (GS); 21: Three Gorges Reservoir Area (TA); 22: desertification control region of Tarim River (DR); 23: biodiversity, soil conservation region in Wuling Mountains (BW); 24: grassland region in Yinshan Mountain (GYM); 25: forest region in Changbai Mountain (FCM).

whole NKEFZ are rare, especially before the implementation of the ecological project and transfer payment. It is not helpful for scientific judgment of the following ecological compensation measures and engineering implantation [12].

Most NKEFZ are in the source area of river and basin and are distributed in different climatic zones. Various ecosystems had undergone significant changes in the impact of climate change and human activities in these regions [12, 13]. Hydrological balance and the cycle process, which could impact the ecological service, had also changed dramatically. In this paper, multisource satellite remote sensing data and ground observation data were used to evaluate the ecosystem and water conservation service in the NKEFZ during 2000–2014. Spatiotemporal features were analyzed with the help of spatial statistics, time series analysis, and simulation scheme comparison. Finally, this paper attempted to identify the impact difference between human activities and climate change.

2. Study Area

NKEFZ includes 25 regions, as Figure 1 showed [7]. Total area of NKEFZ is about 3.86×10^6 km^2, accounting for 40.2% of national land area. In these regions, population is about 0.11 billion, accounting for 8.5% of total population of China. According to the leading ecological service, there are four types of national key ecological services, including water conservation, water and soil conservation, wind break and sand fixation, and biodiversity maintenance (Figure 1).

3. Data Sets

Land use and land cover change data on the NKEFZ from 2000 to 2014 with spatial resolution in 30 m were determined following the standardized methodology outlined in [14, 15]. A hierarchical classification system with 25 types of land use and land cover classes were further grouped into 6 aggregated classes consisting of farmland, forest, grassland, water bodies, built-up areas, and unused land. The comprehensive accuracy was more than 90% [14–17]. Then the land use and land cover change data are classified as farmland, forest, grassland, water body and wetland, settlement, and bare land ecosystems correspondingly. Spatial statistics tools were used to evaluate the characteristics of ecosystem area comprehensively.

Gridded data set of temperature and precipitation data was assembled from the National Meteorological Information Center of China Meteorological Administration. This data set was generated based on the basic meteorological elements of the 2742 National Ground Meteorological Stations; the TPS (Thin Plate Spline) combined with three-dimensional geospatial information was used for spatial interpolation. The spatial resolution of the data set is 0.5 × 0.5 degrees. The boundary of the NKEFZ was used to extract the data needed for this study.

Normalized difference vegetation index (NDVI) was used to reflect the growth and changes of ecological quality in study regions. NDVI data were extracted from the month MODIS vegetation indexes product (Collection 5 MOD13Q1, 250 m spatial resolution, 16-day composites) [18] within the NKEFZ. Data smoothing method based on the Savitzky-Golay filter was used to smooth out noise from cloud and atmosphere in NDVI time series [19, 20]. Annual mean NDVI values were used to reflect interannual variation of vegetation.

4. Methods

4.1. Water Conservation Service Assessment. Because of difference between the NKEFZ and watershed, soil water holding capacity change is very small in climate normal years [21, 22]. In this article, the water yield in pixel scale, which was calculated by precipitation minus evapotranspiration, was used to quantitatively describe the water conservation service capacity. The calculation method is as follows:

$$\mathrm{WR} = P - \mathrm{ET}. \quad (1)$$

Precipitation was spatial gridded data generated from meteorological stations observation data interpolation. The actual evapotranspiration data was calculated from MODIS satellite observation data by Penman-Monteith formula [23, 24]. The accuracy evaluation based observation flux data indicated that the product was suitable for regional scale evapotranspiration analysis [23–26]. At present, ecological protection projects had been implemented in some ecological function zones. Different contribution between human activities and climate change was considered by calculating the water conservation (WR) in two schemes: (1) To describe the impact combined ecological protection project and climate change factor, WR of observation was calculated with precipitation of every year. (2) To describe the impact mainly from human activities, like ecological protection projects, WR of simulation was calculated with mean annual precipitation.

4.2. Trend Analysis. The unitary linear regression can be used to estimate the water conservation trend at pixel scale according to the Ordinary Least Squares (OLS). In this study, python was used to calculate the slope. ArcGIS10.2 software was used to show the spatial distribution of raster data. The slopes were calculated as follows:

$$\text{Slope} = \frac{\sum_{i=1}^{n} m_i X_i - (1/n) \times \sum_{i=1}^{n} m_i \times \sum_{i=1}^{n} X_i}{\sum_{i=1}^{n} m_i^2 - (1/n) \times \left(\sum_{i=1}^{n} m_i\right)^2}, \quad (2)$$

where X_i is the value of water conservation in year i, $i = 1, 2, 3, \ldots, n$. m_i is the number of the year in sequence, and $m_1 = 1, m_2 = 2, m_3 = 3, \ldots, m_n = n$, in which $n = 15$.

5. Result and Discussion

5.1. Ecosystem Distribution and Change. In 2014, grassland was the largest ecosystem in the NKEFZ, the area proportion was 41.12%, and then the forest area proportion was 22.59%. Settlement had the minimum area, whose proportion was only 0.23%. During 2000–2014, the area proportion of forest decreased from 23.41% to 22.59%. Grassland decreased from 42.24% to 41.12%. Water body and wetland decreased from 3.71% to 5.45%. On the contrary, farmland increased slightly from 8.36% to 8.40%. Settlement and bare land showed little change in the NKEFZ (Figure 2).

In the 25 ecological function zones, the TI located at the southernmost tip of China had the largest forest area proportion of 83.10%. While the DT had the lowest forest area proportion in western China, the number is only 0.03%. However, the grassland area proportion in the DT is the highest in the 25 zones. Instead, this number is only 2.30% in the FCM. In general, the natural vegetation area proportion maximum is 98.22% in the GR; the minimum value is 23.51% in the GA (Figure 3).

The main ecosystems in different NKEFZ types were not entirely the same. In the water conservation types zones, the main ecosystems are grassland and forest, and the mean area proportions were 36.82% and 33.55%, such as the GR and FCM. In the water and soil conservation type zones, forest is the main ecosystem with mean area proportion of 46.94%. The representative zones were the TA and KY. Grassland

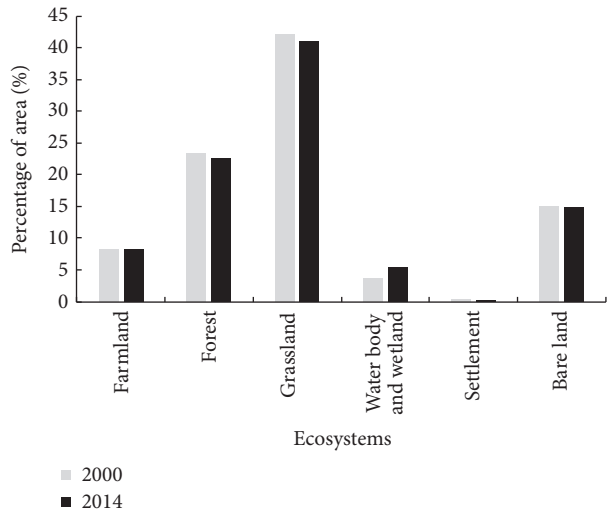

Figure 2: The area proportion change of ecosystems in NKEFZ.

was also the largest ecosystem in the wind break and sand fixation type zones, with mean area proportion of 51.02%. The typical zones were the GB and HD. The biodiversity maintenance type zones mainly included forest and grassland ecosystems with mean area proportion of 46.07% and 26.79%, respectively. The DT and TI were the most representative.

5.2. Vegetation Growth and Change. The normalized difference vegetation index (NDVI) is used to indicate the vegetation growth status. In spite of the close relationship between NDVI and climate change, NDVI can also reflect the characteristics of human activities [27], such as vegetation restoration projects. Statistical analysis showed that the mean NDVI was 0.4307. The TI had the highest NDVI value of 0.8211 in the NKEFZ, while the GA had the lowest NDVI value of 0.0681. In the aspect of function zone type, biodiversity maintenance type zones had the highest NDVI value of 0.5536 and wind break and sand fixation type zones had the lowest NDVI values of 0.1926 (Figure 4).

During 2000–2014, NDVI values showed a slight decrease trend in the MA, FT, and FY, while in the other 22 zones the NDVI values were increased. It is worth noting that there was significant increase in the HP, BQ, TA, and BW ($P < 0.001$). For example, the NDVI increased from 0.6712 in 2000 to 0.7253 in 2014 in the BW. In the 25 function zones, the main ecosystem with NDVI increased was grassland. In the aspect of function zone type, biodiversity maintenance and water and soil conservation type zones showed obvious increasing trend in NDVI, and the change rates were 0.0030 and 0.0012 per year, respectively. These values were 0.0011 and 0.0007 per year, respectively, in wind break and sand fixation and water conservation type zones. The mean NDVI of the NKEFZ had showed a significant increase from 0.4184 in 2000 to 0.4405 in 2014 ($P < 0.001$) (Figure 5).

5.3. Water Conservation Simulation and Evaluation. The mean WR of observation was 174.71 mm in the NKEFZ. The TI had the maximum of WR of observation value

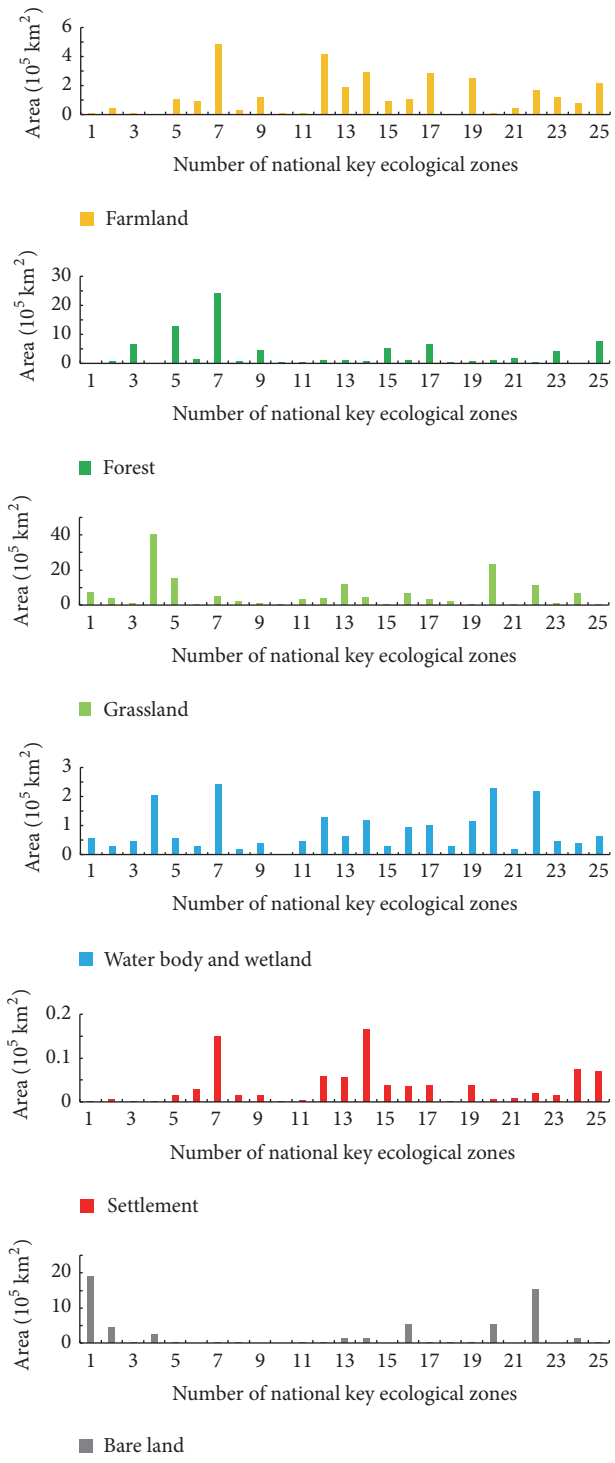

Figure 3: Area of each ecosystem in NKEFZ (the number can refer to Figure 1).

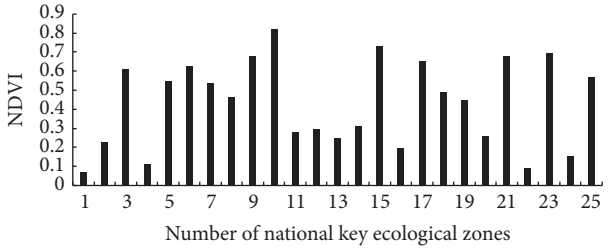

Figure 4: Mean values of NDVI in NKEFZ (the number can refer to Figure 1).

with 985.23 mm. In the GA, WR of observation value was −101.21 mm. In the aspect of function zone type, water and soil conservation and biodiversity maintenance type zones had the largest WR of observation value of 286.19 mm and 286.13 mm, respectively. Then water conservation type zones' mean value was 120.69 mm. The minimum value of WR of observation was in wind break and sand fixation type zones (Figure 6).

There are obvious spatial differences of WR of observation between the north and the south in the NKEFZ. And the value of the south was higher, such as the upper and middle reaches of the Yangtze River Basin (Figures 7(a) and 7(b)). The main reason was the obvious different vegetation types and precipitation.

During 2000–2014, WR of observation change indicated that water conservation was increased obviously in the GS dominated by grassland and the FM dominated by forest, while the water conservation decreased in the zones located in the south of the Yangtze River area. In arid and semiarid zones over northwest China, water conservation had a slight increase on the whole. However, what was unusual was that the WR of simulation change had showed opposite trend with the WR of observation in some zones, such as the HP and GH (Figures 7(c) and 7(d)). WR of simulation decreased year by year. The main reason was that the surface vegetation coverage increased gradually, so the evapotranspiration increased accordingly (Figure 5).

Figure 8 depicted the temporal variation of water conservation and precipitation in different zones. The results showed that the mean WR of observation increased slightly from 192.34 mm to 198.98 mm during 2000–2014 ($P < 0.2$) and had consistent change with precipitation. Specifically, there were six zones of water conservation showing a slight decrease. The zones were the MA, FT, KY, FNM, TA, and DR. The rest of the 19 zones showed an increasing trend. The GS had relatively significantly increased with water conservation from −199.45 mm in 2000 to 40.82 mm in 2014 ($P < 0.1$). Other zones showed increasing volatility. Contrary to NDVI change, water conservation mainly increased in grassland ecosystem. In the aspect of function zone type, water conservation had the largest increase in water conservation type zones. The mean change rate was 4.01 mm/year. Secondly, the change rates were 3.83 mm/year in biodiversity maintenance type zones and 3.20 mm/year in wind break and sand fixation type zones, respectively. Instead, water conservation showed a trend of decrease in water and soil conservation type zones and the change rate was 0.54 mm/year.

However, the WR of simulation showed a slight decrease from 185.18 mm to 174.70 mm during 2000–2014 ($P < 0.5$). Compared with the observation results, WR of simulation had no interference from precipitation change. This could also reduce the uncertainty of climate change and reflect the

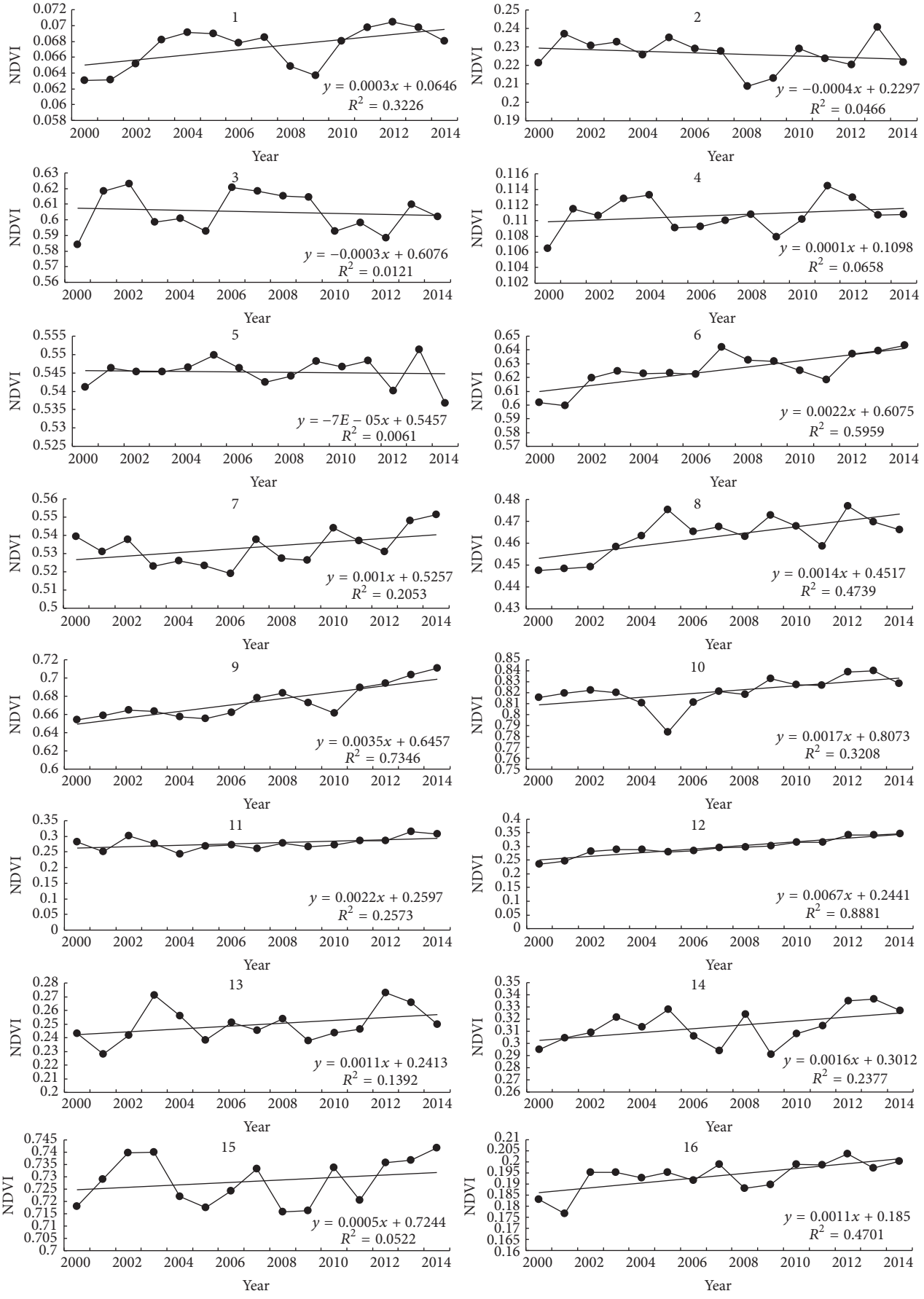

Figure 5: Continued.

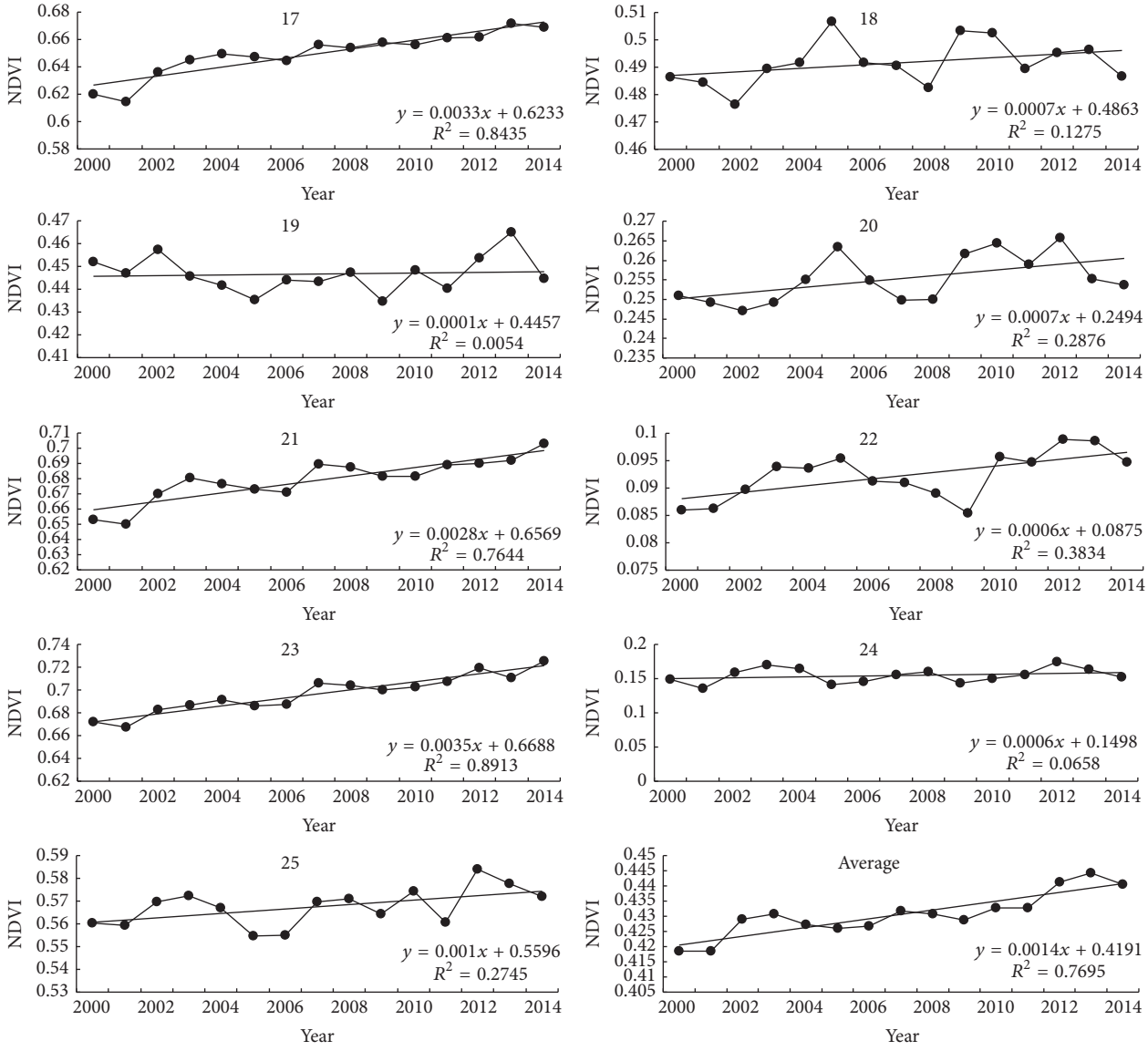

Figure 5: Statistic features of mean values of NDVI in NKEFZ from 2000 to 2014.

change of underlying surface. In the 25 zones, there were 16 zones showing a decrease in water conservation, which was consistent with Figure 7. The most significant change is in the HP ($P < 0.06$). The surface vegetation improvement was the main reason.

6. Discussions

Regional ecological service assessment was affected by climate change and human activities. In recent years, many protection projects and measures were carried out and played an active role in ecosystem restoration in China [4], such as the Grain to Green Program (GTGP), Natural Forest Protection (NFP), Returning Rangeland to Grassland Program (RRGP), and sand control engineering. As a result, the vegetation evapotranspiration increased gradually, and WR of simulation showed a decreasing trend. However, because

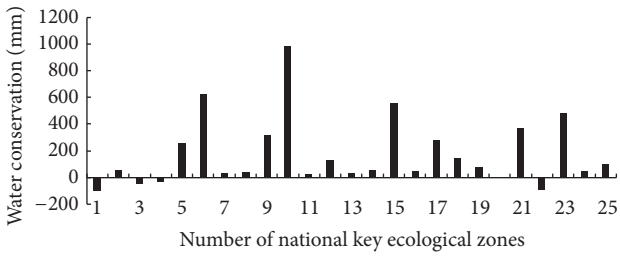

Figure 6: Mean water conservation of observation in NKEFZ (the number can refer to Figure 1).

of the increase of precipitation, WR of observation displays an increasing trend. Therefore, in future research, before the evaluation of water conservation, the models and hypothesis should be determined firstly. Also the climate factors and

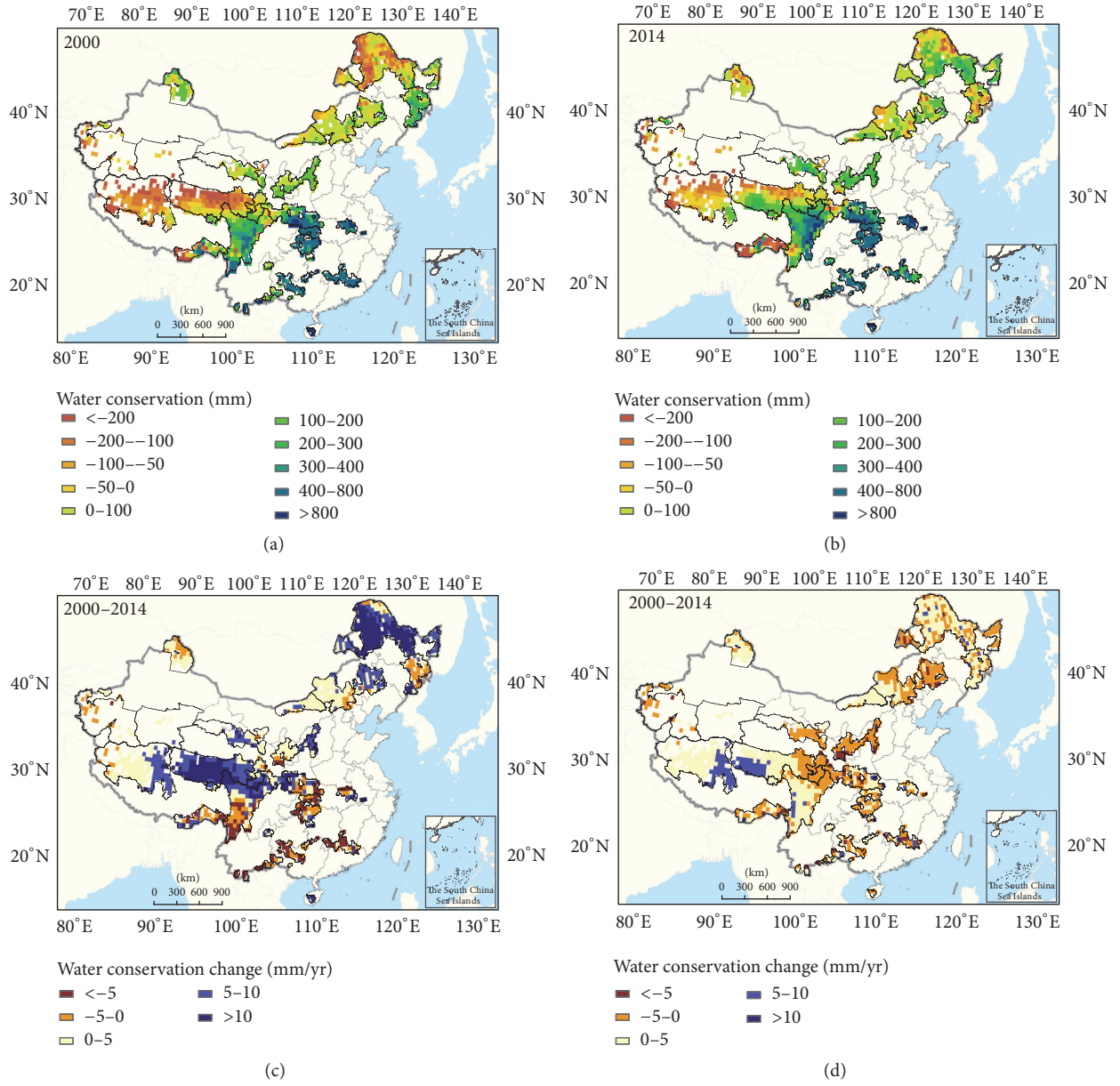

Figure 7: Spatial distribution and change of water conservation in NKEFZ ((a) WR of observation in the NKEFZ of 2000; (b) WR of observation in the NKEFZ of 2014; (c) WR change of observation in the NKEFZ; (d) WR change of simulation in the NKEFZ).

human disturbance should be separated for calculation. Only in this way will assessment results be accurate and credible, and ecology managers and government policy makers could develop targeted management measures and implement different ecological protection projects for ecological function zones.

Regional ecological function assessment should also consider the different features of the underlying surface [28]. It is necessary to characterize the differences of ecological function variation at a local scale. In GS, WR of observation showed increase trend during 2000–2014. Figure 8 also indicated that WR of observation had been negative before 2007 and became positive after 2007. These two stages of change had coincided with the approval time of plan named "the overall planning of ecological protection and construction in Qinghai Three-River Headwater Region nature reserve region." The WR of simulation showed different change features between the eastern and western GS. The possible reason was that the ecological protection projects have promoted vegetation restoration and increased evapotranspiration in the eastern region. However, in the western region, there were the most serious grassland degradation and a large number of secondary bare lands. Saturated water content of soil in this region was only half of the eastern region. Ecological protection projects could not prevent the water content decrease. Accordingly, there was less contribution of vegetation on underlying surface evapotranspiration. Moreover, water and swamps tended to dry in many ways in these regions [29].

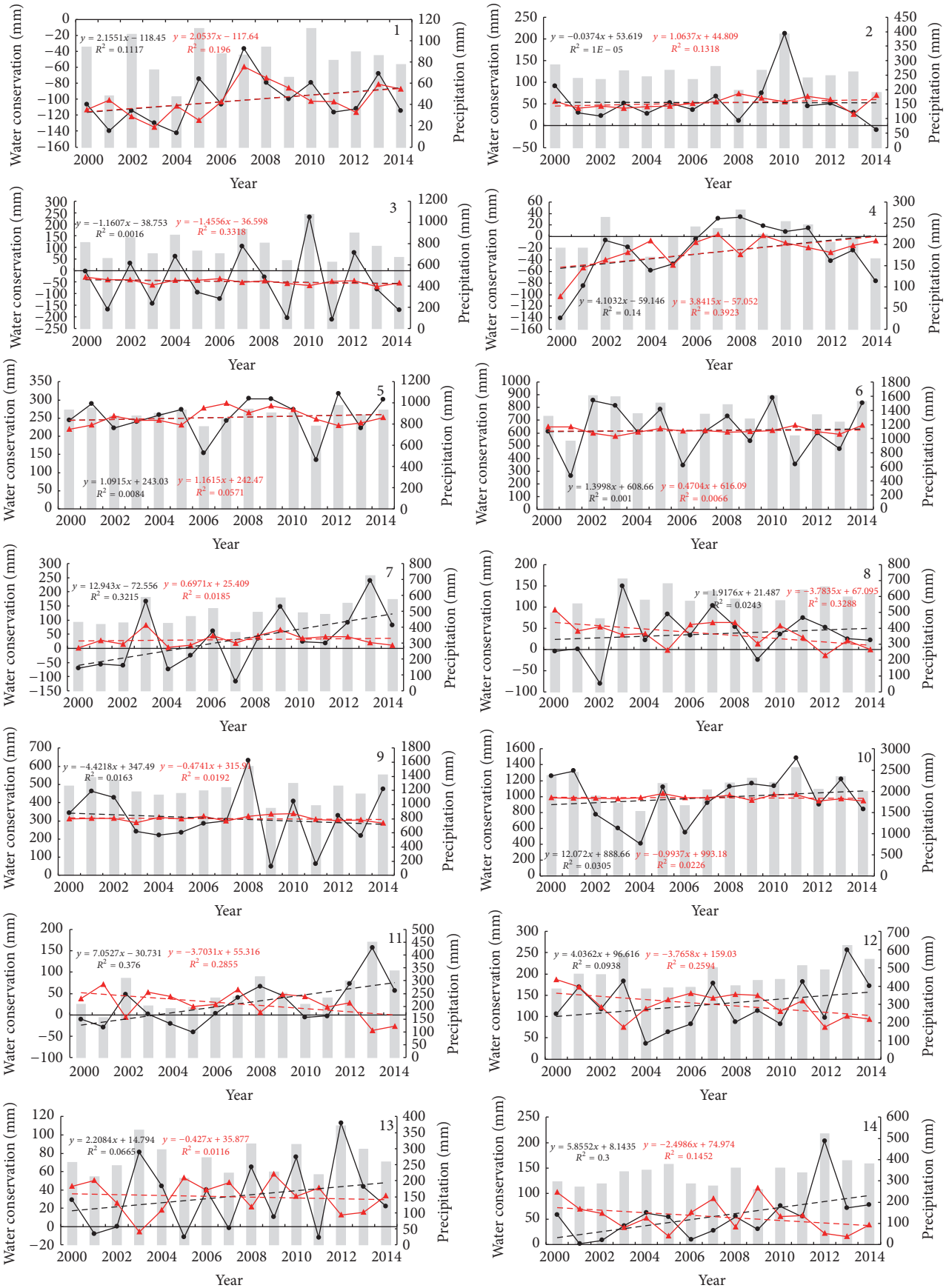

Figure 8: Continued.

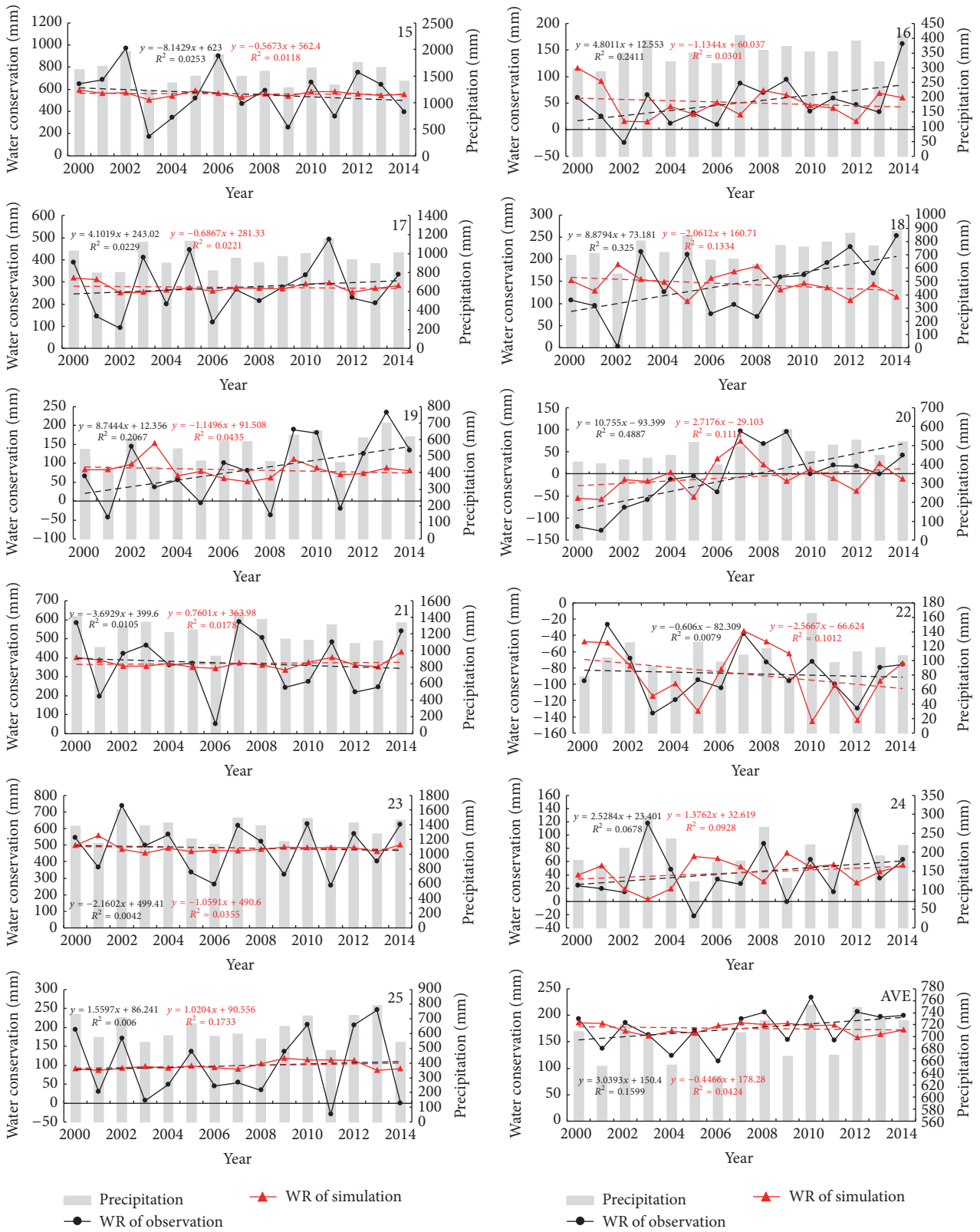

Figure 8: Mean water conservation and annual precipitation change in NKEFZ.

Thus the evapotranspiration decreased and WR of simulation increased instead. However, further research would need more observation data and model simulation to reveal details of reasons of water conservation change on a local scale.

In the arid and semiarid area, evaluation of ecosystem service change caused by ecological protected projects implementation needs to take into account complex surface change. The reason is that maybe more net radiation is absorbed by the restoration vegetation [30]. In the process of energy distribution, more net radiation not only is beneficial to the growth of vegetation, but also could improve surface temperature and then it increases evapotranspiration. Finally, water conservation may be impacted. Therefore, coupled with more ecological parameters, developing land surface process models including energy balance principle is needed to evaluate ecosystem service scientifically in regional scale and provide references for ecological policy makers.

7. Conclusions

(1) The natural vegetation, such as forest and grassland, was the main ecosystem in the NKEFZ. Grassland ecosystem is dominant and largest in area, accounting for 41.12% of the total area. Then forest area proportion was 22.59%. Settlement was minimum in area, whose proportion was only 0.23%. From 2000 to 2014, area proportion of forest and grassland decreased by 0.82% and 1.12%, respectively. Farmland increased by about 0.04%, which suggested that land reclamation and other human activities were still increasing.

(2) Vegetation was growing well as a whole in the NKEFZ. Mean NDVI was 0.4307. Biodiversity maintenance type zones had the highest NDVI value of 0.5536 and wind break and sand fixation type zones had the lowest NDVI values of 0.1926. During 2000–2014, the mean NDVI of the NKEFZ had showed a significant increase from 0.4184 to 0.4405 ($P < 0.001$). On the other hand, NDVI values showed a slight decrease trend in the MA, FT, and FY. Nevertheless, NDVI values were increased in other zones. There was significant increase in the HP, BQ, TA, and BW ($P < 0.001$).

(3) During 2000–2014, mean WR of observation was 174.71 mm in the NKEFZ. The TI had the maximum of WR of observation value with 985.23 mm. In the GA, WR of observation value was −101.21 mm. There are obvious spatial differences of WR of observation between the north and the south in the NKEFZ. WR of observation value of the south was higher, such as the upper and middle reaches of the Yangtze River Basin. Comparing two kinds of water conservation scheme, mean WR of observation increased slightly from 192.34 mm to 198.98 mm during 2000–2014 ($P < 0.2$). It was mainly located in grassland. However, the WR of simulation showed a slight decrease from 185.18 mm to 174.70 mm during 2000–2014 ($P < 0.5$). WR of simulation reduced the uncertainty of climate change and reflected the change of underlying surface. In the important region of ecological protected projects implementation, such as the HP, evapotranspiration increased obviously with improvement of vegetation. Furthermore, WR of simulation showed significant decrease ($P < 0.6$). WR of observation increased mainly because of the increased precipitation.

Competing Interests

The authors declare that there is no conflict of interests regarding the publication of this paper.

Acknowledgments

This research was supported by the Major State Science Research Development Program of China (Grant ID: 2016YFC0500206).

References

[1] H. El Kateb, H. Zhang, P. Zhang, and R. Mosandl, "Soil erosion and surface runoff on different vegetation covers and slope gradients: a field experiment in Southern Shaanxi Province, China," *Catena*, vol. 105, pp. 1–10, 2013.

[2] D. Teka, B. Wesemael, V. Vanacker et al., "Evaluating the performance of reservoirs in semi-arid catchments of Tigray: tradeoff between water harvesting and soil and water conservation," *Catena*, vol. 110, pp. 146–154, 2013.

[3] M. Lee, G. Park, M. Park, J. Park, J. Lee, and S. Kim, "Evaluation of non-point source pollution reduction by applying Best Management Practices using a SWAT model and QuickBird high resolution satellite imagery," *Journal of Environmental Sciences*, vol. 22, no. 6, pp. 826–833, 2010.

[4] X. M. Feng, G. Sun, B. J. Fu, C. H. Su, Y. Liu, and H. Lamparski, "Regional effects of vegetation restoration on water yield across the Loess Plateau, China," *Hydrology and Earth System Sciences*, vol. 16, no. 8, pp. 2617–2628, 2012.

[5] X. H. Wei, G. Sun, J. M. Vose, K. Otsuki, Z. Zhang, and K. Smetterm, "Forest ecohydrological processes in a changing environment," *Ecohydrology*, vol. 4, no. 2, pp. 143–145, 2011.

[6] The State Council of the People's Republic of China, *Major Function-Oriented Zone Planning in China*, The State Council of the People's Republic of China, Beijing, China, 2010 (Chinese).

[7] Ministry of Environmental Protection, *China Ecological Function Regionalization*, Ministry of Environmental Protection, 2008 (Chinese).

[8] J. Fan, "Draft of major function oriented zoning of China," *Acta Geographica Sinica*, vol. 70, no. 2, pp. 186–201, 2015 (Chinese).

[9] Ministry of Environmental Protection, *The Delineation of Ecological Protection Red Technology Guide*, Ministry of Environmental Protection, 2015 (Chinese).

[10] G. P. Li and W. B. Zhang, "Study on the transfer payment differentiation contract of national key ecological function zone," *Modern Economic Sciencem*, vol. 37, no. 6, pp. 92–125, 2015 (Chinese).

[11] G. P. Li and X. Li, "Allocation mechanism of national key ecological function area's transfer paymen," *China Population, Resources and Environment*, vol. 24, no. 5, pp. 124–130, 2015 (Chinese).

[12] H. Lin, C. Wei, W. Dan, G. Guoli, and Z. Guosong, "Assessment on the changing conditions of ecosystems in key ecological function regions in China," *Chinese Journal of Applied Ecology*, vol. 26, no. 9, pp. 2758–2766, 2015 (Chinese).

[13] Q. Wang, P. Hou, F. Zhang, and C. Wang, "Integrated monitoring and assessment framework of regional ecosystem under the global climate change background," *Advances in Meteorology*, vol. 2014, Article ID 896453, 8 pages, 2014.

[14] J. Liu, H. Tian, M. Liu, D. Zhuang, J. M. Melillo, and Z. Zhang, "China's changing landscape during the 1990s: large-scale

land transformations estimated with satellite data," *Geophysical Research Letters*, vol. 32, no. 2, Article ID L02405, 2005.

[15] J. Y. Liu, M. L. Liu, X. Z. Deng, D. F. Zhuang, Z. X. Zhang, and D. Luo, "The land use and land cover change database and its relative studies in China," *Journal of Geographical Sciences*, vol. 12, no. 3, pp. 275–282, 2002.

[16] J. Y. Liu, M. L. Liu, H. Q. Tian et al., "Spatial and temporal patterns of China's cropland during 1990–2000: an analysis based on Landsat TM data," *Remote Sensing of Environment*, vol. 98, no. 4, pp. 442–456, 2005.

[17] J. Liu, W. Kuang, Z. Zhang et al., "Spatiotemporal characteristics, patterns, and causes of land-use changes in China since the late 1980s," *Journal of Geographical Sciences*, vol. 24, no. 2, pp. 195–210, 2014.

[18] A. Huete, K. Didan, T. Miura, E. P. Rodriguez, X. Gao, and L. G. Ferreira, "Overview of the radiometric and biophysical performance of the MODIS vegetation indices," *Remote Sensing of Environment*, vol. 83, no. 1-2, pp. 195–213, 2002.

[19] A. Savitzky and M. J. E. Golay, "Smoothing and differentiation of data by simplified least squares procedures," *Analytical Chemistry*, vol. 36, no. 8, pp. 1627–1639, 1964.

[20] J. Chen, P. Jönsson, M. Tamura, Z. Gu, B. Matsushita, and L. Eklundh, "A simple method for reconstructing a high-quality NDVI time-series data set based on the Savitzky-Golay filter," *Remote Sensing of Environment*, vol. 91, no. 3-4, pp. 332–344, 2004.

[21] R. J. Donohue, M. L. Roderick, and T. R. McVicar, "On the importance of including vegetation dynamics in Budyko's hydrological model," *Hydrology and Earth System Sciences*, vol. 11, no. 2, pp. 983–995, 2007.

[22] G. Sun, G. Y. Zhou, Z. Q. Zhang, X. H. Wei, S. G. McNulty, and J. M. Vose, "Potential water yield reduction due to forestation across China," *Journal of Hydrology*, vol. 328, no. 3-4, pp. 548–558, 2006.

[23] Q. Mu, F. A. Heinsch, M. Zhao, and S. W. Running, "Development of a global evapotranspiration algorithm based on MODIS and global meteorology data," *Remote Sensing of Environment*, vol. 111, no. 4, pp. 519–536, 2007.

[24] Q. Mu, M. Zhao, and S. W. Running, "Improvements to a MODIS global terrestrial evapotranspiration algorithm," *Remote Sensing of Environment*, vol. 115, no. 8, pp. 1781–1800, 2011.

[25] S. M. Liu, Z. W. Xu, Z. L. Zhu, Z. Z. Jia, and M. J. Zhu, "Measurements of evapotranspiration from eddy-covariance systems and large aperture scintillometers in the Hai River Basin, China," *Journal of Hydrology*, vol. 487, pp. 24–38, 2013.

[26] Y. Chen, J. Xia, S. Liang et al., "Comparison of satellite-based evapotranspiration models over terrestrial ecosystems in China," *Remote Sensing of Environment*, vol. 140, pp. 279–293, 2014.

[27] P. Hou, Q. Wang, G. Cao, C. Wang, Z. Zhan, and B. Yang, "Sensitivity analyses of different vegetations responding to climate change in inland river basin of China," *Journal of Geographical Sciences*, vol. 22, no. 3, pp. 387–406, 2012.

[28] P. Hou, Q. Wang, W. M. Shen, J. Zhai, H. M. Liu, and M. Yang, "Progress of integrated ecosystem assessment: concept, framework and challenges," *Geographical Research*, vol. 34, no. 10, pp. 1809–1823, 2015.

[29] J. Liu, X. Xu, and Q. Shao, "Grassland degradation in the 'Three-River Headwaters' region, qinghai province," *Journal of Geographical Sciences*, vol. 18, no. 3, pp. 259–273, 2008.

[30] J. Zhai, R. Liu, J. Liu, L. Huang, and Y. Qin, "Human-induced landcover changes drive a diminution of land surface albedo in the Loess Plateau (China)," *Remote Sensing*, vol. 7, no. 3, pp. 2926–2941, 2015.

Hindawi Publishing Corporation
Advances in Meteorology
Volume 2016, Article ID 9546380, 8 pages
http://dx.doi.org/10.1155/2016/9546380

Research Article

Variation of Main Phenophases in Phenological Calendar in East China and Their Response to Climate Change

Fengyi Zheng,[1,2] Zexing Tao,[1,2] Yachen Liu,[1,3] Yunjia Xu,[1,2] Junhu Dai,[1] and Quansheng Ge[1]

[1]*Key Laboratory of Land Surface Pattern and Simulation, Institute of Geographical Sciences and Natural Resources Research, Chinese Academy of Sciences, Beijing 100101, China*
[2]*University of Chinese Academy of Sciences, Beijing 100049, China*
[3]*School of Geography, Beijing Normal University, Beijing 100875, China*

Correspondence should be addressed to Junhu Dai; daijh@igsnrr.ac.cn and Quansheng Ge; geqs@igsnrr.ac.cn

Received 18 March 2016; Accepted 26 June 2016

Academic Editor: Gang Liu

Based on the phenological data from China Phenological Observation Network, we compiled the phenological calendars of 3 phenological observation stations (Shanghai, Nanjing, and Hefei) in East China for 1987–1996 and 2003–2012 according to the sequences of mean phenophases. We calculated the correlated coefficient and the root mean square error (RMSE) between phenophases and the beginning of meteorological seasons to determine the beginning date of phenological season. By comparing new phenological calendars with the old ones, we discussed the variation of phenophases and their responses to temperature. The conclusions are as follows. (1) The beginning dates of spring and summer advanced, while those of autumn and winter delayed. Thus, summers got longer and winters got shorter. (2) The beginning time of the four phenological seasons was advancing during 1987–1996, while it was delaying during 2003–2012. (3) Most spring and summer phenophases occur earlier and most autumn and winter phenophases occur later in 2003–2012 than in 1987–1996. (4) The beginning time of phenological seasons was significantly correlated with temperature. The phenological sensitivities to temperature ranged from −6.49 to −6.55 days/°C in spring, −3.65 to −5.02 days/°C in summer, 8.13 to 10.27 days/°C in autumn, and 4.76 to 10.00 days/°C in winter.

1. Introduction

Phenology is the study of periodic biological events affected by environment [1, 2]. Besides instrumental measurements, phenology can also reflect the impacts of climate change on the biological and physical systems independently [3] and is regarded as the fingerprints of global warming [4].

Phenological calendar is a specialized calendar recording the sequence of phenological events, which is defined as lists of the starting dates and selected statistics of the phenological phases, their duration, and the intervals between them [5]. The major usage of phenological calendars is to generate a graphically designed phenological spectrum and to study the mean values of records [6]. It is of important value to guide agricultural activities and tourism management [7, 8]. Phenological calendar can also provide a valuable database for dividing phenological seasons. As one of the effective ways to divide the seasons, phenological season is defined by the sequence of various phenophases in a year. The phenological season is objective to embody the seasonal alternations because phenological phenomena could indicate the changes in climate and environment [5, 6]. Wan [8, 9] set a standard to divide one year into 4 phenological seasons (spring, summer, autumn, and winter) and compiled the phenological calendar of the cities in China Phenological Observation Network (CPON) during 1963–1985. However, with climate warming, the timing of phenophases in recent years has evidently shifted [10, 11]. Therefore, it is necessary to compile new phenological calendars to reflect the phenological characters in different regions. To date, people have compiled new phenological calendars in Beijing and Harbin, China [12, 13], but the work in other regions was not reported. In addition, previous phenological studies mainly focused on phenological variation in temperate regions at middle and high latitudes and revealed that most of the spring phenophases advanced while phenophases in autumn

Table 1: Geographical information of the 3 phenological observation stations.

Station	Longitude (°E)	Latitude (°N)	Sea level (m)	Number of species	Number of phenophases
Shanghai	121.48	31.22	4	14	35
Nanjing	118.78	32.04	9	45	344
Hefei	117.25	31.83	30	20	136

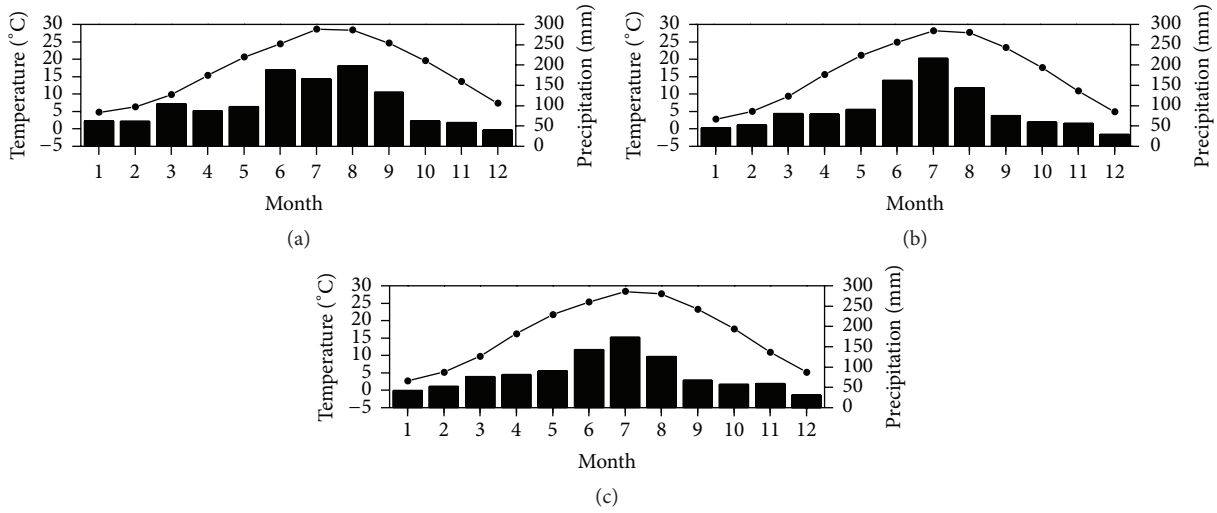

Figure 1: Annual mean temperature and average annual precipitation of the 3 stations (1987–2012). (a) Shanghai; (b) Nanjing; and (c) Hefei. The curves stand for monthly mean temperature, and the bars stand for monthly mean precipitation.

tended to delay in China [13–16] and other places in Northern Hemisphere [17–21]. Nevertheless, few of them discussed the timing and variations of phenology in subtropical areas. As a result, further studies are essential for the completion of the phenological calendar and better understanding of the climatic impact on vegetation phenology in these regions.

We conducted this study in East China, which is located at the margin of subtropical humid monsoon zone and temperate monsoon zone. In this region, phenological observations are organized by CPON since 1963, which provides sufficient data for phenological calendar compilation. Firstly, we used the phenological records from CPON in three representative stations, Shanghai, Nanjing, and Hefei, to compile the phenological calendars for 1987–1996 and 2003–2012. Secondly, we determined the beginning times of phenological seasons for each year and analyzed their trends for the two periods separately. Then, the differences of the mean phenophases between the two periods were calculated to discuss the phenological variations. Finally, we applied linear correlation analysis to study the climatic impacts on plant phenology. This study intends to provide theoretical and data basis for a better understanding of the biological response to regional climate change.

2. Materials and Methods

2.1. Study Area. The three stations are located in central of East China with typical subtropical climate and zonal vegetation of evergreen and deciduous broadleaved mixed forest and evergreen broadleaf forest [22]. The annual mean temperature is 19.1 to 20.3°C. Average annual precipitation is 1000.8 to 1259.3 mm. We selected three phenological observation stations in this area: Shanghai, Nanjing, and Hefei (Table 1), all located in the Middle-Lower Yangtze Plain. The phenological data of the 3 stations were the most complete among the stations in East China. The climate condition of the 3 stations could also represent the climate features of the study area (Figure 1).

2.2. Phenological and Meteorological Data. The phenological data in this paper were from China Phenological Observation Network (CPON), a nationwide system of phenological observation stations administered by the Institute of Geographic Sciences and Natural Resources Research (IGSNRR), Chinese Academy of Sciences. We divided the study period into two parts, 1987–1996 and 2003–2012, choosing 11 major phenophases, namely, bud expansion (BE), bud burst (BB), first flowering (FF), 50% of full flowering (50F), end of flowering (EF), first leaf (FL), 50% of full leaf expansion (50L), beginning of leaf coloring (BLC), end of leaf coloring (ELC), beginning of leaf fall (BLF), and end of leaf fall (ELF).

The meteorological data were from China Meteorological Administration (http://data.cma.cn/). We used the daily mean air temperature at the above-mentioned 3 stations from 1987 to 2012 to determine the beginning time of the four meteorological seasons and carry on linear correlation analysis between phenophases and temperatures.

2.3. Methods. Based on phenological data referred to above, we listed the phenophases of the 3 stations. For each station,

Table 2: Temperature standard for four meteorological seasons.

Season	Spring	Summer	Autumn	Winter
Standards	Above 3°C	Above 19°C	Below 19°C	Below 10°C

we selected phenophases with 3 or more observation records during each 10-year period and neglected the rest. Then, we calculated the mean dates of the selected phenophases and sorted them according to their sequence to compile the phenological calendars.

According to the division method proposed by Wan [8] (Table 2), we divided each year into 4 meteorological seasons. After 10 consecutive days in which the temperature reached the referential standard, we determined the first day of the 10 consecutive days as the beginning time of the season.

In order to decide the beginning time of the four phenological seasons, the correlated coefficients and the root mean square error (RMSE) between each phenophase and the beginning of corresponding meteorological season were calculated (see (1)), and the phenophases which had the maximum correlation coefficients and minimum RMSE value were chosen as the beginning time of the four phenological seasons:

$$\mathrm{RMSE} = \sqrt{\frac{1}{n}\sum_{i=\mathrm{YF}}^{\mathrm{YL}} \left(\mathrm{DP}_i - \mathrm{DM}_i\right)^2}. \quad (1)$$

In the equation, i, YF, YL, n, DP_i, and DM_i represent the year, the first year of calculation, the last year of calculation, the quantity of years with observation records, the date of phenophases in year i, and the beginning date of meteorological season in year i, respectively.

Subsequently, we compared the beginning time and its trend, as well as the length of the phenological seasons for the two periods.

After that, in order to verify whether the phenophases in spring and summer tended to advance and the phenophases in autumn and winter tended to delay, we calculated the differences between mean phenophases in phenological calendar for the two periods of each station.

Finally, linear correlation analysis between the beginning time of phenological season and the mean temperature in the previous 60 days during the whole period 1987–2012 was carried out to reveal the response of phenophases to climate change.

3. Results

3.1. The Beginning Time and Length of Phenological Seasons. By compiling phenological calendars (Appendix, in Supplementary Material available online at http://dx.doi.org/10.1155/2016/9546380) of the 3 stations, the beginning time of the four phenological seasons was determined. In all the three stations, spring and summer started earlier in 2003–2012 than in 1987–1996, with the beginning time of spring advancing by 3, 1, and 2 days and that of summer advancing by 5, 1, and 8 days in Shanghai, Nanjing, and Hefei, respectively (Table 3). However, autumn and winter in the three stations started later in the latter period than in the former period, and the beginning time of autumn delayed by 16 days, 2 days, and 1 day and that of winter delayed by 14, 3, and 16 days in Shanghai, Nanjing, and Hefei, respectively.

Regarding to the length of different seasons summarized from the two phenological calendars, it is learned that the length of all the four seasons changed regularly. Among them, spring shortened in Shanghai and Hefei, by 2 days and 6 days, respectively, but without so clear change in Nanjing. Summer lengthened in all the three sites, by 21, 3, and 9 days in Shanghai, Nanjing, and Hefei, respectively. Overall speaking, autumn lengthened in East China, but with regional differences. Autumn in Nanjing and Hefei lengthened by 1 and 15 days, respectively, while, in Shanghai, it shortened by 2 days. Winter became shorter in all the three sites, shortening by 17, 4, and 18 days in Shanghai, Nanjing, and Hefei, respectively.

3.2. Changing Trends of the Beginning of Phenological Seasons. Comparing the changing trend of the beginning time of each season during 1987–1996 to that during 2003–2012, we found out how the season beginning time had been changing (Figure 2).

In the phenological calendar of 1987–1996, the beginning time of spring advanced in Shanghai and Nanjing by 0.04 and 1.02 days/year, respectively, while it delayed in Hefei by 0.54 days/year, with an average advancing trend of 0.17 days/year (Figure 2(a), Table 4). Whereas, in phenological calendar of 2003–2012, beginning time of spring in all 3 stations delayed, by 0.67 days/year in Shanghai, 1.88 days/year in Nanjing, 2.98 days/year in Hefei, respectively, and 1.84 days/year on average.

Figure 2(b) presents that the beginning time of summer delayed in Shanghai by 0.45 days/year while it advanced in Nanjing by 0.99 days/year and that in Hefei delayed by 0.66 days/year and advanced by 0.40 days/year on average in 1987–1996, and it delayed in all 3 stations, by 0.40 days/year in Shanghai, 0.48 days/year in Nanjing, 0.69 days/year in Hefei, respectively, and 0.52 days/year on average in 2003–2012.

The changing trend of autumn beginning time was advancing in the 3 stations, by 1.17 days/year in Shanghai, 1.56 days/year in Nanjing, 2.96 days/year in Hefei, respectively, and 1.90 days/year on average in 1987–1996 (Figure 2(c)). The overall changing trend in 2003–2012 was 1.01 days/year, indicating a delayed autumn beginning in this period. Regarding the 3 stations, the beginning of autumn in Shanghai and Nanjing delayed by 2.19 and 1.06 days/year while it advanced in Hefei by 0.21 days/year.

Figure 2(d) shows that the winter beginning time advanced in Shanghai and Hefei by 0.54 and 1.82 days/year, respectively, and delayed in Nanjing by 1.32 days/year. On average, the beginning of winter advanced by 0.38 days/year in the phenological calendar of 1987–1996. During the period of 2003–2012, the beginning time of winter in all the 3 stations delayed, by 0.40 days/year in Shanghai, 0.48 days/year in Nanjing, and 0.69 days/year in Hefei, respectively, with an average changing trend of 0.52 days/year.

Table 3: Division of phenological seasons for 1987–1996 and 2003–2012.

Station	Season	Species	Phenophase	Beginning time (1987–1996)	Beginning time (2003–2012)	Season length (1987–1996)	Season length (2003–2012)
Shanghai	Spring	*Jasminum nudiflorum*	FF	43	40	78	76
	Summer	*Robinia pseudoacacia*	FF	121	116	153	174
	Autumn	*Platanus acerifolia*	BLF	274	290	64	62
	Winter	*Magnolia denudata*	ELF	338	352	70	53
Nanjing	Spring	*Salix babylonica*	FL	54	53	61	61
	Summer	*Robinia pseudoacacia*	FF	115	114	165	168
	Autumn	*Hibiscus syriacus*	EF	280	282	66	67
	Winter	*Pterocarya stenoptera*	ELF	346	349	73	69
Hefei	Spring	*Ulmus pumila*	FF	58	56	58	52
	Summer	*Robinia pseudoacacia*	FF	116	108	155	164
	Autumn	*Metasequoia glyptostroboides*	BLF	271	272	58	73
	Winter	*Pterocarya stenoptera*	ELF	329	345	94	76

Unit of beginning time: day of the year, DOY.

Table 4: Parameters of regression for phenological trends.

Season	Station	1987–1996			2003–2012		
		Slope (days/year)	R^2	P	Slope (days/year)	R^2	P
Spring	Shanghai	−0.04	0.01	0.97	0.67	0.09	0.46
	Nanjing	−1.02	0.08	0.46	1.88	0.65	0.05
	Hefei	0.54	0.04	0.59	2.98	0.46	0.05
Summer	Shanghai	0.45	0.14	0.32	0.40	0.11	0.35
	Nanjing	−0.99	0.20	0.23	0.48	0.20	0.26
	Hefei	−0.66	0.28	0.11	0.69	0.12	0.34
Autumn	Shanghai	−1.17	0.16	0.50	2.19	0.54	0.02
	Nanjing	−1.56	0.10	0.41	1.06	0.11	0.39
	Hefei	−2.96	0.22	0.29	−0.21	0.02	0.07
Winter	Shanghai	−0.54	0.04	0.56	1.70	0.65	0.01
	Nanjing	1.32	0.15	0.35	1.85	0.44	0.07
	Hefei	−1.82	0.16	0.25	0.21	0.01	0.88

3.3. Variations of Phenophases in Different Seasons. The frequency distribution of seasonal phenophases (Figure 3) can be used to explain the overall variation and characteristics of phenological seasons. At the 3 stations, the majority of phenophases in spring (83.3% in Shanghai, 72.8% in Nanjing, and 90.8% in Hefei) and summer (all in Shanghai, Nanjing, and Hefei) occurred earlier in 2003–2012 than in 1987–1996, while the majority of phenophases in autumn (87.5% in Shanghai, 77.1% in Nanjing, and 86.2% in Hefei) and winter (100% in Shanghai, 50% in Nanjing, and 83.3% in Hefei) occurred later in 2003–2012 than in 1987–1996. During the period of 2003–2012, phenophases averagely advanced by 7.6, 3.9, and 9.6 days in spring in Shanghai, Nanjing, and Hefei, respectively, compared to the spring phenophases during 1987–1996. Similar changes happened to phenophases in summer, showing by earlier occurrences of 8.1, 4.3, and 7.5 days averagely during 2003–2012 than during 1987–1996 in Shanghai, Nanjing, and Hefei, respectively.

Phenophases in autumn and winter all delayed averagely during the latter period compared to the former. Specifically, autumn phenophases delayed by 7.3, 6.6, and 13.2 days, and winter phenophases delayed by 19.5, 1.1, and 13.5 days on average in Shanghai, Nanjing, and Hefei, respectively. It is indicated that the overall variation of phenophases in each phenological season is similar to that of the beginning time of the corresponding season.

3.4. The Relationship between Phenological Changes and Temperature. Figure 4 exhibits correlations between the beginning of phenological seasons and 60-day preseason mean temperature. Notably, the beginning time of spring and summer shows significant negative correlation with temperature. The significance levels of correlations in Shanghai, Nanjing, and Hefei were $P < 0.01$, $P < 0.05$, and $P < 0.01$, respectively, for spring and all were $P < 0.01$ for summer. The beginning time of autumn and winter shows significant

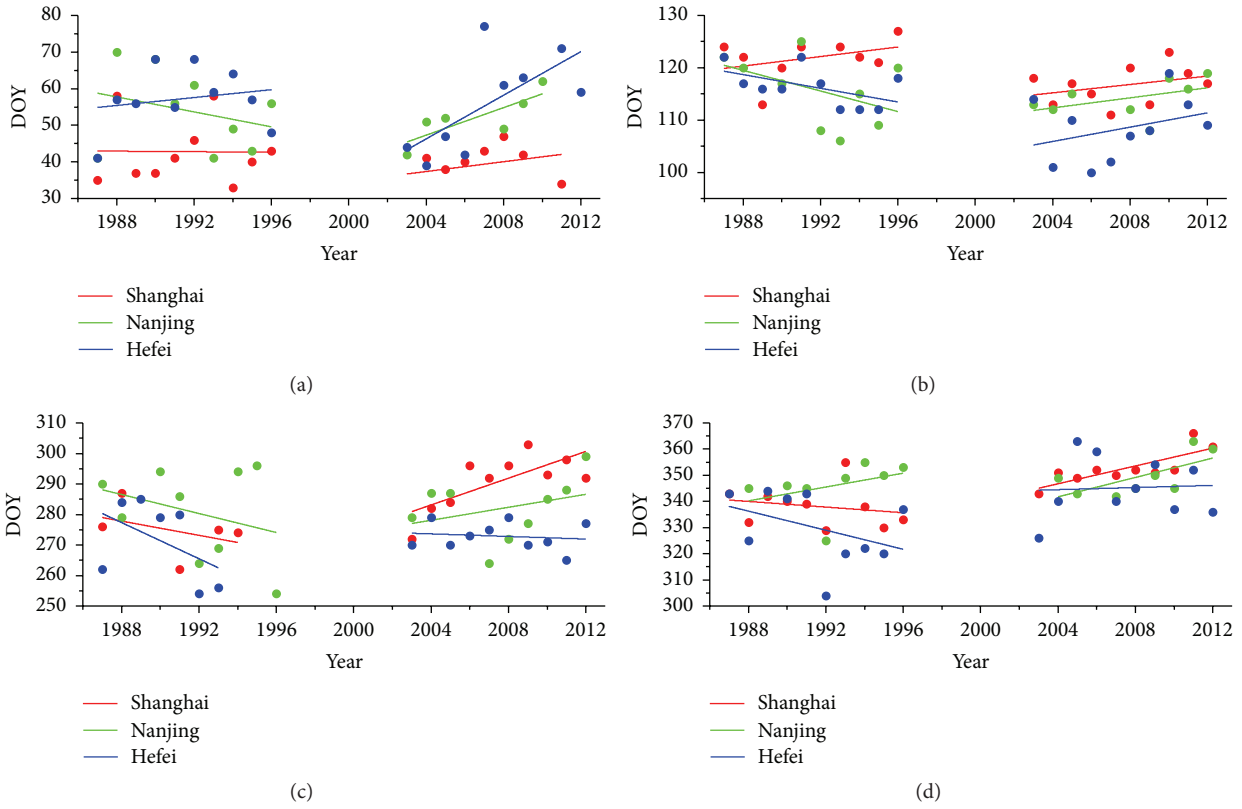

Figure 2: The changing trends in the beginning time of phenological seasons. (a) Spring; (b) summer; (c) autumn; and (d) winter. DOY: day of the year.

positive correlation with temperature. The significance levels of correlations in Shanghai, Nanjing, and Hefei were $P < 0.05$, $P < 0.05$, and $P < 0.001$, respectively, for autumn, and all were $P < 0.05$ for winter. That is, the increase in previous temperature will lead to an advance in spring and summer beginning time and a delay in autumn and winter beginning time and vice versa. The slopes of the linear regression, herein, represent the sensitivities of the beginning of phenological seasons to temperature. The sensitivities ranged from −6.49 to −6.55 days/°C in spring, −3.65 to −5.02 days/°C in summer, 8.13 to 10.27 days/°C in autumn, and 4.76 to 10.00 days/°C in winter.

4. Discussion and Conclusion

4.1. Discussion. The compilation of phenological calendars by applying phenological observation data from CPON was very unique in China. The systematical results were published in 1986 and 1987 [8, 9]. They were used for instruction in agricultural activities in the past by arranging cultivation times for crops and providing references for pest control [1]. This study developed a new approach in the application of phenological calendar in the field of climate changes. As phenological seasons defined by phenological calendar were with good geographical representation and described the relatively stable phenophases during a certain period of time and the sequence of these phenophases was usually put in regular order, they were of high significance when used in the comparison of phenophases between different time periods. Therefore, the phenophase changes in each season of a year during different time periods were indicated very evidently in this study. Besides, changes of length for phenological seasons together with the phenological sensitivities to temperature in different time period were also studied very sufficiently.

Another important finding of this study is that the spring phenological sensitivity to temperature was from −6.49 to −6.55 days/°C in East China. The result of a former study shows that the phenological sensitivities to temperature in Northeast China were between −1.99 and −6.18 days/°C, with an average of −3.00 days/°C [13], which was almost half of our result. It further demonstrated that the phenological sensitivities to temperature were greater at lower latitudes than those at higher latitudes [23, 24]. This discrepancy can be possibly explained by spring GDD (Growing Degree Days) Models [24]. Owing to the longer duration of heat accumulation, the plants in warmer areas receive greater extra heat accumulation than those in colder areas with the temperature increase by the same amount, and this leads to the plant phenophases more sensitive to temperature at lower latitudes.

This is the beginning of studying phenological changes in subtropical areas in China and such conclusions remain to be strengthened by further studies in the future.

4.2. Conclusion. With phenological data from China Phenological Observation Network of Chinese Academy of Sciences

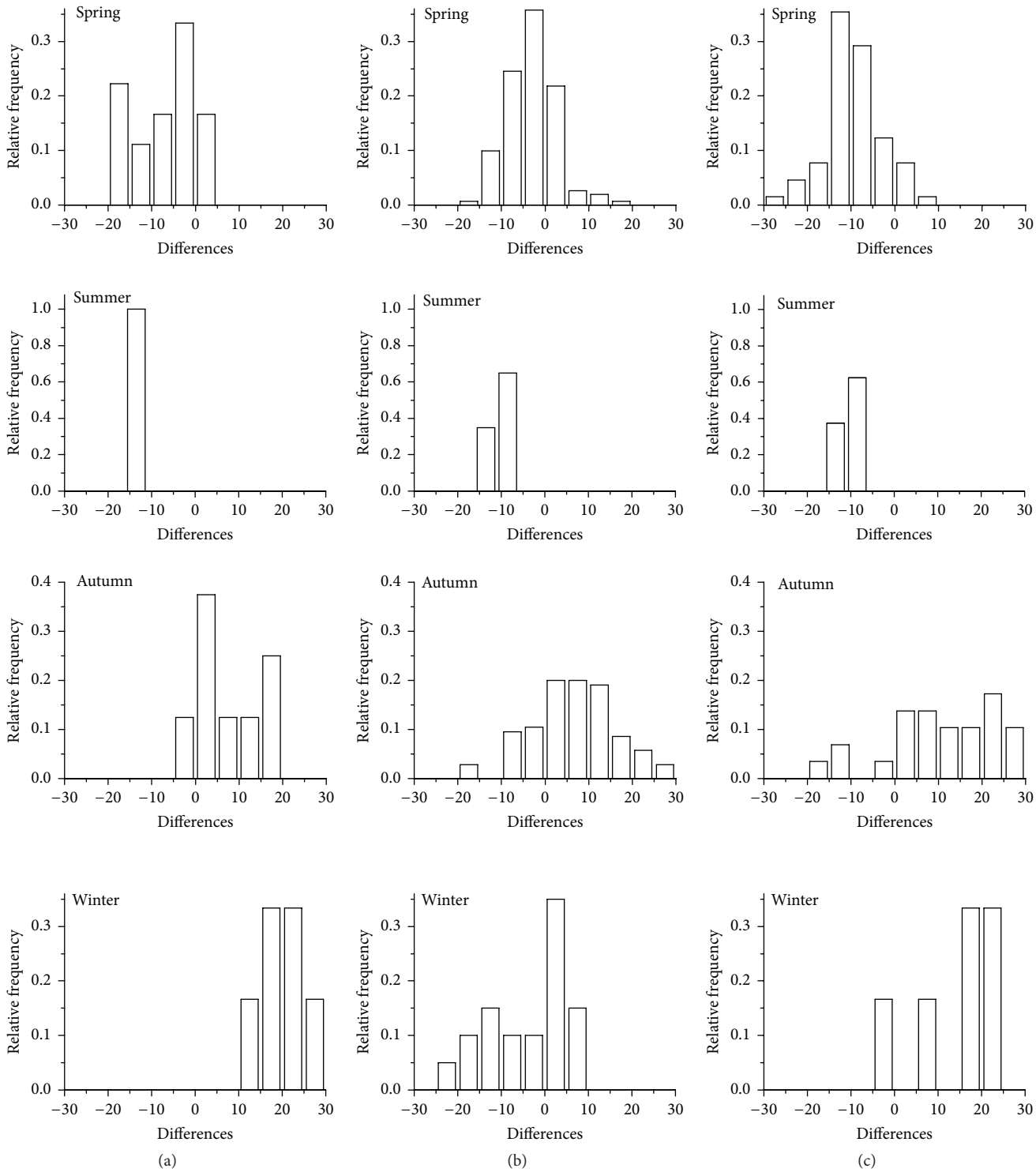

Figure 3: Frequency distribution of the differences in mean phenological dates between the phenological calendar of 1987–1996 and 2003–2012. The columns stand for Shanghai (a), Nanjing (b), and Hefei (c), respectively.

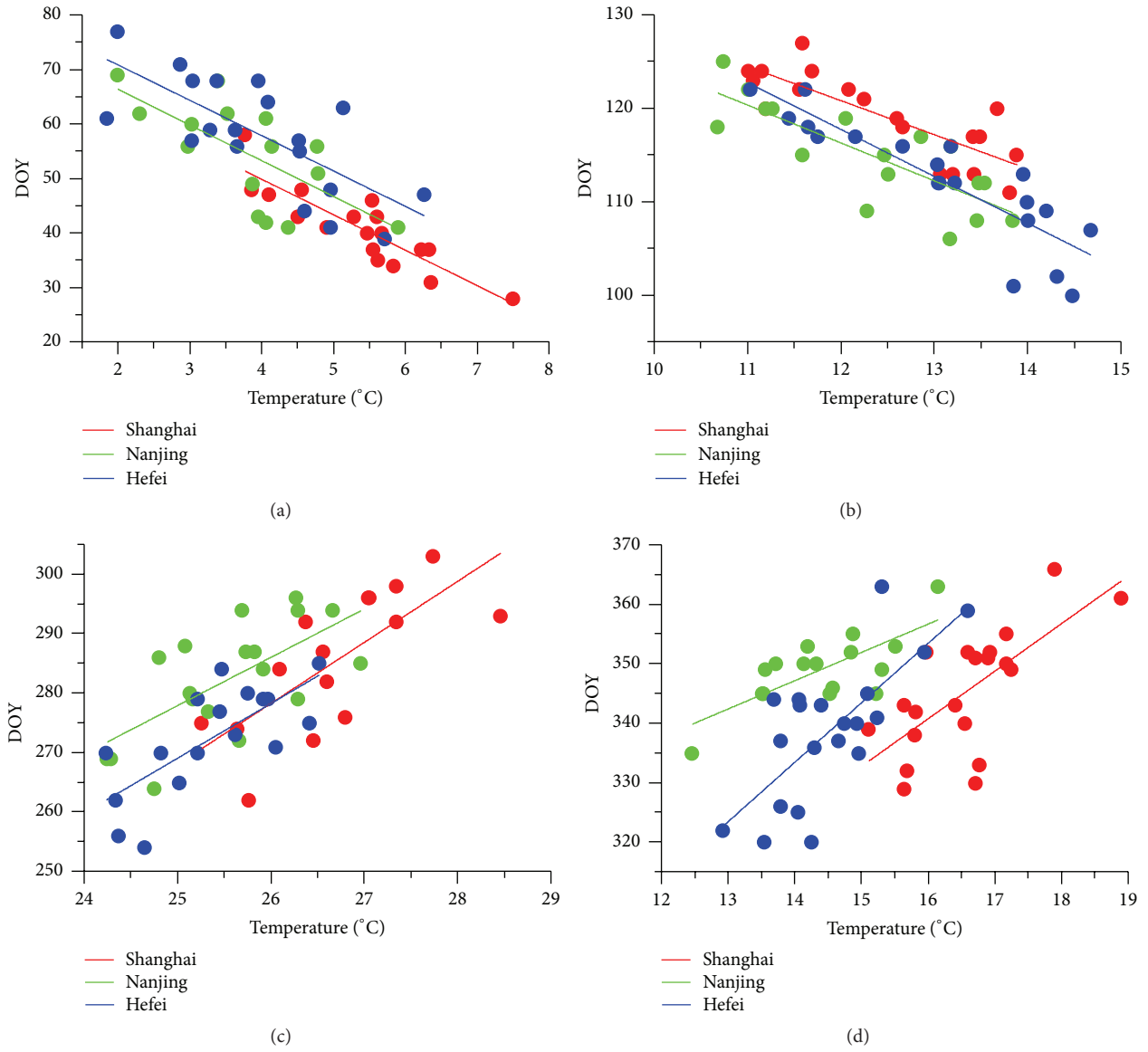

FIGURE 4: Linear correlation analysis between the beginning time of phenological season and the mean temperature of the previous 60 days in 1987–2012. (a) Spring, Shanghai: $y = -6.51x + 75.86$ ($R^2 = 0.77$, $P < 0.01$); Nanjing: $y = -6.55x + 79.45$ ($R^2 = 0.47$, $P < 0.05$); and Hefei: $y = -6.49x + 83.79$ ($R^2 = 0.53$, $P < 0.01$). (b) Summer, Shanghai: $y = -3.65x + 164.59$ ($R^2 = 0.67$, $P < 0.01$); Nanjing: $y = -4.06x + 164.94$ ($R^2 = 0.64$, $P < 0.01$); and Hefei: $y = -5.02x + 177.93$ ($R^2 = 0.77$, $P < 0.01$). (c) Autumn, Shanghai: $y = 10.27x + 11.22$ ($R^2 = 0.55$, $P < 0.05$); Nanjing: $y = 8.13x + 74.72$ ($R^2 = 0.44$, $P < 0.05$); and Hefei: $y = 9.22x + 38.44$ ($R^2 = 0.53$, $P < 0.001$). (d) Winter, Shanghai: $y = 8.00x + 212.65$ ($R^2 = 0.48$, $P < 0.05$); Nanjing: $y = 4.76x + 280.48$ ($R^2 = 0.54$, $P < 0.05$); and Hefei: $y = 10.00x + 193.34$ ($R^2 = 0.53$, $P < 0.05$).

and the meteorological data from China Meteorological Administration, this paper reveals the characteristics of variations between the phenological calendar for 2003–2012 and that for 1987–1996 and the response of phenophases to climate change. The conclusions are as follows:

(1) The beginning of spring and summer in East China was earlier and the beginning of autumn and winter was later in 2003–2012 than in 1987–1996. Summer lengthened by 21, 3, and 9 days, and winter shortened by 17, 4, 18, days, respectively, in Shanghai, Nanjing, and Hefei.

(2) The beginning time of all four seasons showed advancing trends of 0.17 days/year in spring, 0.40 days/year in summer, 1.90 days/year in autumn, and 0.38 days/year in winter during 1987–1996, while the beginning time of all four seasons showed delaying trends of 1.84 days/year in spring, 0.52 days/year in summer, 1.01 days/year in autumn, and 0.52 days/year in winter during 2003–2012.

(3) Most spring and summer phenophases occurred earlier and most autumn and winter phenophases occurred later during 2003–2012 than during 1987–1996, indicating that the advancing and delaying

of mean phenophases were in accordance with the change of the beginning time of the corresponding phenological season.

(4) The beginning time of spring and summer shows significant negative correlation with temperature, while the beginning time of autumn and winter shows significant positive correlation with temperature. The phenological sensitivities to temperature ranged from −6.49 to −6.55 days/°C in spring, −3.65 to −5.02 days/°C in summer, 8.13 to 10.27 days/°C in autumn, and 4.76 to 10.00 days/°C in winter.

Competing Interests

The authors declare that there is no conflict of interests regarding the publication of this paper.

Acknowledgments

This study is supported by National Key Basic Research Program of China (Grant no. 2012CB955304), Major National Research Program of Scientific Instruments from National Natural Science Foundation (Grant no. 41427805), and Strategic Priority Research Program of the Chinese Academy of Sciences (Grant no. XDA05090301).

References

[1] K. Z. Zhu and M. W. Wan, *Phenology*, Science Press, Beijing, China, 1973.

[2] M. D. Schwartz, *Phenology: An Integrative Environmental Science*, Kluwer Academic, Dordrecht, The Netherlands, 2013.

[3] F. Zwiers and G. Hegerl, "Climate change: attributing cause and effect," *Nature*, vol. 453, no. 7193, pp. 296–297, 2008.

[4] T. L. Root, J. T. Price, K. R. Hall, S. H. Schneider, C. Rosenzweig, and J. A. Pounds, "Fingerprints of global warming on wild animals and plants," *Nature*, vol. 421, no. 6918, pp. 57–60, 2003.

[5] R. Ahas, J. Jaagus, and A. Aasa, "The phenological calendar of Estonia and its correlation with mean air temperature," *International Journal of Biometeorology*, vol. 44, no. 4, pp. 159–166, 2000.

[6] A. Menzel, N. Estrella, and P. Fabian, "Spatial and temporal variability of the phenological seasons in Germany from 1951 to 1996," *Global Change Biology*, vol. 7, no. 6, pp. 657–666, 2001.

[7] G. D. Yang, *The Phenological Calendar of Beijing and Its Application*, Capital Normal University Press, Beijing, China, 1995.

[8] M. W. Wan, *Selected Phenological Calendars of China*, Science Press, Beijing, China, 1986.

[9] M. W. Wan, *Continuation of Phenological Calendars of China*, Science Press, Beijing, China, 1987.

[10] H. J. Wang, J. H. Dai, and Q. S. Ge, "The spatiotemporal characteristics of spring phenophase changes of *Fraxinus chinensis* in China from 1952 to 2007," *Science China Earth Sciences*, vol. 55, no. 6, pp. 991–1000, 2012.

[11] E. E. Cleland, I. Chuine, A. Menzel, H. A. Mooney, and M. D. Schwartz, "Shifting plant phenology in response to global change," *Trends in Ecology & Evolution*, vol. 22, no. 7, pp. 357–365, 2007.

[12] S. Y. Zhong, Q. S. Ge, J. Y. Zheng et al., "Variations of main phenophases of natural calendar and phenological seasons in Beijing for the last 30 years," *Chinese Journal of Plant Ecology*, vol. 36, no. 12, pp. 1217–1225, 2012.

[13] Y. J. Xu, J. H. Dai, H. J. Wang et al., "Variations of main phenophases of natural calendar and analysis of responses to climate change in Harbin in 1985–2012," *Geographical Research*, vol. 34, no. 9, pp. 1662–1674, 2015.

[14] X. Q. Fang and W. H. Yu, "Progress in the studies on the phenological responding to global warming," *Advance in Earth Sciences*, vol. 17, no. 5, pp. 714–719, 2002.

[15] Q. S. Ge, H. J. Wang, T. Rutishauser, and J. Dai, "Phenological response to climate change in China: a meta-analysis," *Global Change Biology*, vol. 21, no. 1, pp. 265–274, 2015.

[16] J. Dai, H. Wang, and Q. Ge, "Multiple phenological responses to climate change among 42 plant species in Xi'an, China," *International Journal of Biometeorology*, vol. 57, no. 5, pp. 749–758, 2013.

[17] D. W. Wolfe, M. D. Schwartz, A. N. Lakso, Y. Otsuki, R. M. Pool, and N. J. Shaulis, "Climate change and shifts in spring phenology of three horticultural woody perennials in northeastern USA," *International Journal of Biometeorology*, vol. 49, no. 5, pp. 303–309, 2005.

[18] A. Menzel, T. H. Sparks, N. Estrella et al., "European phenological response to climate change matches the warming pattern," *Global Change Biology*, vol. 12, no. 10, pp. 1969–1976, 2006.

[19] M. D. Schwartz, R. Ahas, and A. Aasa, "Onset of spring starting earlier across the Northern Hemisphere," *Global Change Biology*, vol. 12, no. 2, pp. 343–351, 2006.

[20] C. Defila and B. Clot, "Phytophenological trends in Switzerland," *International Journal of Biometeorology*, vol. 45, no. 4, pp. 203–207, 2001.

[21] C. Parmesan and G. Yohe, "A globally coherent fingerprint of climate change impacts across natural systems," *Nature*, vol. 421, no. 6918, pp. 37–42, 2003.

[22] J.-Y. Fang, Y.-C. Song, H.-Y. Liu, and S.-L. Piao, "Vegetation-climate relationship and its application in the division of vegetation zone in China," *Acta Botanica Sinica*, vol. 44, no. 9, pp. 1105–1122, 2002.

[23] Y. Y. Xie, P. L. Lu, and Q. Yu, "Sensitivity of leaf unfolding date for woody plant to temperature variability in spring in China's eastern monsoonal region," *Chinese Journal of Agrometeorology*, vol. 31, no. 4, pp. 495–500, 2010.

[24] J. H. Dai, H. J. Wang, and Q. S. Ge, "The spatial pattern of leaf phenology and its response to climate change in China," *International Journal of Biometeorology*, vol. 58, no. 4, pp. 521–528, 2014.

Hindawi Publishing Corporation
Advances in Meteorology
Volume 2016, Article ID 6809749, 10 pages
http://dx.doi.org/10.1155/2016/6809749

Research Article

Evapotranspiration Trend and Its Relationship with Precipitation over the Loess Plateau during the Last Three Decades

Zesu Yang,[1,2] Qiang Zhang,[2] and Xiaocui Hao[3]

[1] *Plateau Atmospheric and Environment Key Laboratory of Sichuan Province, College of Atmospheric Sciences, Chengdu University of Information Technology, Chengdu 610225, China*
[2] *Institute of Arid Meteorology, China Meteorological Administration, Key Laboratory of Arid Climatic Change and Reducing Disaster of Gansu Province, Key Open Laboratory of Arid Climatic Change and Disaster Reduction of CMA, Lanzhou 730020, China*
[3] *Northwest Regional Climate Center, Lanzhou 730020, China*

Correspondence should be addressed to Zesu Yang; zesuyang@outlook.com

Received 25 December 2015; Accepted 5 June 2016

Academic Editor: Gang Liu

There have been few studies conducted on the changes in actual ET over the Loess Plateau, due to the lack of reliable ET data. Based on ET data simulated by the Community Land Model, the present study analyzed the changes in ET over the Loess Plateau. The results showed the domain-average ET to have decreased in the past 31 years, at a rate of 0.78 mm year^{-1}. ET fluctuated much more strongly in the 1990s than in the 1980s and 2000s, and, apart from in autumn, ET decreased in all seasons. In particular, ET in summer comprised about half of the annual ET trend and had the sharpest trend, dominating the interannual decline. ET also decreased more sharply in the semiarid than semihumid regions. The declining trend of ET was attributed to declining precipitation and air humidity. Locally, the ET trend was closely related to local mean annual precipitation: in areas with precipitation less than 400 mm, ET showed a decreasing trend; in areas with precipitation larger than 600 mm, ET showed an increasing trend; and in areas with precipitation in the range of 400–600 mm could be classified as a transitional zone.

1. Introduction

Evapotranspiration (ET)—the process of transferring water from the land surface to the atmosphere—is the link between the global water cycle, energy cycle, and carbon cycle and is of critical importance for agriculture, hydrology, ecology, and the climate system [1, 2]. Changes in ET will also change the energy partitioning between sensible and latent heat, altering atmospheric dynamics and influencing weather and climate [3]. A detailed understanding of changes in global and regional ET could in turn help us to understand the global water cycle and its role in the climate system.

Against the background of increased air temperature associated with global warming, the atmosphere is able to hold more water, leading to increases in the fluxes of water globally via the water cycle [4]. Usually, the evidence put forward to support this conclusion involves increases in precipitation and runoff, but not ET trends, because the latter are very hard to observe. Potential ET—the upper limit of ET, indicative of evaporative ability—is relatively easy to obtain, plus, there are also some other variables that can represent evaporative ability, including pan evaporation and reference ET. Many studies have investigated trends of pan evaporation, potential ET, and reference ET regionally or globally. These trends, however, are not consistent among different regions of the globe. Theoretically, global warming would increase pan evaporation, but there are only a few regions where the evidence supports this inference, including Israel [5], northeast Brazil [6], Australia [7], and China [8]. In fact, most regions indicate an opposite conclusion, that is, a decrease in pan evaporation, for example, America [9, 10], Canada [11], Greece [12], India [13], Thailand [14], Japan [15], China [16, 17], Australia [18], and New Zealand [19]. Likewise, two studies on potential ET have also concluded opposite trends

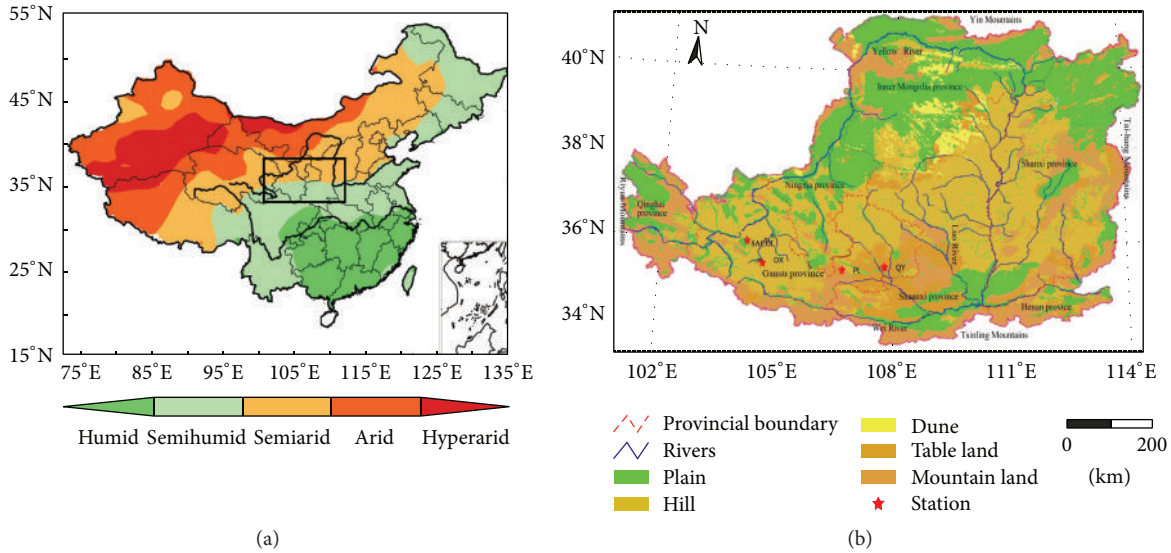

Figure 1: The (a) location and climate of the Loess Plateau (black line) and (b) its land cover and the locations of the ET observatories (red stars).

in different regions [20, 21]. Actual ET is closely related to potential ET or pan evaporation, but the implication of the trend in pan evaporation for the trend in actual ET has long been disputed. Some scientists argue that the declining trend in pan evaporation indicates a declining trend in actual ET. Others suggest that a complementary relationship between potential and actual ET exists, with declining ET meaning an increase in actual ET. Recent studies have shown that these two relationships are correct under certain conditions [17, 22, 23]. Apparently, the positive relationship is satisfied under conditions of sufficient water, while the complementary relationship is satisfied under water-limited conditions.

Potential ET is decreasing in most regions of China; however, pan evaporation and potential ET are increasing in the Loess Plateau [24, 25]. Since the trend of pan evaporation and potential ET only provides us with a clue for the possible trend of actual ET, and because potential ET and pan evaporation have a special trend in the Loess Plateau compared to other regions of China, our goal in the present study was to probe the characteristics of actual ET by examining whether the trend in actual ET in the Loess Plateau also shows distinct regional features, like potential ET. Besides, because the Loess Plateau is situated in the boundary zones influenced by the Asian summer monsoon, precipitation demonstrates considerable spatial variation [26], which in turn causes spatial variation in land surface hydrothermal processes. It is therefore also of interest to investigate the relationship between ET trends and precipitation on the local scale.

For a long time, research on actual ET has been limited by a lack of reliable ET data [1]. In recent years, however, the Global Land Data Assimilation System (GLDAS) has become an important dataset for global change and water cycle research [27, 28]. Employing the Community Land Model (CLM), GLDAS produces land surface ET data on the global scale, and its land surface variables are reported to be highly consistent with observations in the Loess Plateau [27]. In this study, we first validated the ET products of GLDAS using ET data observed by an eddy covariance (EC) system at four land surface observatories in the Loess Plateau. Then, on the basis of GLDAS ET data, we analyzed the trends of ET, and their reasons, over the Loess Plateau. In addition, the relationship between ET trends and mean annual precipitation locally was also analyzed.

2. Study Area and Data

2.1. Study Area. The Loess Plateau—located to the north of the Yin Mountains, south of the Tsinling Mountains, east of the Tai-hang Mountains, and west of the Riyue Mountains—is a highly unique land type with special ecosystems. The average altitude is approximately 1000 m above sea level, increasing from southeast to northwest. The most common topography is gully and hilly terrain, and the specific geomorphology is shown in Figure 1. The Loess Plateau is located in the boundary zone of the Asian summer monsoon. It is a transitional region from the humid climate in the southeast, under the influence of the summer monsoon, to the arid climate in the northwest (Figure 1, rectangle), and thus can be divided into two parts, that is, the semiarid zone in the northwest and the semihumid zone in the southeast [29] (Figure 1). The annual average rainfall is approximately 466 mm, with 700 mm in the southeastern regions and 120 mm in the northwestern regions. The mean annual temperature ranges from 4°C to 12°C. The main soil type is loess, which has a weak ability to resist wind and soil erosion.

2.2. Data and Data Processing

2.2.1. Simulated ET Data. The simulated ET data were downloaded from GLDAS. As the main dynamic framework, the land surface model is the key part of GLDAS. The forcing

Table 1: Information on the validation sites.

Site	Location	Elevation (m)	Land cover	Precipitation (mm)	Temperature (°C)	Climate
Dingxi	35°35′N, 104°37′E	1896	Cropland	386	6.7	Semiarid
SACOL	35°57′N, 104°08′E	1966	Grassland	381.8	6.7	Semiarid
Qingyang	35°41′N, 107°51′E	1280	Cropland	562	8.8	Semihumid
Pingliang	35°34′N, 106°35′E	1480	Cropland	511.2	8.7	Semihumid

data were provided by the Global Data Assimilation System of the National Centers for Environmental Prediction and the Data Assimilation System of the Goddard Space Flight Center. This study used monthly ET data simulated by the Community Land Model (CLM), with a horizontal resolution of 1° × 1°, from January 1982 to December 2013. A rectangular region of (34°–41°N, 101°–114°E), including the Loess Plateau, was selected. The simulation data can be obtained directly from the website of GLDAS: http://disc.sci.gsfc.nasa.gov/hydrology/data-holdings.

CLM was developed from three land models: the Land Surface Model of the National Center for Atmospheric Research; the land model of the Institute of Atmospheric Physics, Chinese Academy of Sciences land model; and the Biosphere-Atmosphere Transfer Scheme. As such, it has the best features of these three land models and offers improvements regarding certain parameterization schemes. CLM was developed as the land surface module of the Community Earth System Model and the Community Atmosphere Model. Land biogeophysical and hydrological processes are the main processes simulated by CLM, including (1) vegetation composition, structure, and phenology; (2) absorption, reflection, and transmittance of solar radiation; (3) absorption and emission of longwave radiation; (4) momentum, sensible heat (ground and canopy), and latent heat (ground evaporation, canopy evaporation, and transpiration) fluxes; (5) heat transfer in the soil and snow, including phase changes; (6) canopy hydrology (interception, throughfall, and drip); (7) snow hydrology (snow accumulation and melt, compaction, and water transfer between snow layers); (8) soil hydrology (surface runoff, infiltration, subsurface drainage, and redistribution of water within the column); (9) stomatal physiology and photosynthesis. When simulating latent heat flux, the equations used for the ET calculation are [30]

$$
\begin{aligned}
E &= E_v + E_g,\\
E_v &= -\rho_{\text{atm}} \frac{\left(q_s - q_{\text{sat}}{}^{T_v}\right)}{r_{\text{total}}},\\
E_g &= -\rho_{\text{atm}} \frac{\left(q_s - q_g\right)}{r'_{\text{aw}}},\\
\frac{1}{r_{\text{total}}} &= \frac{L^{\text{sun}}}{r_b + r_s^{\text{sun}}} + \frac{L^{\text{sha}}}{r_b + r_s^{\text{sha}}},\\
r_b &= \frac{1}{C_v}\left(\frac{U_*}{d_{\text{leaf}}}\right)^{-1/2},\\
r'_{\text{aw}} &= \frac{1}{C_s u^*},\\
\frac{1}{r_s} &= m\frac{A}{c_s}\frac{e_s}{e_i}P_{\text{atm}} + b,
\end{aligned}
\tag{1}
$$

where q_s is the specific humidity of the canopy roof; q_g is the specific humidity of the land surface; $q_{\text{sat}}{}^{T_v}$ is the humidity of the canopy; E_v is the vegetation transpiration; E_g is the evaporation; r_{total} is the total resistance to water vapor transfer from the canopy to the canopy air, including the leaf boundary resistance r_b and stomatal resistance r_s; r'_{aw} is the aerodynamic resistance to water vapor transfer between the ground and the canopy air; A is the photosynthesis; m is a parameter associated with atmospheric conditions and plant type; b is an empirical parameter; u^* is friction velocity; C_s is the turbulent transfer coefficient; L^{sun} and L^{sha} are the sunlit and shaded leaf area indices, respectively; r_s^{sun} and r_s^{sha} are the sunlit and shaded stomatal conductance, which can use the average absorbed photosynthetically active radiation for sunlit and shaded leaves, respectively; c_s is the CO_2 concentration at the leaf surface; e_s is the vapor pressure at the leaf surface; e_i is the saturation vapor pressure inside the leaf at the vegetation temperature; and P_{atm} is the atmospheric pressure.

2.2.2. In Situ ET Data. ET was measured by an EC (eddy covariance) system at four land surface observatories in the Loess Plateau (see Figure 1 and Table 1). The EC system included a three-dimensional ultrasonic anemometer (CSAT-3, Campbell, USA) and a quick response infrared analyzer (Li7500, Li-Cor, USA) and was set at a height of 2.5 m. The sampling frequency was 10 Hz. Latent heat flux was calculated by

$$
\text{LE} = \rho\lambda\overline{\omega' q'}, \tag{2}
$$

where LE is latent heat flux, ρ is air density, λ is the latent heat of vaporization, and ω' and q' are the fluctuations around the averages of vertical wind speed and specific humidity, respectively.

The data from the EC system were processed as follows [31]: first, quality control and gap filling: (i) half-hourly data from periods of sensor malfunction were deleted; (ii) half-hourly data within 1 h before or after rainfall were deleted; (iii) half-hourly data (x_i) were deleted when $x_i \geq (+4\delta)$ or $x_i \leq (-4\delta)$, where δ is standard deviation. On average, the datasets contained 18.9% missing or rejected ET data. Missing data were filled using a look-up table method [32]. For each

Table 2: Correlation statistics between predicted ET and observations at four sites in the Loess Plateau.

Site	Fitting coefficient	Correlation coefficient	Root-mean-square error (mm)	Relative error (%)
SACL	0.969	0.94	7.9	18.1
Dingxi	0.834	0.87	9.4	21.5
Pingliang	0.918	0.95	8.4	19.3
Qingyang	0.935	0.96	6.8	22.4

Correlation coefficients passed the significance test at all sites ($P < 0.01$).

study site, tables were created based on the four seasons. For each season, ET was classified by 20 R_n-classes × 35 VPD (R_n, net radiation; VPD, vapor pressure deficit). R_n consisted of 50 W m^{-2} intervals from −200 to 800 W m^{-2}. Similarly, VPD consisted of 0.15 kPa intervals ranging from 0 to 5.1, with a separate class for VPD = 0. Gaps with no mean assigned in the look-up tables were interpolated linearly. Tables of ET means and standard deviation were produced by the procedure. Thus, we filled the missing data by referring to the synchronous R_n and VPD. Then, half-hourly LE data were transformed to half-hourly ET. Finally, half-hourly ET data were aggregated to monthly ET.

Since energy disclosure is an inevitable problem for EC [33]. The energy closure ratio of ET across all sites was evaluated, and the results showed that the averaged energy closure ratio was 86.2%, which is superior to the typical energy closure ratio of EC measurements (15–30%) [34]. Thus, observed ET at the validation sites were considered reliable. Unaccounting for advection fluxes is one of the reasons for energy disclosure at EC sites. Another reason is that EC towers cannot capture the large eddies (with low frequency) associated with stationary secondary circulations that generate over tall canopies and heterogeneous landscapes [35–39].

2.2.3. Regional Climate Data. Climate data, including daily precipitation, temperature, air humidity, sunshine duration, and wind speed, were obtained from the National Climate Center, China. At the time of study, there were 106 meteorological stations across the Loess Plateau. These stations' climate data were aggregated to the monthly timescale to match that of the ET data. When analyzing the domain-average trend of these climate variables, we averaged them for the 106 stations.

2.2.4. Vegetation Index. Vegetation indices are radiometric measures of photosynthetically active radiation absorbed by chlorophyll in the green leaves of vegetation canopies and are therefore good surrogate measures of the physiologically functioning surface greenness level of a region. The latest version of the GIMMS NDVI (Global Inventory Modeling and Mapping Studies Normalized Difference Vegetation Index) dataset spans the period July 1981 to December 2013 and is termed NDVI3g (third-generation GIMMS NDVI from Advanced Very High Resolution Radiometer (AVHRR) sensors). The NDVI3g time series is an improved 8 km NDVI dataset produced from AVHRR instruments and can be downloaded from http://ecocast.arc.nasa.gov/data/pub/gimms/. This study used gridded NDVI data over the Loess Plateau for the period of January 1982 to December 2013. During data preprocessing, we spliced the images, transformed the projection, and extracted the study area (the Loess Plateau). The horizontal resolution of NDVI was set to 1°× 1°, to match the horizontal resolution of the ET data simulated by CLM, with the grid values interpolated by linear averages of the surrounding area.

2.3. Validation of GLDAS ET Product. A mismatch existed between the scales of the simulated and measured ET, which could have introduced uncertainty in the results. To date, an efficient way to overcome this problem remains elusive. However, *in situ* ET data can provide a reference for the simulated ET [40]. Given this, the ET produced by GLDAS was validated using the ET observed by the eddy covariance system at four sites in the Loess Plateau. Figure 2 compares the monthly CLM-simulated and measured ET at the four sites. It can be seen that the simulated ET was highly consistent with the measured ET at the four validation sites. As shown in Table 2, the fitting coefficient was close to 1, the average coefficient of determination (R^2) was about 0.87, the average root-mean-square error was about 8.12 mm, and the relative error was about 20.32%. The precision of remote sensing methods for estimating regional ET is within the range of 15–30% [1]. CLM produced ET that achieved an upper-middle level of precision, indicating that the CLM-simulated ET was reliable for the Loess Plateau.

3. Results and Discussion

3.1. Trends of Annual, Decadal, and Seasonal ET. Figure 3(a) shows the time series of domain-average annual ET over the Loess Plateau. It can be seen that ET decreased from 1982 to 2013 over the Loess Plateau, at a rate of 0.78 mm year^{-1}. The decreasing trend was weak before 1998 and then accelerated after 1998. The accelerated decrease in ET after 1998 may be related to severe drought caused by strong El Niño events in 1998 [41] and the temperature increase slowing down [27]. Figure 3(b) shows the time series of the ratio of ET to precipitation, which also shows an obvious decreasing trend. The decreasing trend implies that ET decreased more sharply than precipitation during the study period; water recycling from the land surface to the atmosphere was becoming weaker, as was the regional water cycle.

In terms of the interdecadal characteristics of changes in ET over the Loess Plateau (Table 3), ET decreased by 4.1 mm from the 1980s to the 1990s and then decreased more

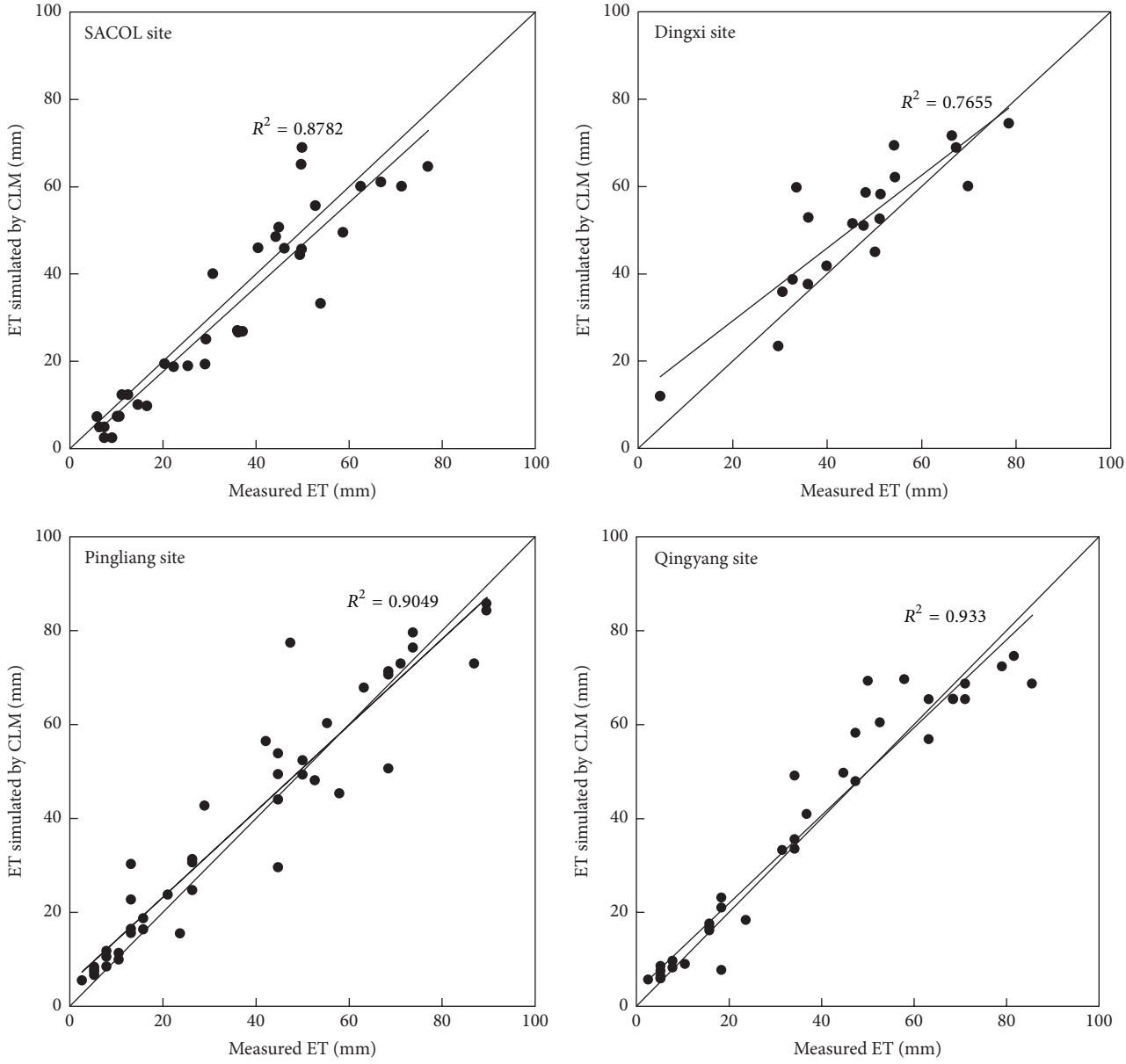

Figure 2: Comparison of simulated and observed ET at four sites (SACOL, Dingxi, Pingliang, and Qingyang) in the Loess Plateau.

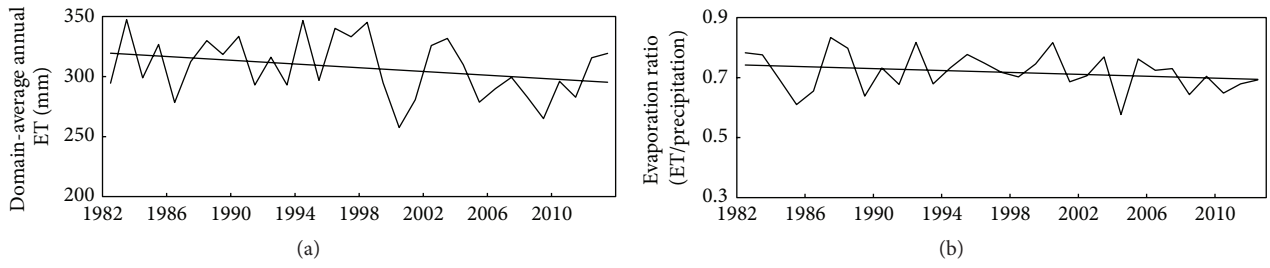

Figure 3: Trend of the (a) ET and (b) ET to precipitation ratio over the Loess Plateau during the period 1982–2013.

Table 3: Interdecadal characteristics of ET over the Loess Plateau.

Decade	Mean (mm)	Standard deviation (mm)
1980s	315.7	21.7
1990s	311.6	29.4
2000s	294.8	20.6

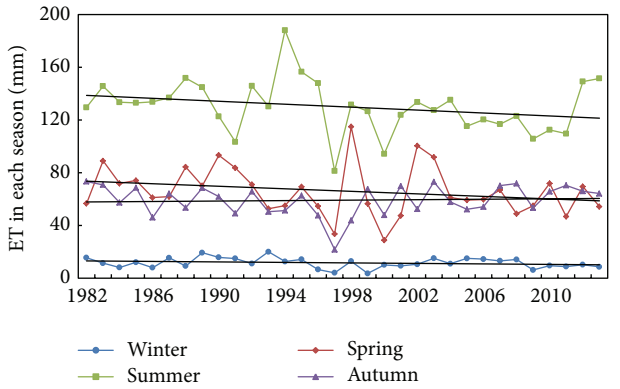

Figure 4: Trend of ET in each season over the Loess Plateau during 1982–2013.

rapidly from the 1990s to the 2000s (by 16.8 mm). Besides, the standard deviation for the 1990s was much larger than that of the 1980s and 2000s, implying that ET fluctuated abnormally strongly in the 1990s, which could have caused disturbance of the water cycle leading to drought [42].

The ET trend in each season and their contribution to the overall ET trend were also investigated (Figure 4). For each year, the seasonal ET was calculated by summing the monthly ET within the separate seasons. It can be seen that ET decreased in all seasons except autumn. Summer had the largest magnitude, accounting for around half of the annual ET. ET also decreased most rapidly during summer, at a rate of 0.43 mm year^{-1}. In spring, ET fluctuated strongly, especially around 1998, and had a relatively small rate of decrease. ET had a small mean and rate of decrease in winter, and in autumn, ET increased slightly but nonsignificantly. Overall, the summer trend dominated the declining ET trend over Loess Plateau.

3.2. Local ET Trend over the Loess Plateau. Although the domain-average ET decreased over the Loess Plateau during 1982–2013, it was possible that local ET trends may have differed due to the complicated topography and distinct features of local climate. Figure 5 shows the local ET trends over the Loess Plateau during the study period. As can be seen, ET decreased in most parts of the Loess Plateau, with the rate of decrease ranging from 1 to 3 mm year^{-1}. An ET increase was apparent in only a few parts of the Loess Plateau, with the rate of increase being less than 2 mm year^{-1} in most cases. This small increasing ET trend was dominated by the larger decreasing ET trend, meaning the domain-average ET showed an overall decreasing trend. The areas with an increasing ET trend were located in Tianshui District and the intersection of the Yellow River, Luo River, and Wei River, where there is a relatively high level of water availability.

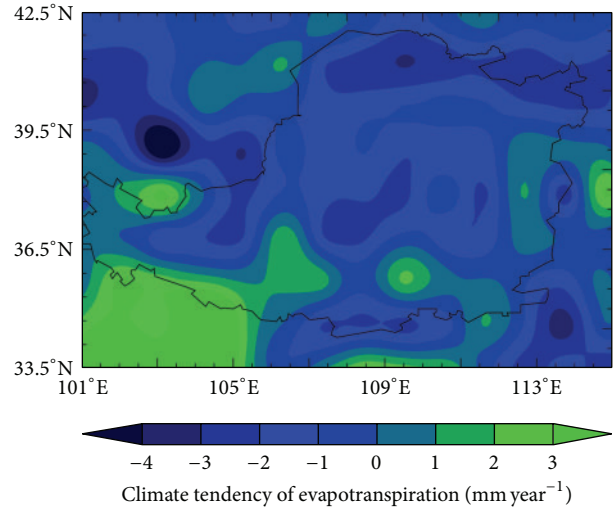

Figure 5: Distribution of the climate tendency of ET over the Loess Plateau.

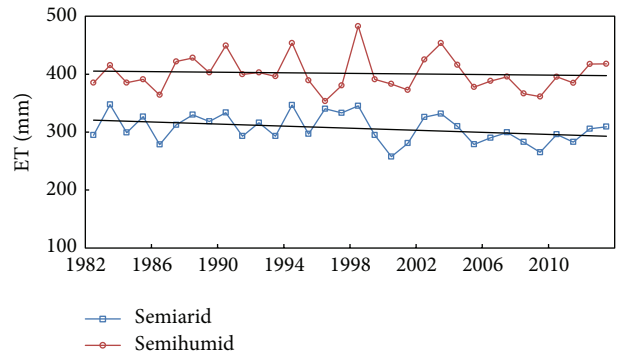

Figure 6: Trend of ET in the semiarid and semihumid areas of the Loess Plateau.

Figure 6 further breaks down the ET trend into that of the semiarid and that of semihumid region of the Loess Plateau. It can be seen that ET was much larger in the semihumid region than in the semiarid region. Furthermore, ET decreased more rapidly in the semiarid region than in the semihumid region, with their rates of decrease being 0.025 mm year^{-1} and 0.89 mm year^{-1}, respectively. A larger availability of water slowed the rate of decrease in the semihumid region.

3.3. Attribution of the ET Trend. To elucidate the factors causing the decreasing ET trend, we examined the temporal evolution and trends of annual precipitation, air humidity, temperature, sunshine duration, wind speed, and vegetation conditions. Annual precipitation and air humidity showed an obvious decreasing trend during the study period (Figures 7(a) and 7(b)), meaning that water availability was decreasing over the Loess Plateau. The trend in sunshine duration was not significant (Figure 7(c)). Temperature and wind speed showed marked increasing trend, indicating that the evaporation potential was increasing (Figures 7(d) and 7(e)). NDVI also increased (Figure 7(f)), which may have contributed to an increase in transpiration. These results indicate that

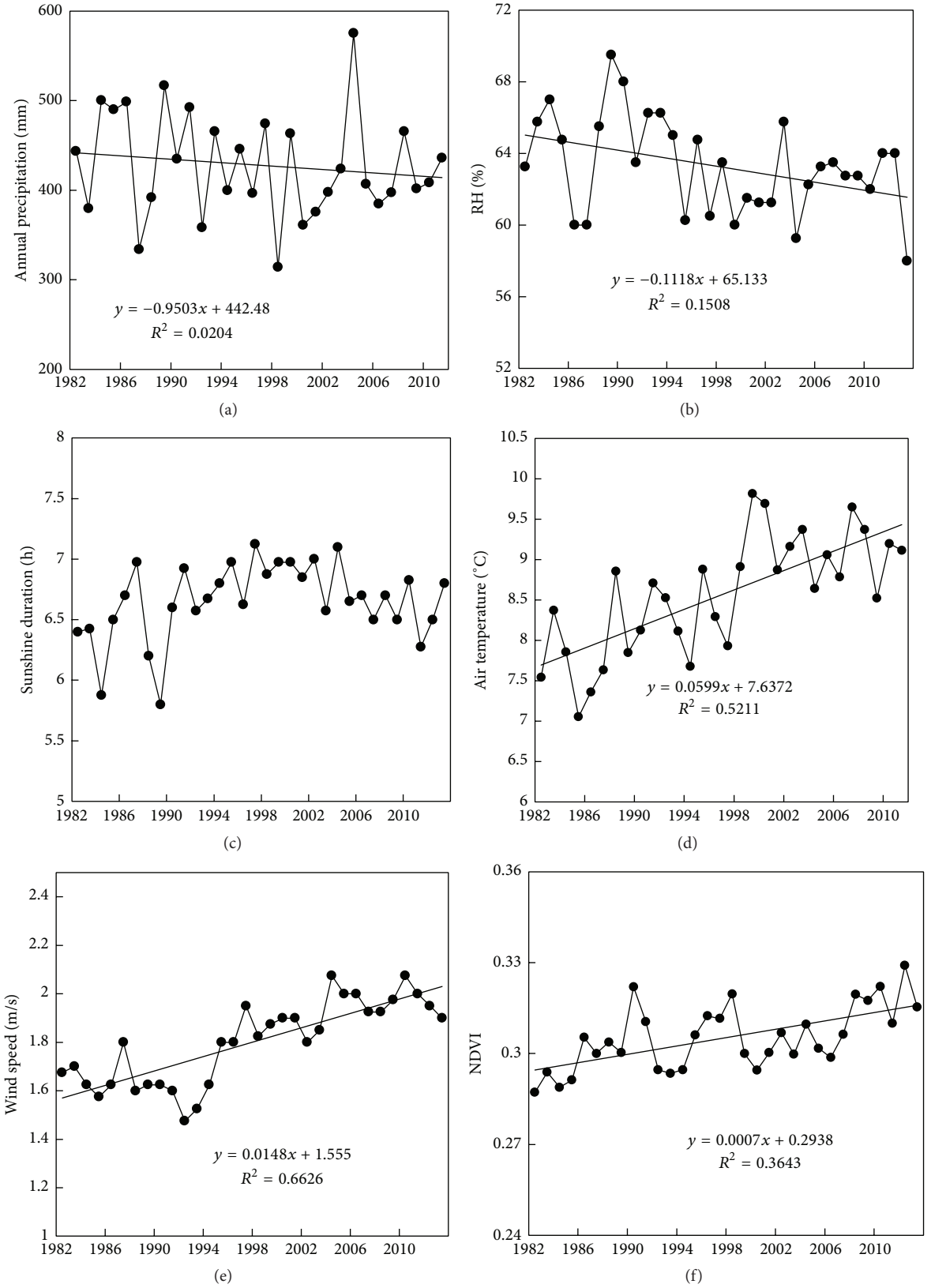

Figure 7: Trends of annual (a) precipitation, (b) air humidity, (c) sunshine duration, (d) air temperature, (e) wind speed, and (f) NDVI over the Loess Plateau.

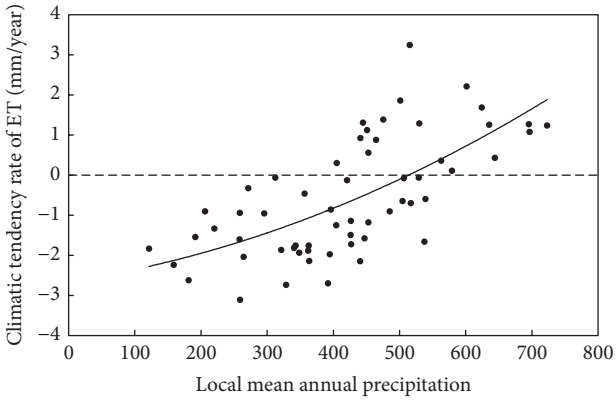

Figure 8: Relationship between the climate tendency rate of ET and local mean annual precipitation.

the declining trend in annual precipitation and air humidity caused the decreasing trend in ET, which outweighed the effects of increasing temperature, wind speed, and NDVI.

Increased potential ET [24, 25] and decreased actual ET imply that a complementary relationship between the two exists over the Loess Plateau. Similar research on different regions of China [17] showed that potential and actual ET were both controlled by available energy and both showed decreasing trends in humid and semihumid regions, while in arid and semiarid regions, potential ET was controlled by available energy and showed a decreasing trend, and actual ET was controlled by available water and showed an increasing trend. The Loess Plateau, however, shows an opposite ET trend compared to the arid and semiarid regions of China as a whole. The increasing ET trend in other arid and semiarid regions was attributed to increased precipitation, relative humidity, and cloud cover [43]. Our results showed that water availability, represented by precipitation and air humidity, was decreasing during the study period, which caused the decreasing trend of actual ET. In the study area, potential evapotranspiration (ET) is the upper limit of evapotranspiration when there is no water limit and represents the evaporative demand. Actual evapotranspiration is evapotranspiration mainly limited by the water supply of the area. Potential ET is higher than actual ET; it means that the ET demand is higher than the actual ET, indicating that precipitation cannot meet the ET demand and all precipitation (except run-off) transforms into ET, resulting in a better correlation between actual ET and precipitation.

3.4. Local ET Trends in Response to Mean Annual Precipitation. From the above analysis, it is apparent that water availability is the dominant factor controlling ET over the Loess Plateau. Therefore, the different local ET trends may be related to local water availability. Figure 8 shows the relationship between the climate tendency rate of local ET and mean annual precipitation. It can be seen that the climate tendency rate of local ET was closely related to local mean annual precipitation. The climate tendency rate of local ET changed from negative to positive when local mean annual precipitation increased. This implies that ET changed from being supply-limited to energy-limited due to increased water availability. The climate tendency rate was negative in supply-limited areas where local mean annual precipitation was less than 400 mm, because water supply was decreasing in these areas; it could be negative or positive in the transition zone where local mean annual precipitation was within the range 400–600 mm, and it was positive in energy-limited areas where local mean annual precipitation was greater than 600 mm, because the ET potential was increasing and water availability was sufficient in these areas. In the semiarid region, local mean annual precipitation was less than 400 mm, so the local climate tendency was negative and local ET showed a decreasing trend. In most of the semihumid region, local mean annual precipitation was within the range 400–600 mm, so the local climate tendency was either negative or positive and local ET showed a decreasing or increasing trend in different areas. For the intersection areas of the Yellow River, Luo River, and Wei River, local mean annual precipitation was greater than 600 mm, the local climate tendency rate was positive, and the local ET showed an increasing trend.

The strong solar radiation of the Loess Plateau means relatively high levels of available energy, and therefore the only limit for ET is the availability of water. An increase in water resources leads to changes in the climate tendency rate of ET from negative to positive, and this causes two opposing feedback mechanisms in the region. In areas with little precipitation (less than 400 mm), the decreasing ET contributes less moisture to the atmosphere and decreases precipitation locally, further intensifying aridity. In areas with large quantities of precipitation (greater than 600 mm), the increasing ET contributes more moisture to the atmosphere and increases precipitation locally, further intensifying humidity. These mechanisms are quite different from those in humid regions, where ET increases under low-precipitation conditions and decreases under high-precipitation conditions, due to available energy being reduced under high-precipitation conditions [44].

4. Conclusion

Based on CLM-simulated ET, the trend of ET was analyzed over the Loess Plateau from 1982 to 2013. The domain-average ET decreased during the study period, at a rate of 0.78 mm year^{-1}. In particular, the decreasing trend accelerated after 1998, with ET decreasing more from the 1990s to 2000s compared to the 1980s to 1990s. Stronger variation was also apparent for the 1990s, leading to an easier facilitation of drought. Apart from autumn, all seasons showed a decreasing trend, with summer dominating the interannual ET trend. Regionally, most of the Loess Plateau showed a decreasing ET trend, with only a few small areas showing an increasing trend (located in Tianshui District and the intersection areas of the Yellow River, Luo River, and Wei River). ET decreased more rapidly in the semiarid region than in the semihumid region. The declining trend of ET was attributed to declining precipitation and air humidity over the Loess Plateau during the study period. Local ET trends were closely

related to local mean annual precipitation. Areas with mean annual precipitation less than 400 mm showed decreasing ET trends; areas with mean annual precipitation larger than 600 mm showed increasing ET trends; and areas with mean annual precipitation within the range 400–600 mm were transitional. Overall, the decreasing trend of ET indicates local water cycling weakened over the Loess Plateau during the study period, causing an energy partitioning preference toward sensible heat rather than latent heat, which accelerated surface warming and intensified land-atmosphere interactions.

Competing Interests

The authors declare that they have no competing interests.

Acknowledgments

The CLM-simulated ET data were provided by GLDAS. This work was jointly supported by the Major National Basic Research Program of China 2013CB430200 (2013CB430206), the National Science Foundation of China (31300376), and the Postdoctoral Science Foundation of China (2012M512044).

References

[1] K. Wang and R. E. Dickinson, "A review of global terrestrial evapotranspiration: observation, modeling, climatology, and climatic variability," *Reviews of Geophysics*, vol. 50, no. 2, Article ID RG2005, 2012.

[2] Y. Huang, D. Jiang, D. Zhuang, Y. Zhu, and J. Fu, "An improved approach for modeling spatial distribution of water use profit—a case study in Tuhai Majia Basin, China," *Ecological Indicators*, vol. 36, pp. 94–99, 2014.

[3] K. E. Trenberth, J. T. Fasullo, and J. Kiehl, "Earth's global energy budget," *Bulletin of the American Meteorological Society*, vol. 90, no. 3, pp. 311–323, 2009.

[4] P. J. Durack, S. E. Wijffels, and R. J. Matear, "Ocean salinities reveal strong global water cycle intensification during 1950 to 2000," *Science*, vol. 336, no. 6080, pp. 455–458, 2012.

[5] S. Cohen, A. Ianetz, and G. Stanhill, "Evaporative climate changes at Bet Dagan, Israel, 1964–1998," *Agricultural and Forest Meteorology*, vol. 111, no. 2, pp. 83–91, 2002.

[6] V. D. P. R. Da Silva, "On climate variability in Northeast of Brazil," *Journal of Arid Environments*, vol. 58, no. 4, pp. 575–596, 2004.

[7] D. G. C. Kirono, R. N. Jones, and H. A. Cleugh, "Pan-evaporation measurements and Morton-point potential evaporation estimates in Australia: are their trends the same?" *International Journal of Climatology*, vol. 29, no. 5, pp. 711–718, 2009.

[8] J. Q. Xu, S. Haginoya, K. Saito, and K. Motoya, "Surface heat balance and pan evaporation trends in Eastern Asia in the period 1971–2000," *Hydrological Processes*, vol. 19, no. 11, pp. 2161–2186, 2005.

[9] M. L. Roderick and G. D. Farquhar, "The cause of decreased pan evaporation over the past 50 years," *Science*, vol. 298, no. 5597, pp. 1410–1411, 2002.

[10] M. T. Hobbins, J. A. Ramírez, and T. C. Brown, "Trends in pan evaporation and actual evapotranspiration across the conterminous U.S.: paradoxical or complementary?" *Geophysical Research Letters*, vol. 31, no. 13, Article ID L13503, 2004.

[11] D. H. Burn and N. M. Hesch, "Trends in evaporation for the Canadian Prairies," *Journal of Hydrology*, vol. 336, no. 1-2, pp. 61–73, 2007.

[12] G. Papaioannou, G. Kitsara, and N. Melanitis, "Temporal analysis of hydrometeorological characteristics in Crete," in *Proceedings of the Symposium on Water Resources Management: New Approaches and Technologies (EWRA '07)*, Chania, Greece, 2007.

[13] N. Chattopadhyay and M. Hulme, "Evaporation and potential evapotranspiration in India under conditions of recent and future climate change," *Agricultural and Forest Meteorology*, vol. 87, no. 1, pp. 55–73, 1997.

[14] T. Tebakari, J. Yoshitani, and C. Suvanpimol, "Time-space trend analysis in pan evaporation over Kingdom of Thailand," *Journal of Hydrologic Engineering*, vol. 10, no. 3, pp. 205–215, 2005.

[15] J. Asanuma and H. Kamimera, "Long-term trend of pan evaporation measurements in Japan and its relevance to the variability of the hydro-logical cycle," in *Proceedings of the Symposium on Water Resource and its Variability in Asia*, Meteorological Research Institute, Tsukuba, Japan, March 2004.

[16] H.-C. Zuo, Y. Bao, C.-J. Zhang, and Y.-Q. Hu, "An analytic and numerical study on the physical meaning of pan evaporation and its trend in recent 40 years," *Chinese Journal of Geophysics*, vol. 49, no. 3, pp. 680–688, 2006.

[17] B. Liu, Z. N. Xiao, and Z. G. Ma, "Relationship between pan evaporation and actual evaporation in different humid and arid regions of China," *Plateau Meteorology*, vol. 29, no. 3, pp. 629–636, 2010.

[18] M. L. Roderick and G. D. Farquhar, "Changes in Australian pan evaporation from 1970 to 2002," *International Journal of Climatology*, vol. 24, no. 9, pp. 1077–1090, 2004.

[19] M. L. Roderick and G. D. Farquhar, "Changes in New Zealand pan evaporation since the 1970s," *International Journal of Climatology*, vol. 25, no. 15, pp. 2031–2039, 2005.

[20] W. Abtew, J. Obeysekera, and N. Iricanin, "Pan evaporation and potential evapotranspiration trends in South Florida," *Hydrological Processes*, vol. 25, no. 6, pp. 958–969, 2011.

[21] X. F. Qiu, Y. Zeng, and Q. L. Miu, "Calculating land surface actual evapotranspiration using Conventional meteorological data," *Science in China, Series D-Earth Sciences*, vol. 33, no. 3, pp. 281–288, 2004.

[22] A. J. Teuling, M. Hirschi, A. Ohmura et al., "A regional perspective on trends in continental evaporation," *Geophysical Research Letters*, vol. 36, no. 2, Article ID L02404, 2009.

[23] Y. J. Wang, B. Liu, and J. Q. Zhai, "Relationship between potential and actual evaporation in Yangtze River Basin," *Advances in Climate Change Research*, vol. 7, no. 6, pp. 393–399, 2011.

[24] X. Q. Xie and L. Wang, "Changes of potential evaporation in Northern China over the past 50 years," *Journal of Nature Resources*, vol. 22, no. 5, pp. 683–691, 2007.

[25] Z. Li, "Spatiotemporal variations in the reference crop evapotranspiration on the Loess Plateau during 1961–2009," *Acta Ecologica Sinica*, vol. 32, no. 13, pp. 4139–4145, 2012.

[26] S. Lin and Y. R. Wang, "Spatial-temporal evolution of precipitation in China loess plateau," *Journal of Desert Research*, vol. 27, no. 3, pp. 502–508, 2007.

[27] Q. Zhang, J. Huang, L. Zhang, and L. Y. Zhang, "Warming and drying climate over Loess plateau area in China and its effect on land surface energy exchange," *Acta Physica Sinica*, vol. 62, no. 13, Article ID 019202, 2013.

[28] W. Wang, X. J. Wang, and P. Wang, "Assessing the applicability of GLDAS monthly precipitation data in China," *Advances in Water Science*, vol. 25, no. 6, pp. 769–778, 2014.

[29] J. Y. Zheng, Y. H. Yin, and B. Y. Li, "A new scheme for climate regionalization in China," *Acta Geographica Sinica*, vol. 65, no. 1, pp. 3–13, 2010.

[30] K. W. Oleson, Y. Dai, G. Bonan, M. Bosilovich, R. Dickson, and P. Dirmeyer, *Technical Description of the Community Land Model (CLM)*, 2004.

[31] S. M. Liu, Z. W. Xu, Z. L. Zhu, Z. Z. Jia, and M. J. Zhu, "Measurements of evapotranspiration from eddy-covariance systems and large aperture scintillometers in the Hai River Basin, China," *Journal of Hydrology*, vol. 487, pp. 24–38, 2013.

[32] E. Falge, D. Baldocchi, R. Olson et al., "Gap filling strategies for long term energy flux data sets," *Agricultural and Forest Meteorology*, vol. 107, no. 1, pp. 71–77, 2001.

[33] S. M. Liu, Z. W. Xu, W. Z. Wang et al., "A comparison of eddy-covariance and large aperture scintillometer measurements with respect to the energy balance closure problem," *Hydrology and Earth System Sciences*, vol. 15, no. 4, pp. 1291–1306, 2011.

[34] T. Foken, "The energy balance closure problem: an overview," *Ecological Applications*, vol. 18, no. 6, pp. 1351–1367, 2008.

[35] M. Mauder, T. Foken, R. Clement et al., "Quality control of CarboEurope flux data—part 2: inter-comparison of eddy-covariance software," *Biogeosciences*, vol. 5, no. 2, pp. 451–462, 2008.

[36] T. Foken, R. Leuning, S. R. Oncley, M. Mauder, and M. Aubinet, "Corrections and data quality control," in *Eddy Covariance.*, M. Aubinet, T. Vesala, and D. Papale, Eds., pp. 85–131, Springer, Berlin, Germany, 2012.

[37] J. Cuxart, L. Conangla, and M. A. Jiménez, "Evaluation of the surface energy budget equation with experimental data and the ECMWF model in the Ebro Valley," *Journal of Geophysical Research D: Atmospheres*, vol. 120, no. 3, pp. 1008–1022, 2015.

[38] J. Cuxart, B. Wrenger, D. Martínez-Villagrasa et al., "Estimation of the advection effects induced by surface heterogeneities in the surface energy budget," *Atmospheric Chemistry and Physics Discussions*, vol. 2016, pp. 1–16, 2016.

[39] Z. Gao, H. Liu, E. S. Russell, J. Huang, T. Foken, and S. P. Oncley, "Large eddies modulating flux convergence and divergence in a disturbed unstable atmospheric surface layer," *Journal of Geophysical Research: Atmospheres*, vol. 121, no. 4, pp. 1475–1492, 2016.

[40] Q. P. Liu, Y. C. Yang, H. Z. Tian, B. Zhang, and L. Gu, "Assessment of human impacts on vegetation in built-up areas in China based on AVHRR, MODIS and DMSP_OLS nighttime light data, 1992–2010," *Chinese Geographical Science*, vol. 24, no. 2, pp. 231–244, 2014.

[41] M. Jung, M. Reichstein, P. Ciais et al., "Recent decline in the global land evapotranspiration trend due to limited moisture supply," *Nature*, vol. 467, no. 7318, pp. 951–954, 2010.

[42] D. Li, "Assessing the impact of interannual variability of precipitation and potential evaporation on evapotranspiration," *Advances in Water Resources*, vol. 70, pp. 1–11, 2014.

[43] B. Liu, Z. Ma, J. Feng, and R. Wei, "The relationship between pan evaporation and actual evapotranspiration in Xinjiang since 1960," *Acta Geographica Sinica*, vol. 63, no. 11, pp. 1131–1139, 2008.

[44] Y. Song, Y. Ryu, and S. Jeon, "Interannual variability of regional evapotranspiration under precipitation extremes: a case study of the Youngsan River basin in Korea," *Journal of Hydrology*, vol. 519, pp. 3531–3540, 2014.

Hindawi Publishing Corporation
Advances in Meteorology
Volume 2016, Article ID 4629235, 13 pages
http://dx.doi.org/10.1155/2016/4629235

Research Article

Statistics and Analysis of the Relations between Rainstorm Floods and Earthquakes

Baodeng Hou,[1] Yongxiang Wu,[2] Jianhua Wang,[1] Kai Wu,[2] and Weihua Xiao[1]

[1] *China Institute of Water Resources and Hydropower Research, State Key Laboratory of Simulation and Regulation of Water Cycle in River Basin, Beijing 100038, China*
[2] *Nanjing Hydraulic Research Institute, State Key Laboratory of Hydrology-Water Resources and Hydraulic Engineering, Nanjing 210029, China*

Correspondence should be addressed to Jianhua Wang; jhwangiwhr@126.com

Received 13 November 2015; Revised 21 February 2016; Accepted 4 April 2016

Academic Editor: Paolo Madonia

The frequent occurrence of geophysical disasters under climate change has drawn Chinese scholars to pay their attention to disaster relations. If the occurrence sequence of disasters could be identified, long-term disaster forecast could be realized. Based on the Earth Degassing Effect (EDE) which is valid, this paper took the magnitude, epicenter, and occurrence time of the earthquake, as well as the epicenter and occurrence time of the rainstorm floods as basic factors to establish an integrated model to study the correlation between rainstorm floods and earthquakes. 2461 severe earthquakes occurred in China or within 3000 km from China and the 169 heavy rainstorm floods occurred in China over the past 200+ years as the input data of the model. The computational results showed that although most of the rainstorm floods have nothing to do with the severe earthquakes from a statistical perspective, some floods might relate to earthquakes. This is especially true when the earthquakes happen in the vapor transmission zone where rainstorms lead to abundant water vapors. In this regard, earthquakes are more likely to cause big rainstorm floods. However, many cases of rainstorm floods could be found after severe earthquakes with a large extent of uncertainty.

1. Introduction

The Global Climate Change led to the frequent hazards like flood and draught; meanwhile, it also exerted a certain impact on geological hazards like earthquake [1, 2]. The related research concluded that the earthquake had a certain impact on the climate change [3]. China is one of the countries with the most types of natural calamities in the world. Occurrence of natural calamities will lead to certain losses of human lives and damage to our living environment. In particular, concentrated or successive occurrence of such severe disasters within a short period of time may result in even greater harms to personal safety and social and economic fortunes [4].

Frequent occurrence of rainstorm flood, drought, earthquake, and other natural disasters has driven the rapid development of some emerging sciences, for example, geosystemics [5] and disaster physics [6]. The researches on the disaster chain (DC) [7] are also gradually deepening; for example, geophysical disaster chain (GDC) has been rapidly developed in recent years [8]. GDC as a new transdisciplinary science primarily studies such disaster chains as earthquake and flood, drought and earthquake, earthquake and typhoon, earthquake and desertification/sand storm, and earthquake and cold wave as well as air pollution and lightning, wherein the chains of earthquake and flood, flood and earthquake, and drought and earthquake as well as earthquake and drought have major impacts on people's daily life and urban development and therefore have become a focus of relevant experts and scholars.

But few people study GDC out of China. GDC was first put forward by three academics in China named Z. J. Guo, A. N. Guo, and K. X. Zhou. Y. Q. Wang, Q. Hou, L. T. Du, J. G. Gao, and Q. G. Geng also studied it. They defined DC as a phenomenon of different kinds of significant disasters occurring in the neighborhood or remote areas within a certain period and believe that GDC is a member of DC, which can lead to large disaster, so the most attention was

paid to it. At present, the studies mainly focused on the definition of DC, formation mechanism and characteristics, damage assessment, risk assessment, and integrated disaster reduction countermeasures [9–11].

Whether DC or GDC, the key lies in the "Chain," namely, whether the relationships among these disasters existed, whether these disasters will be able to form a "Chain," and whether to produce "Chain Reaction" [12] or "Catastrophe" [13–16], thus leading to greater disasters. As the "Butterfly Effect" [17] implies, there may be significant relationships among some seemingly unrelated things. There are many complicated trigger factors of these geophysical disasters, such as earthquakes, rainstorm floods, droughts, and typhoons. Each factor appears to be independent, but some small relationship may exist among them, and then they influence each other to form a "Chain Reaction." Now that the "Chain Reaction" does exist, it will always be repeated and present some regularity. This paper was studied based on this fact to explore the regularity between the successively occurred rainstorm floods and earthquakes.

It is well known that earthquake can be induced by external factors. Fluid injection in the subsurface can generate earthquake. Some examples are the KTB site-1994 in Germany [18], Soultz-2000 in France [19], or Basel-2006 in Switzerland [20]. It is noteworthy that injection of fluids, such as magma or water, can initiate seismic swarms: for example, reservoir (or large artificial lake) induced earthquake [21], water table changes or stream discharge connected with microearthquake [22], intraplate earthquake swarms [23], fluid injections [24–26], magma injection [27], and aftershocks of strong earthquakes [28, 29]. As suggested by Shapiro et al. [30], microseismic series associated with fluid injection (including magma) could be linked to big earthquakes.

But there are limited researches on the correspondence between rainstorm floods and earthquakes abroad; the researches are mainly concentrated on the relations between earthquakes and tsunamis [31–33] and earthquakes and fire [34, 35]. In 1965, the international tsunami prewarning system was formally launched. In 1966, 26 countries and regions cooperated to set up Pacific Tsunami Warning Center [36] in Hawaii at the request of the IOC (Intergovernmental Oceanographic Commission) [37]. Thereafter, a couple of regional and national tsunami warning centers were established successively, for example, Hawaii Tsunami Warning Center, Alaska and Western Coast Tsunami Warning Center, and Japan Tsunami Warning Center. In the 1990s, the UN established an international coordination group for the Pacific Tsunami Prewarning System. In 1997, someone proposed including the Indian Ocean into the tsunami prewarning system but failed. In October 2003, Australian seismologist Dr. Phil Cummins proposed expanding the scope of prewarning to the Indian Ocean again during the International Tsunami Organization Conference but was also rejected. Through the computer-synthesized tsunami wave height diagrams of four stations including Cocos Islands, he simulated the tsunami induced by the Mw8.5 earthquake of Sumatra in 1833 in a highly similar way to the earthquake-induced tsunami of 2004.

Several Chinese researchers believed that there was a certain relation between rainstorm floods and earthquakes [38–40]. They proposed that the occurrence of flood, drought, and other natural calamities after an earthquake might relate to the earth degassing effect which is both the cause and effect of an earthquake. This indicates that the foregoing viewpoints are basically in line with each other; that is, substantial humid and hot gases are released after an earthquake, thus causing severe rainstorm floods, namely, the earth degassing effect (EDE) [41].

Are earthquake and rainstorm flood related? Will a severe earthquake spark off a severe flood? Will the occurrence of a severe flood induce a severe earthquake? There have always been disputes about these questions in the academic field. Both earthquakes and floods relate to an enormous spatial and temporal system and have highly complicated physical causes, so the mechanism-related researches are very difficult. It is noteworthy that there is still no solution to earthquake forecast worldwide today. As such, it is highly difficult to research into the "Disaster Chain" that may exist between earthquakes and floods and the relevancy and physical causes thereof. Therefore, this study ignored the physical mechanism and only performed a preliminary study on the spatial and temporal correspondence between rainstorm floods and earthquakes from a statistical perspective. Meanwhile, a quantitative computing model was established to study the rules of spatial and temporal correspondence between rainstorm floods and earthquakes when EDE was considered.

2. The Concept of EDE and Preliminary Analysis

2.1. The Concept of EDE. The concept of EDE was first proposed by former Soviet scholars in the early 1900s. With subsequent development over centuries, the New Independent States of the former Soviet Union remain dominant power in terms of in-depth research [40]. The essence of this concept is that mantle ichor (HACONS supercritical fluid) [42] is spontaneously emitted in an upward and outward direction, resulting in the formation of five gas rings and gas geodynamics. Through alkali metasomatism, upwelling mantle ichor could lead to alteration and magma. Meanwhile, it could also cause original upper mantle and crust in the solid form to degenerate. As a result, under a combined effect of the three basic dynamics of the earth (i.e., gravity, earth's rotation, and differential rotation) and celestial tidal force (e.g., mainly from the moon), the tectonic movement of the earth, associated evolutionary process, and natural disasters could be induced.

2.1.1. Gases in the Earth Crust. In recent hundreds of years, under the constraints of solid earth concept, the EDE was ignored, although the combustible gases in underground were mined by humans and the huge plume of gases were spewed by strong volcanos. The evidences of gases in the earth's crust were as follows: (i) Germany KTB Well: there was a high conductivity layer in the depth of 7.0 km, with hot brine flow of gas [43]; (ii) Russia Cora KTB Well: there

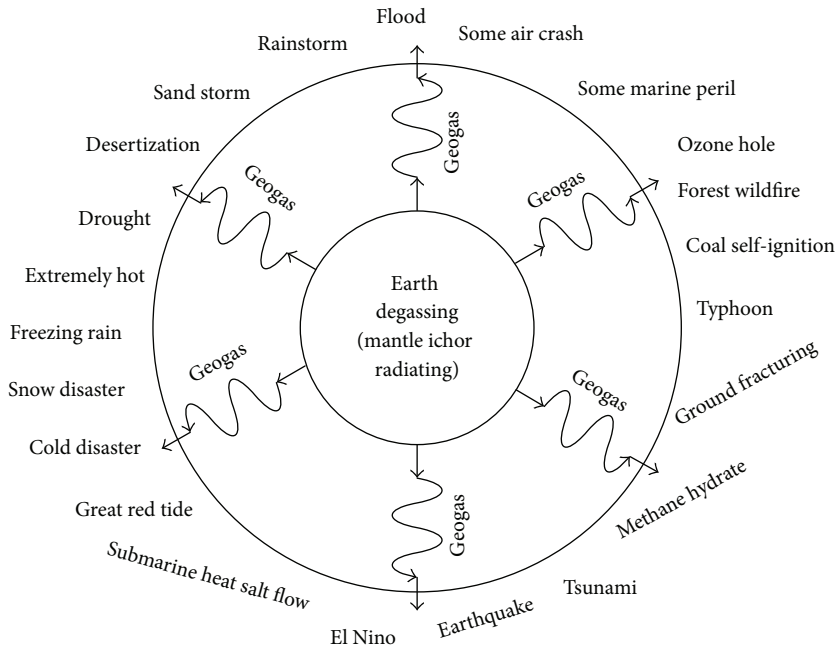

Figure 1: The relationship between earth degassing and some disasters.

was a high permeability zone and gas flow in the depth of 11.5 km [44]; (iii) Russia Kolva KTB Well: high porosity hole was found in the depth of 5.2 km [44]; (iv) Russia Tyumen region: there was rich water and gas in the depth of 7416 m [44]; (v) Kazakhstan Tengiz region: there was low density, low stress, porosity, and saturation fluid from the oil and gas layer to 15 km [45]; (vi) there was some finding recently in [46, 47]. The research of Vernadsky [48], Rubey [49], Goldschmidt [50], Fanale [51], Bailey [52], Gold [53], Pineau and Javoy [54], Graf et al. [55], Chiodini et al. [56], and other scholars has improved the recognition of the importance of EDE. EDE is likely to be the inoculated disaster condition and trigger factor of the disasters such as earthquake, drought, rainstorm, and flood (Figure 1) [40].

2.1.2. Degassing in the Earthquake. Driven by the huge earthquake, the gas in the interior of the earth will overflow up powerfully [41]. In the earthquake of Haicheng in 1975 and Longling, Tangshan, and Songpan in 1976, the black fog or odd fog appeared or black or white gas was jetted out, warm and wet. The temperature of the gas spewed before Songpan earthquake was 80~120°C, and the plant leaves were scorched by the gas [57].

The gases in the upper mantle balloon are 120 times more than in the entire atmosphere, and the gases in the core are more than those in the upper mantle. Seismic activity caused the gathered gases in deep crust upward along the fault fracture zone and formed the gas accumulated in the local soil.

2.1.3. Degassing after Earthquake. Because of the complexity and obstruction of the underground fissure, the gases upward to the surface can be lagging more than one year after the earthquake.

Six months after the Sumatran earthquake in 2004, there were a large number of gases released in the quake zone. About 2 years later, the satellite thermal infrared image showed that the bright temperatures of the degassing sites were higher than surrounding region in the quake zone of the west of Kunlun Mountain Pass Ms8.1 earthquake in 2001. Research suggests that earthquake may play an important role in gas degassing from the solid earth [58].

As to the application of earth degassing-related theories to the flood-earthquake relevancy research, Du and other researchers believe that such relevancy exists because, during the process of earthquake preparation, accumulation, and outbreak, the produced earth degassing effect could lead to humid low-pressure environment in the lower layer of the atmosphere, which is conducive to the formation of heavy rain and subsequent flood events. In addition, a wide range of areas surrounding the border of Inner Mongolia, Xinjiang, and Gansu province in China where severe earthquakes hit exhibit relatively intense tectonic movement before, after, or when such events occur. The escaped hot water vapors from underground areas might also affect the dynamics of the westerly lands and cause big flood or drought events in the Yellow River Basin. After the occurrence of severe earthquake events in Yunnan province and Burma, a wide range of escaped water vapors are accumulated over the Bay of Bengal. Meanwhile, among water vapors transported towards Yangtze River Basin, the component of plum rain vapors is mostly from the Bay of Bengal, which brings about abundant supply of water vapors. As a result, big flood or drought events are likely to occur in this region. Moreover, the occurrence of large earthquake events in Sumatra Island, Indonesia, is closely related to the occurrence of large flood events in the Pearl River Basin.

Table 1: The list of "earthquake-flood relevancy" events under the "earth degassing effect."

Number	Earthquakes	Floods
1	6 destructive earthquakes in Shaanxi, Shanxi, and Henan provinces from 1568 to 1569	Severe flood at the borders of Shaanxi, Shanxi, and Henan provinces in 1570
2	Earthquakes higher than Ms7 in the mountainous areas in the upper reaches of the Yangtze River on April 11, 1870	Severe flood along the Yangtze River in 1870
3	One earthquake higher than Ms7 and two earthquakes higher than Ms6 at the border of Guangdong and Fujian provinces from 1918 to 1921	Landing of a super typhoon at the border of Guangdong and Fujian provinces in 1922
4	An earthquake of Ms8.6 leading to 1,200 deaths in Mongolia on December 4, 1957	Severe flood along the Yellow River in July 1958 (peak flowrate of 22,300 m^3/s at Huayuankou on the 16th)
5	Two earthquakes higher than Ms8 in Tibet in 1950 and 1951; two earthquakes of Ms7.5 in Tibet and Gansu in 1952 and 1954	Severe floods along the Yangtze River, the Huai River and the Yellow River in 1954; severe flood on Songhua River in 1956
6	An earthquake of Ms7.5 in Ulan Bator of Mongolia on January 5, 1967	Severe flood along the Yellow River in August 1967 (peak flowrate of 21,000 m^3/s at Longmen on the 11th)
7	An earthquake of Ms7.1 in the southwest of Mongolia on July 4, 1974	Severe flood in Zhumadian of Henan province on August 8, 1975
8	Earthquakes of Ms7.3 and 7.4 in Longling of Yunnan on May 29, 1976 Earthquake of Ms7.8 in Tangshan of Hebei province on July 28, 1976, leading to 242,000 deaths Earthquake of Ms7.2 in Songpan-Pingwu of Sichuan province on August 16 and August 23, 1976	Severe flood on the Yellow River in July and August 1977 (peak flowrate of 8,780 m^3/s at Dongguan Bridge, YanAn on July 6, a millennial flood; peak flowrate of 14,500 m^3/s at Longmen on July 20; peak flowrate of 10,800 m^3/s at Huayuankou on August 7)
9	Earthquake of Ms7.5 in the north of Mandalay Burma on January 5, 1991	Flood on Huai River in 1991
10	Earthquake of Ms8.1 in the west of Kunlun Mountain, Qinghai province on November 14, 2001	Flood in the middle reaches of the Yellow River from August to October 2003
11	Earthquake of Ms9.3 in Sumatra, Indonesia on December 26, 2004	Flood on Xijiang River on June 17, 2005
12	Four earthquakes of Ms6–6.5 in Yunnan and Burma from May to June 2007	Super flood on Xijiang River in June 2008

Table 1 for the "earthquake-flood relevancy" events may be subjected to the EDE in their view.

2.2. Preliminary Analysis. The foregoing analysis of the "earthquake-flood relevancy" events and "relevancy rules" shows the following.

2.2.1. The "Earthquake-Flood Relevancy" Events Are Mostly Single without Any Systematic and Comprehensive Researches Thereon. From the perspective of earthquake and flood scales, the earthquake scale was basically above 7 while the scales of floods were diverse, covering a range from several thousand square kilometers to several hundred thousand square kilometers. Any comparison of an earthquake higher than Ms7.0 with floods of different scales (e.g., comparison of a flood on the trunk of a large river and a flood on a certain small branch) might not be practically feasible.

From the perspective of occurring time, the two events occurred at an interval of at least half a year, and most over 1 year, or even 6 years at the maximum; for example, the earthquake on Ms8.5 at Chayu, Tibet, in August 1950 was associated with the floods on the Yangtze River in 1954 and the floods on Songhua River in 1956. Severe floods were focused in the period from June to August in China while severe earthquakes might occur every month.

From the regional perspective, typical severe floods were mostly concentrated in the middle and lower reaches of the seven major rivers in the east of China while major earthquakes were mostly concentrated in Xinjiang and Gansu in the northwest of China, Yunnan in the southwest, and Taiwan region. An initial comparison showed that the nearest pairs were more than 1,000 km away from each other. The distance was even farther if overseas earthquakes were considered; for example, the earthquake taking place in Sumatra of Indonesia was more than 4,000 km away from the severe flood along the Pearl River Delta. According to the earthquake-flood relevancy theory of Guo, this is the remote relevancy. According to such a viewpoint, however, most earthquakes and floods are related based on Table 1.

2.2.2. Superficial Understanding of the Physical Mechanism of "Earthquake-Flood Relevancy". According to the EDE, "earthquake-flood relevancy" mainly arises from the gases discharged during an earthquake. However, the foregoing analysis showed that earth degassing was both the cause and effect of an earthquake and the low-pressure environment

Table 2: Summary of the eras of the representative rainstorm floods.

Era	Before 1900	1900–1949	1950s	1960s	1970s	1980s	1990s	After 2000	Total
Count	15	75	17	18	10	11	24	9	169
Percentage	8.9%	44.4%	10.1%	10.7%	5.9%	6.5%	14.2%	5.3%	100.0%

Table 3: Summary of the occurrence periods of the representative rainstorm floods.

Occurrence period	May	Jun.	Jul.	Aug.	Sept.	Oct.	Total
Count	4	41	64	51	7	2	169
Percentage	2.4%	24.3%	37.9%	30.2%	4.1%	1.2%	100.0%

Table 4: Summary of the region of the representative rainstorm floods.

Drainage area or region	Songhua River	Liao River	Hai River	Yellow River	Huai River	Yangtze River	Pearl River	Northwest	Southwest	Zhejiang, Fujian, and Taiwan	Total
Count	14	17	17	9	17	47	28	4	4	12	169
Percentage	8.3%	10.1%	10.1%	5.3%	10.1%	27.8%	16.6%	2.4%	2.4%	7.1%	100.0%

resulting from the earth degassing might attract humid and hot vapors and cold airs. Therefore, observation of substantial earth degassing effects may indicate the occurrence of a severe earthquake on the one hand and a severe flood or substantial local temperature decline on the other hand. Meanwhile, earth degassing is only a local effect which is not on the same level as the atmospheric circumfluence and the weather system that cause the flood. In terms of energy, the energy level of an earthquake is incomparable with the solar energy level that causes atmospheric circumfluence and weather system changes. Moreover, how can vapors discharged in an earthquake flow in the air for some years and then come back to the same drainage area in the same country? If the temperature increases due to an earthquake, what is the relation with an overseas earthquake? These questions cannot be well addressed.

Therefore, the relation between rainstorm floods and earthquakes as concluded by the foregoing researches is highly subjective, coincident, and uncertain.

3. Data and Model

3.1. Rainstorm Flood Data. After extensive examination of the rainstorm floods data in China, a total of 169 representative regional rainstorm floods characterized by long duration (over 3 days), wide coverage (covering area more than 100,000 km^2), large scale, and rare occurrence (recurrence interval more than 20 years) from 1800 to 2012 were systematically summarized. For the convenience of analysis, each rainstorm flood was collectively taken as one event, and it was assumed that all the 169 rainstorm floods were rainstorm flood events with no further classification. As shown in Tables 2–4, the era, period, and region of the representative rainstorm floods were presented.

3.2. Seismic Data. Totally 2,461 cases of earthquakes were summarized (Figure 2), including 987 earthquakes on or higher than Ms6.0 in China mainland and neighboring

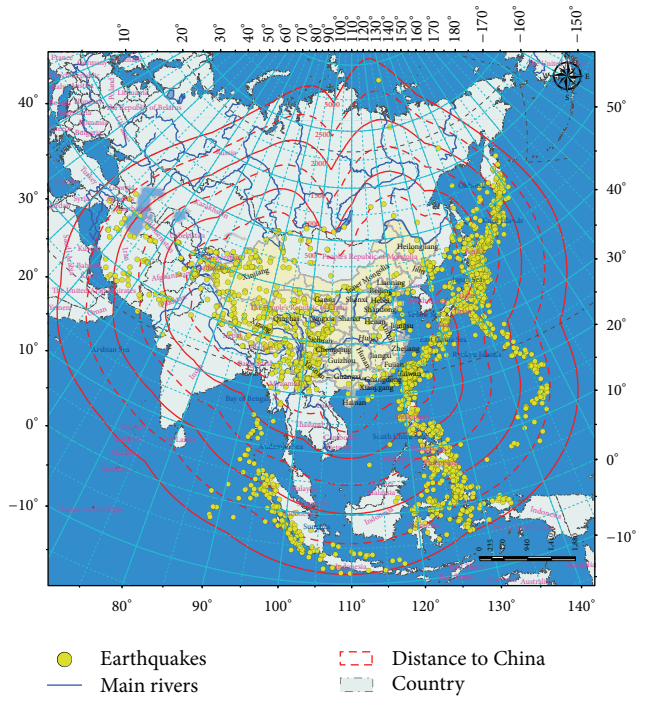

Figure 2: Distribution of the earthquakes higher than Ms6.0 in China and surrounding regions.

regions (Taiwan and territorial waters) from 1800 to 2012 and 1,474 earthquakes on or higher than Ms6.0 (higher than scale 6.5 for most earthquakes) within a distance of 3,000 km from China from 1900 to 2012. Among these earthquakes, there were 3 earthquakes on or higher than Mw9.0, 46 earthquakes on a scale of 8.0 to 9.0 (including 8.0 but excluding 9.0), 693 earthquakes on a scale of 7.0 to 8.0, and 1,719 earthquakes on a scale of 6.0 to 7.0.

As rainstorm flood events mostly occur in the east and south of China, the earthquakes taking place in neighboring

countries are all far away from the place where the rainstorm flood events take place. Therefore, a preliminary screening was performed on the overseas earthquakes. According to the relevant data, the initial conclusion was that the overseas earthquakes lower than Ms6.5 had weak impacts on the rainstorm floods in China. As such, a total of 2,354 cases of severe earthquakes were screened out, including domestic earthquakes higher than Ms6.0 and overseas earthquakes higher than Ms6.5.

3.3. Model

3.3.1. Basic Philosophies of the Model. In order to further probe into the spatial and temporal correspondences between rainstorm flood events and earthquakes, it was assumed that the impacts of an earthquake on rainstorm flood will increase when the earthquake scale is higher, the time interval is shorter, and the distance is smaller. Considering earth degassing effects, the impact of an earthquake on a rainstorm flood will increase when the orientation of the epicenter to the rainstorm zone is less different from the orientation of vapor transmission above the rainstorm zone. According to this basic concept, only the postearthquake occurrence of rainstorm flood events was considered in the general calculation. Meanwhile, for the convenience of statistical analysis, the domestic territory and the regions within 3000 km from China firstly underwent a gridding process and were numbered according to some rules (see below). Secondly, the factors that affect the correspondence between the rainstorm floods and earthquakes were analyzed, identified, classified, and scored. Thirdly, various influential factors were weighted and the calculation model was established for general scoring and calculation of the relations between rainstorm floods and earthquakes. Finally, the possible correspondences between rainstorm floods and earthquakes were determined through classification of the general scores.

3.3.2. Gridding and Numbering. For the convenience of statistics, China and the regions within 3,000 km from China were first gridded with a size of 2.5° × 2.5°. The geographic range was 40° east longitude and 10° south latitude at the minimum and 170° east longitude and 80° north latitude at the maximum. For grid numbering, there was one grid at an interval of 2.5° starting from (40°, –10°). The number was changed by 1 for each grid in the longitudinal direction and 100 for each grid in the latitudinal direction. The first grid was numbered as 101.

For any point (x, y), x is the longitudinal coordinate, "+" is the east longitude, and "–" is the west longitude; y is the latitudinal coordinate, "+" is the north latitude, and "–" is the south latitude. The calculation formula of grid number AABB (AA may stand for one or two bits) is as follows:

$$\mathrm{AABB} = \left\{\left[\frac{(y+10)}{2.5}\right]+1\right\}\times 100 + \left[\frac{(x-40)}{2.5}\right]+1, \quad (1)$$

where [] is the rounding symbol.

For any grid number AABB, the central longitudinal and latitudinal coordinate (x, y) of the grid is

$$\begin{aligned} x &= (\mathrm{BB}-1)\times 2.5 + 40 + 1.25, \\ y &= (\mathrm{AA}-1)\times 2.5 - 10 + 1.25. \end{aligned} \quad (2)$$

3.3.3. Identification and Processing of Influential Factors. The above analysis showed that the following factors might affect the relations between earthquakes and rainstorm floods: earthquake scale, time interval and distance between the earthquake and the rainstorm flood, and the orientation of the earthquake relative to the rainstorm flood. In order to describe the spatial and temporal correspondence between earthquakes and rainstorm flood events as accurately as possible, it is necessary to classify the above factors and assign corresponding weights to them:

(1) Classify earthquake scales and weigh accordingly. It is believed that higher earthquake scale will cause greater impact on the rainstorm flood, so that the weight will be higher.

(2) Classify the time intervals between the earthquake and rainstorm flood (on a monthly basis) and weigh accordingly. It is believed that the impacts of an earthquake on the rainstorm flood will decline, and thus the weight will be smaller when the time interval between an earthquake and a rainstorm flood is longer.

(3) Classify the distance between the earthquake and rainstorm flood (in kilometers) and weigh accordingly. It is believed that the impacts of an earthquake on the rainstorm flood will decline, and the weight will be smaller when the distance between an earthquake and a rainstorm flood is farther.

(4) When EDE is substantiated, it is believed that the probability for an earthquake to impact the rainstorm flood will be higher and the weight should be higher if the earthquake and the vapors causing the rainstorm floods are in the same or similar orientation.

Eight orientations, that is, north, northeast, east, southeast, south, southwest, west, and northwest, were adopted herein to indicate the orientations of the earthquakes and the vapors causing the rainstorm floods, and eight codes from 1 to 8 were awarded thereto accordingly. The relative orientation of the earthquake to the rainstorm flood could be calculated based on the longitude and latitude of the epicenter and the rainstorm center. The orientation of vapors causing the rainstorm floods might be acquired according to relevant research results [59]. As rainstorms are mostly concentrated from June to August in most parts of China and heavy rainstorms in specific regions may occur in May or September to October, only the sources and relative orientations of vapors of various regions from May to October were summarized. Considering the gridding process, the sources and the relative orientations of the vapors causing the heavy rainstorms in the regions located in various grids in China from May to October will be summarized finally. If the orientation

Table 5: Classification and weights of the influential factors for the relations between an earthquake and a rainstorm flood event.

Magnitude		Time interval (months)		Distance (km)		Orientation	
Scale	Weight	Scale	Weight	Scale	Weight	Orientation difference	Weight
6.0~6.9	0.1	0	1.0	0~499	1.0	The same orientation	1.0
7.0~7.4	0.2	1~3	0.8	500~999	0.9	Different by 1 orientation	0.8
7.5~7.9	0.4	4~6	0.7	1000~1499	0.8	Different by 2 orientations	0.4
8.0~8.4	0.6	7~9	0.6	1500~1999	0.7	Different by over 2 orientations	0.1
8.5~8.9	0.8	10~12	0.5	2000~2499	0.6		
Higher than scale 9	1.0	13~15	0.4	2500~2999	0.5		
		16~18	0.3	3000~3499	0.4		
		19~21	0.2	3500~3999	0.3		
		22~24	0.1	4000~4499	0.2		
				Higher than 4500	0.1		

of an earthquake to a rainstorm center is the same as the orientation of the transmission of the vapors within the grid where the rainstorm center is located, the code difference will be 0; if they are different by 1 orientation, the code difference will be 1 or 7; if they are different by 2 orientations, the code difference will be 2 or 6; if they are different by 3 orientations, the code difference will be 3 or 5; if they are different by 4 orientations, the code difference will be 4.

Table 5 showed the classification and weights of various influential factors.

3.3.4. Weighing and General Calculation of the Influential Factors. After classification and weighing of various influential factors, a general calculation and analysis can be performed on the different earthquakes corresponding to each rainstorm flood. The weights of various classes of the influential factors were assigned as X_{ij} ($i = 1, 2, 3, 4$; j is different due to different classes of the influential factors); meanwhile, various influential factors were assigned with weight W_i ($\sum_{i=1}^{4} W_i = 1.0$); hence the general score P of various earthquakes could be indicated as follows:

$$P = \sum_{i=1}^{4} X_{ij} \times W_i. \quad (3)$$

Regarding the weights of various influential factors, it was hypothesized that the impacts of earthquake scale and relative orientation to the rainstorm flood event on the correspondence between them were relatively high, while the time interval and distance between them would generate lower impacts.

As shown in Table 6, the weight W_i of various influential factors was listed.

Table 6: Weights of various influential factors.

Influential factor	Weight
Earthquake scale	0.3
Time interval between the earthquake and the rainstorm flood event	0.2
Distance between the earthquake and the rainstorm flood event	0.2
Orientation of the earthquake to the rainstorm flood event	0.3

According to the general score P, five possible correspondences between rainstorm flood events and earthquakes can be set (Table 7).

4. Results and Analysis

The possible correspondences between the 165 rainstorm floods and the 1,932 earthquakes that happened two years before them are calculated and shown in Table 8.

The foregoing statistics showed that none of the 165 severe rainstorm floods had strong correspondence to the previous severe earthquakes; 99 of the severe rainstorm floods, or 58.6% of all rainstorm floods, might have a high correspondence to the severe earthquakes taking place in the past 2 years. Only 2 of the severe rainstorm floods had low correspondences to the severe earthquakes taking place in the past 2 years. Meanwhile, 144 of the 1,932 severe earthquakes had a high correspondence to the rainstorm floods that took place 2 years later, or 7.5% of all severe earthquakes, 6.1% of the preliminarily-screened 2,354 severe earthquakes, and only 5.9% of the 2,461 severe earthquakes higher than Ms6.0.

Table 7: Judgment of possible correspondences between rainstorm floods and earthquakes.

Class	General score P	Possible correspondence
Class 1	[0.8, 1.0]	Correspondence is extremely probable
Class 2	[0.6, 0.8)	Correspondence is highly probable
Class 3	[0.4, 0.6)	Correspondence is probable
Class 4	[0.2, 0.4)	Correspondence is impossible
Class 5	[0.1, 0.2)	Correspondence is highly impossible

Table 8: Summary of the probable correspondences between rainstorm floods and earthquakes.

Class	Rainstorm flood event	Corresponding earthquake
Class 1	0	0
Class 2	99	144
Class 3	64	906
Class 4	2	856
Class 5	—	26
Total	*165*	*1,932*

It showed that most earthquakes had a low correspondence to the rainstorm floods taking place within 2 years after them.

Among the 99 rainstorm floods with a highly possible correspondence to earthquakes, 38 rainstorm floods had a high correspondence to multiple previous earthquakes, with 1 rainstorm flood corresponding to 8 severe earthquakes at the maximum. It meant that multiple earthquakes might have impacts on 1 rainstorm flood. On the contrary, 24 earthquakes of the 144 earthquakes may correspond to multiple rainstorm flood events, with 1 earthquake corresponding to 3 rainstorm floods at the maximum. This indicated that most earthquakes and rainstorm floods corresponded to each other on a one-to-one basis although one-sixth of the earthquakes might generate certain impacts on multiple rainstorm floods.

Judging from the correspondence between the numbers of grids where rainstorm floods and earthquakes were located, the grids of 36 (65.5% of all 55 grids) rainstorm floods corresponded to the grids of multiple epicenters, with 1 grid of rainstorm flood corresponding to the grids of 11 epicenters at the maximum (including 1 rainstorm flood corresponding to multiple earthquakes). On the contrary, the grid of the same epicenter corresponded to the grids of multiple rainstorm floods, with the grid of 1 epicenter corresponding to the grids of 13 rainstorm floods at the maximum (similarly including repetitions). Accordingly, no rainstorm flood located in the same grid or some adjacent grids was found always corresponding to the earthquake of a certain grid or some adjacent grids and vice versa (Figures 3 and 4). It meant that none of the earthquakes in a certain region was always found to cause the rainstorm floods in the some regions.

Further analysis of the 99 rainstorm floods and 144 earthquakes that had a high correspondence showed that there were cumulatively 172 repeated correspondences between the rainstorm floods and the earthquakes (Figure 5). Rainstorm floods basically happened in the main rainstorm regions of China, most of which were along the Yangtze River, followed by the Pearl River and the fewest in the southwest of China, and they mostly happened during the rainy period of these regions (June to August). The earthquake scale distribution rules were similar to the general rules, and scale 7 and scale 8 earthquakes were the most. Rainstorm floods mostly occurred within 1 year after an earthquake, especially from January to March. The rainstorm zone was mostly within 3,000 km away from the epicenter, particularly between 1,000 km and 2,000 km. Earthquake zones were mostly located to the west or southwest of the rainstorm zones and on the path of exotic vapors towards the rainstorm zones. Meanwhile, the four influential factors were all very important to the general score during the survey of the same rainstorm flood corresponding to multiple earthquakes. However, none of the influential factors played a decisive role in the general score (Table 9).

5. Discussions

Through the summarization of the severe earthquakes and the rainstorm floods that may have spatial and temporal correspondence in China and adjacent regions in the past 200+ years and also by general computation and statistical analysis, it was found that only 144 severe earthquakes had a high correspondence with the rainstorm floods that occurred within 2 years after their occurrence, or only 5.9% of the 2,461 severe earthquakes higher than Ms6.5. As we all know, this computation and statistical results were based on some parameters and weights, and the values of weights are subjective and could be criticized. So we need to change the weights values, computation, and statistical analysis again.

First, we will change the weights values of the influential factors. The results are shown in Table 10.

The data in Table 10 shows different distribution ratios of the four factors' weights; the statistical results are different. The greater the differentiation of the distribution ratios, the higher the corresponding number. In the four factors, the weights of orientation bear the biggest influence on statistical results; the bigger the weights of orientation, the higher the corresponding number. Increasing the weights of orientation and distance, the corresponding number of class 1 is also on the increase. In order to prevent the single factor's influence on the statistical results, we set the weights as the above (Table 6); it is very reasonable.

Now, we come to have a further discussion about the rules of the high corresponding relationships between earthquakes and rainstorm floods. In order to obtain more earthquake series, we shuffled the earthquake occurring time, location, and magnitude of the former earthquake series, respectively and randomly, to form a new set of earthquake series [60] (diagram as shown in Figure 6). The synthetic earthquake series and the original rainstorm flood series were input to the model; after calculation the statistical results were shown in Table 11.

We analyzed the regularity of the correspondence results and found that there were still no rules in the correspondence. It is consistent with the analysis results in Section 4.

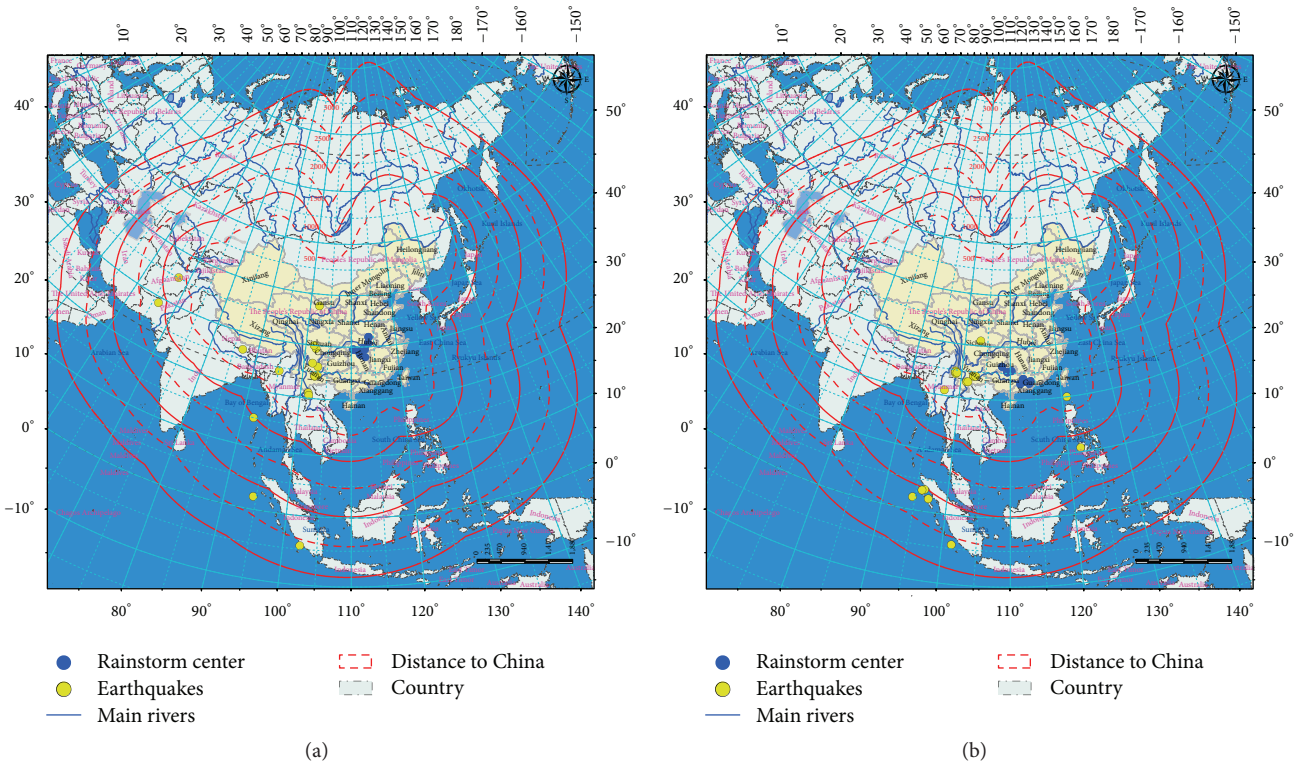

Figure 3: Distribution of typical regional rainstorm floods and previous earthquakes.

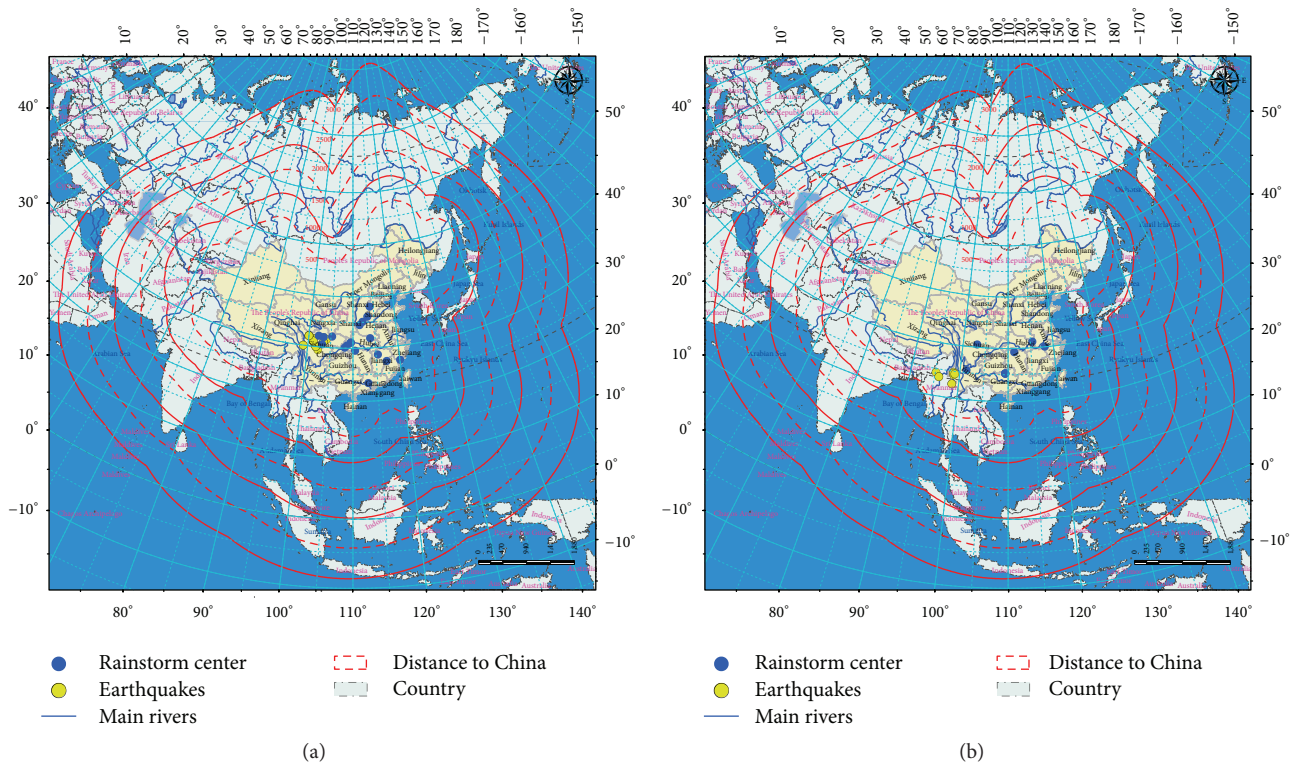

Figure 4: Distribution of typical regional earthquakes and subsequent rainstorm floods.

Table 9: Summary of the correspondences between the 99 rainstorm floods and the 144 earthquakes.

Drainage area or region		Magnitude		Time interval (month)		Distance (km)		Orientation	
Name	Count	Class	Count	Class	Count	Class	Count	Orientation difference	Count
Yangtze River	48	6.0~6.9	64	0	30	0~499	16	The same orientation	83
Hai River	15	7.0~7.4	46	1~3	51	500~999	32	Different by one orientation	86
Huai River	21	7.5~7.9	36	4~6	37	1000~1499	40	Different by two orientations	3
Yellow River	12	8.0~8.4	18	7~9	23	1500~1999	22	Different by over two orientations	0
Liao River	6	8.5~8.9	6	10~12	12	2000~2499	25		
Songhua River	6	>9	2	13~15	10	2500~2999	16		
Pearl River	35			16~18	4	3000~3499	9		
Southwest	2			19~21	1	3500~3999	4		
Zhejiang, Fujian, and Taiwan	20			22~24	4	4000~4499	6		
Northwest	7					Over 4500	2		

Table 10: The correspondence results based on different weights values of the influential factors.

Weights				Class 1		Class 2		Classes 1 and 2	
Magnitude	Time interval	Distance	Orientation	Rainstorm flood	Earthquake	Rainstorm flood	Earthquake	Rainstorm flood	Earthquake
1	0	0	0	23	9	53	30	76	39
0	1	0	0	156	610	3	746	159	1356
0	0	1	0	154	589	11	601	165	1190
0	0	0	1	160	785	0	0	160	785
0.7	0.1	0.1	0.1	2	2	33	18	35	20
0.1	0.7	0.1	0.1	71	113	87	740	158	853
0.1	0.1	0.7	0.1	32	60	128	668	160	728
0.1	0.1	0.1	0.7	110	179	50	605	160	784
0.4	0.2	0.2	0.2	1	1	37	34	38	35
0.2	0.4	0.2	0.2	1	1	136	337	137	338
0.2	0.2	0.4	0.2	1	1	129	312	130	313
0.2	0.2	0.2	0.4	0	0	148	437	148	437
0.4	0.4	0.1	0.1	1	1	61	58	62	59
0.4	0.1	0.4	0.1	0	0	45	33	45	33
0.4	0.1	0.1	0.4	1	1	89	91	90	92
0.1	0.4	0.4	0.1	15	16	137	603	152	619
0.1	0.4	0.1	0.4	41	44	115	527	156	571
0.1	0.1	0.4	0.4	32	42	120	505	152	547
0.3	0.3	0.3	0.1	0	0	78	115	78	115
0.3	0.3	0.1	0.3	1	1	107	174	108	175
0.3	0.1	0.3	0.3	0	0	100	158	100	158
0.25	0.25	0.25	0.25	0	0	124	226	124	226
0.3	0.2	0.2	0.3	0	0	99	144	99	144

6. Conclusions

Currently, there is a big controversy surrounding the topic of EDE. Under the hypothesis that EDE is valid, this paper tests the relationship between rainstorm floods and earthquakes. When EDE is substantiated, it is believed that most of the rainstorm floods may relate to severe earthquakes. However, most of the rainstorm floods have nothing to do with the severe earthquakes from a statistical perspective.

The foregoing calculation showed that the correspondence between a severe earthquake and a rainstorm flood was related to the earthquake scale, geographic location of

Table 11: The correspondence results based on shuffled series of earthquakes.

Shuffle or not			Class 1		Class 2		Classes 1 and 2	
Time	Epicenter location	Earthquake scale	Rainstorm flood	Earthquake	Rainstorm flood	Earthquake	Rainstorm flood	Earthquake
Yes	No	No	2	2	111	151	113	153
No	Yes	No	2	1	115	142	117	143
No	No	Yes	4	2	96	134	100	136
Yes	Yes	No	3	2	94	133	97	135
Yes	No	Yes	1	1	91	121	92	122
No	Yes	Yes	3	2	93	146	96	148
Yes	Yes	Yes	0	0	101	143	101	143

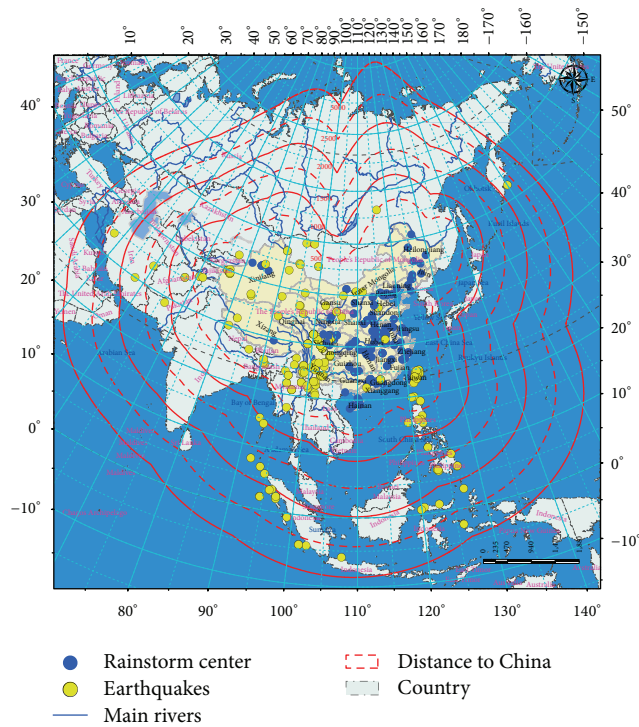

Figure 5: General distribution of the 144 earthquakes corresponding to the 99 rainstorm floods.

Number	Time	Epicenter location	Earthquake scale
1	1812.3.8	83.0°E, 43.7°N	7.8
2	1906.3.28	118.5°E, 24.5°N	6.5
3	1922.5.15	144.2°E, 40.3°N	6.5
4	1938.8.16	93.9°E, 23.0°N	7.1
5	1948.5.25	100.5°E, 29.5°N	7.3
6	1976.7.28	118.0°E, 39.4°N	7.8
7	1990.2.8	124.6°E, 9.8°N	6.8
8	2000.6.4	102.0°E, 4.8°S	7.8
9	2004.12.26	95.86°E, 3.27°N	9.3
10	2008.5.12	103.4°E, 31.0°N	8.0

Number	Time	Epicenter location	Earthquake scale
1	2008.5.12	118.0°E, 39.4°N	6.8
2	1938.8.16	144.2°E, 40.3°N	7.8
3	2004.12.26	93.9°E, 23.0°N	6.5
4	1906.3.28	124.6°E, 9.8°N	7.8
5	2000.6.4	118.5°E, 24.5°N	9.3
6	1922.5.15	83.0°E, 43.7°N	8.0
7	1990.2.8	100.5°E, 29.5°N	7.3
8	1948.5.25	103.4°E, 31.0°N	7.1
9	1812.3.8	95.86°E, 3.27°N	7.8
10	1976.7.28	102.0°E, 4.8°S	6.5

Figure 6: Schematic diagram of shuffling the series of earthquakes.

the rainstorm zone, and epicenter as well as the time interval, distance, and relative orientation between the rainstorm flood and the earthquake. Therefore, it is highly probable for an earthquake to spark off a severe rainstorm flood if the earthquake is located on the transmission path of vapors leading to the rainstorm.

From a statistical point of view, some severe earthquakes and rainstorm floods have certain intrinsic linkage. From a physical perspective, however, it is necessary to carry out a further systematic research on the impacts of orientation, scope, time interval, and weather system of an earthquake on rainstorm floods.

Competing Interests

The authors declare that they have no competing interests.

Acknowledgments

The research is financially supported by the National Natural Science Foundation of China (Grant no. 51509267) and the National Basic Research Program of China ("973" Program) (Grants nos. 2013CB036406 and 2015CB452701). Thanks are due to Dr. Yuyan Zhou in China Institute of Water Resources and Hydropower Research and Professors Quansheng Liu and Jinxing Xu for assisting in revising this paper.

References

[1] United Nations Office for Disaster Risk Reduction (UNISDR), *Global Assessment Report on Disaster Risk Reduction*, United Nations Office for Disaster Risk Reduction (UNISDR), Geneva, Switzerland, 2009.

[2] M. J. Crozier, "Deciphering the effect of climate change on landslide activity: a review," *Geomorphology*, vol. 124, no. 3-4, pp. 260–267, 2010.

[3] D.-H. Yang, D.-B. Yang, and X.-X. Yang, "The influence of tides and earthquakes in global climate changes," *Chinese Journal of Geophysics*, vol. 54, no. 4, pp. 926–934, 2011.

[4] A. Bunde, J. Kropp, and H. J. Schellnhuber, Eds., *The Science of Disasters: Climate Disruptions, Heart Attacks, and Market Crashes*, Springer, Berlin, Germany, 2002.

[5] A. De Santis, "Geosystemics," in *Proceedings of the 3rd IASME/WSEAS International Conference on Geology and Seismology (GES '09)*, pp. 36–40, Cambridge, UK, February 2009.

[6] S. Homma, K. Fujita, and T. Ichimura, "A physics-based monte carlo earthquake disaster simulation accounting for uncertainty in building structure parameters," *Procedia Computer Science*, vol. 29, pp. 855–865, 2014.

[7] J. Li and C. K. Chen, "Modeling the dynamics of disaster evolution along causality networks with cycle chains," *Physica A: Statistical Mechanics and Its Applications*, vol. 401, pp. 251–264, 2014.

[8] H. Hasanzadeh and M. Bashiri, "An efficient network for disaster management: model and solution," *Applied Mathematical Modelling*, vol. 40, no. 5-6, pp. 3688–3702, 2016.

[9] Q. W. Li, C. Wang, and H. Zhang, "A probabilistic framework for hurricane damage assessment considering non-stationarity and correlation in hurricane actions," *Structural Safety*, vol. 59, pp. 108–117, 2016.

[10] S. C. Li, Z. Q. Zhou, L. P. Li, P. Lin, Z. Xu, and S. Shi, "A new quantitative method for risk assessment of geological disasters in underground engineering: Attribute Interval Evaluation Theory (AIET)," *Tunnelling and Underground Space Technology*, vol. 53, pp. 128–139, 2016.

[11] K. S. Sagun-Ongtangco, M. A. D. Abenir, C. T. Bermejo, E. D. C. Shih, J. V. O. Wales, and J. Plaza, "Perspectives of the UST NSTP facilitators on disability and disaster risk reduction and management: a qualitative case study," *International Journal of Disaster Risk Reduction*, vol. 16, pp. 134–141, 2016.

[12] T. Nagatani, "Chain-reaction crash on a highway in high visibility," *Physica A: Statistical Mechanics and Its Applications*, vol. 450, pp. 466–472, 2016.

[13] R. Thom, *Structural Stability and Morphogenesis*, W. A. Benjamin, New York, NY, USA, 1972.

[14] D. Liu, J. Wang, and Y. Wang, "Application of catastrophe theory in earthquake hazard assessment and earthquake prediction research," *Tectonophysics*, vol. 167, no. 2–4, pp. 179–186, 1989.

[15] M. Scheffer, S. Carpenter, J. A. Foley, C. Folke, and B. Walker, "Catastrophic shifts in ecosystems," *Nature*, vol. 413, no. 6856, pp. 591–596, 2001.

[16] G. Woo, *Calculating Catastrophe*, Imperial College Press, 2011.

[17] D. L. Turcotte, *Fractals and Chaos in Geology and Geophysics*, Cambridge University Press, Cambridge, UK, 1997.

[18] S. A. Shapiro, E. Huenges, and G. Borm, "Estimating the crust permeability from fluid-injection-induced seismic emission at the KTB site," *Geophysical Journal International*, vol. 131, no. 2, pp. F15–F18, 1997.

[19] N. Delépine, N. Cuenot, E. Rothert, M. Parotidis, S. Rentsch, and S. A. Shapiro, "Characterization of fluid transport properties of the Hot Dry Rock reservoir Soultz-2000 using induced microseismicity," *Journal of Geophysics and Engineering*, vol. 1, no. 1, pp. 77–83, 2004.

[20] N. Deichmann and D. Giardini, "Earthquakes induced by the stimulation of an enhanced geothermal system below Basel (Switzerland)," *Seismological Research Letters*, vol. 80, no. 5, pp. 784–798, 2009.

[21] P. Talwani, "Seismogenic properties of the crust inferred from recent studies of reservoir-induced seismicity—application to Koyna," *Current Science*, vol. 79, no. 9, pp. 1327–1333, 2000.

[22] M.-K. Lee- and L. W. Wolf, "Analysis of fluid pressure propagation in heterogeneous rocks: implications for hydrologically-induced earthquakes," *Geophysical Research Letters*, vol. 25, no. 13, pp. 2329–2332, 1998.

[23] M. Parotidis, E. Rothert, and S. A. Shapiro, "Pore-pressure diffusion: a possible triggering mechanism for the earthquake swarms 2000 in Vogtland/NW-Bohemia, central Europe," *Geophysical Research Letters*, vol. 30, no. 20, 2003.

[24] S. A. Shapiro, E. Rothert, V. Rath, and J. Rindschwentner, "Characterization of fluid transport properties of reservoirs using induced microseismicity," *Geophysics*, vol. 67, no. 1, pp. 212–220, 2002.

[25] S. A. Shapiro, C. Dinske, C. Langenbruch, and F. Wenzel, "Seismogenic index and magnitude probability of earthquakes induced during reservoir fluid stimulations," *Leading Edge*, vol. 29, no. 3, pp. 304–309, 2010.

[26] B. P. Goertz-Allmann, A. Goertz, and S. Wiemer, "Stress drop variations of induced earthquakes at the Basel geothermal site," *Geophysical Research Letters*, vol. 38, no. 9, 2011.

[27] A. Díaz-Moreno, J. M. Ibáñez, S. De Angelis et al., "Seismic hydraulic fracture migration originated by successive deep

magma pulses: the 2011–2013 seismic series associated to the volcanic activity of El Hierro Island," *Journal of Geophysical Research: Solid Earth*, vol. 120, no. 11, pp. 7749–7770, 2015.

[28] W. Bosl and A. Nur, "Aftershocks and pore fluid diffusion following the Landers earthquake," *Journal of Geophysical Research*, vol. 107, no. B12, p. 2366, 1992.

[29] S. A. Shapiro, R. Patzig, E. Rothert, and J. Rindschwentner, "Triggering of seismicity by pore-pressure perturbations: permeability-related signatures of the phenomenon," *Pure and Applied Geophysics*, vol. 160, no. 5-6, pp. 1051–1066, 2003.

[30] S. A. Shapiro, S. Rentsch, and E. Rothert, "Characterization of hydraulic properties of rocks using probability of fluid-induced microearthquakes," *Geophysics*, vol. 70, no. 2, pp. F27–F33, 2005.

[31] B. W. Levin, "Nonlinear oscillating structures in the earthquake and seaquake dynamics," *Chaos*, vol. 6, no. 3, pp. 405–413, 1996.

[32] C. D. Williams, "The Mary Celeste: a classic seaquake encounter?" *Marine Observer*, vol. 72, no. 355, 2002.

[33] F. Dall'Osso, D. Dominey-Howes, C. Moore, S. Summerhayes, and G. Withycombe, "The exposure of Sydney (Australia) to earthquake-generated tsunamis, storms and sea level rise: a probabilistic multi-hazard approach," *Scientific Reports*, vol. 4, article 7401, 2014.

[34] J. Mohammand and P. Grobbel, "An investigation of earthquake fire hazard in urban areas," in *Proceedings of the World Conference on Earthquake Engineering (WCEE '96)*, Acapulco, Mexico, June 1996.

[35] M. Kobayashi, "Urban post-earthquake fires in Japan," in *Proceedings of the 2nd Japan-US Workshop on Urban Earthquake Hazard Reduction*, 2002.

[36] G. Papadopoulos, "Tsunami early warning systems and risk mitigation," in *Tsunamis in the European-Mediterranean Region*, pp. 179–226, 2016.

[37] E. Okemwa, "The Intergovernmental Oceanographic Commission of UNESCO and regional capacity building," *Marine Policy*, vol. 22, no. 3, pp. 197–207, 1998.

[38] Y. Q. Wang and Q. Hou, "Earthquake flood disaster chain—research on early-stage earthquakes of super-scale floods on Xijiang River in the past 500 years," in *Proceedings of the Natural Disaster Forecast and Summarization Academic Workshop*, Beijing, China, 2010 (Chinese).

[39] Z. J. Guo, B. Y. Qin, and G. P. Li, "Remote relevancy between severe Earthquake, severe flood and severe drought," *Northwest Earthquake Journal*, no. 3, article 37, 1991 (Chinese).

[40] L. T. Du, "Significance research and development of earth degassing," *Geological Review*, vol. 51, no. 2, pp. 174–180, 2005 (Chinese).

[41] G. Chiodini, C. Cardellini, A. Amato et al., "Carbon dioxide Earth degassing and seismogenesis in central and southern Italy," *Geophysical Research Letters*, vol. 31, no. 7, Article ID L07615, 2004.

[42] E. A. Gaiduk, Y. D. Fomin, V. N. Ryzhov, E. N. Tsiok, and V. V. Brazhkin, "Dynamical crossover in supercritical core-softened fluids," *Fluid Phase Equilibria*, vol. 417, pp. 237–241, 2016.

[43] A. Rauen, J. Duyster, S. Heikamp et al., "Electrical conductivity of a KTB core from 7000 m: effects of cracks and ore minerals," *Scientific Drilling*, vol. 4, no. 5-6, pp. 197–206, 1994.

[44] B. N. Khakhaev, L. A. Pevzner, I. I. Samkhan et al., "Geothermal technology of formation water utilization," *Razvedka I Okhrana Nedr*, no. 1, pp. 34–36, 1994.

[45] I. A Garagash, V. N. Nikolaevsky, and V. I. Shatilov, "Connection of the deep anomalies of the crust stresses with under salt hydrocarbon deposits of the North Caspian," in *Proceedings of the RAS*, vol. 338, pp. 383–386, 1994.

[46] A. Caracausi, M. Martelli, P. M. Nuccio, M. Paternoster, and F. M. Stuart, "Active degassing of mantle-derived fluid: a geochemical study along the Vulture line, southern Apennines (Italy)," *Journal of Volcanology and Geothermal Research*, vol. 253, pp. 65–74, 2013.

[47] P. Sella, A. Billi, I. Mazzini et al., "A newly-emerged (August 2013) artificially-triggered fumarole near the Fiumicino airport, Rome, Italy," *Journal of Volcanology and Geothermal Research*, vol. 280, pp. 53–66, 2014.

[48] V. I. Vernadsky, "Gas exchange in earth's crust," *Proceedings of St. Petersburg Royal Academy of Sciences*, vol. 6, pp. 141–162, 1912 (Russian).

[49] W. W. Rubey, "Geologic history of sea water: an attempt to state the problem," *Geological Society of America Bulletin*, vol. 62, pp. 1111–1148, 1951.

[50] V. M. Goldschmidt, "Geochemistry," *Soil Science*, vol. 78, no. 2, p. 156, 1954.

[51] F. P. Fanale, "A case for catastrophic early degassing of the earth," *Chemical Geology*, vol. 8, no. 2, pp. 79–105, 1971.

[52] D. K. Bailey, "Volcanism, earth degassing and replenished lithosphere mantle," *Philosophical Transactions of the Royal Society A: Mathematical, Physical & Engineering Sciences*, vol. 297, no. 1431, pp. 309–322, 1980.

[53] T. Gold, "The deep, hot biosphere," *Proceedings of the National Academy of Sciences of the United States of America*, vol. 89, no. 13, pp. 6045–6049, 1992.

[54] F. Pineau and M. Javoy, "Strong degassing at ridge crests: the behaviour of dissolved carbon and water in basalt glasses at 14°N, Mid-Atlantic Ridge," *Earth and Planetary Science Letters*, vol. 123, no. 1–3, pp. 179–198, 1994.

[55] H.-F. Graf, B. Langmann, and J. Feichter, "The contribution of Earth degassing to the atmospheric sulfur budget," *Chemical Geology*, vol. 147, no. 1-2, pp. 131–145, 1998.

[56] G. Chiodini, F. Frondini, C. Cardellini, F. Parello, and L. Peruzzi, "Rate of diffuse carbon dioxide Earth degassing estimated from carbon balance of regional aquifers: the case of central Apennine, Italy," *Journal of Geophysical Research: Solid Earth*, vol. 105, no. 4, Article ID 1999JB900355, pp. 8423–8434, 2000.

[57] Z. J. Qiang, X. D. Xu, and C. G. Dian, "Thermal infrared anomaly precursor of impending earthquakes," *Chinese Science Bulletin*, vol. 36, no. 4, pp. 319–323, 1991.

[58] Y. Sano, N. Takahata, G. Igarashi, N. Koizumi, and N. C. Sturchio, "Helium degassing related to the Kobe earthquake," *Chemical Geology*, vol. 150, no. 1-2, pp. 171–179, 1998.

[59] G. W. Liu, *Atmospheric Process of Hydrological Circulation*, Science Press, Beijing, China, 1997 (Chinese).

[60] J. Theiler, S. Eubank, A. Longtin, B. Galdrikian, and J. Doyne Farmer, "Testing for nonlinearity in time series: the method of surrogate data," *Physica D: Nonlinear Phenomena*, vol. 58, no. 1–4, pp. 77–94, 1992.

Hindawi Publishing Corporation
Advances in Meteorology
Volume 2016, Article ID 8714209, 11 pages
http://dx.doi.org/10.1155/2016/8714209

Research Article

Evaluating Spatiotemporal Variation of Groundwater Depth/Level in Beijing Plain, a Groundwater-Fed Area from 2001 to 2010

Yuyan Zhou,[1] Weihua Xiao,[1] Jianhua Wang,[1] Yong Zhao,[1] Ya Huang,[1,2] Jiyang Tian,[1] and Yan Chen[1]

[1]*State Key Laboratory of Simulation and Regulation of Water Cycle in River Basin, China Institute of Water Resources and Hydropower Research, Beijing 100038, China*
[2]*Guangxi University, Nanning 530004, China*

Correspondence should be addressed to Jianhua Wang; jhwangiwhr@126.com

Received 7 November 2015; Accepted 18 January 2016

Academic Editor: Gang Liu

Groundwater has always been a valuable resource in Beijing, facing a great decline of groundwater level during the past decades. However, few previous researches have revealed the spatial variation of groundwater level within Beijing Plain. In this study, spatiotemporal variation of groundwater level from 2001 to 2010 in Beijing Plain has been investigated. Factor analysis has been conducted to identify the primary influencing factor. Results showed that the groundwater level decreased by 8.41 m from 2001 to 2010, with a linear decreasing rate of 0.954 m per year averagely. Significant spatial variation characteristics have been detected. The north area suffered more groundwater depletion than the south part in general. The lowest groundwater level has been identified downstream Miyun Reservoir, central part of the Plain. Nevertheless, the most of the south part witnessed a slight revival between 2001 and 2010. This may be due to the differences of socioeconomic circumstances in the Plain. Three influencing factors, that is, "demand factor," "supply factor," and "loss factor," have been identified in the water balance model. Eigenvalues of these factors are 3.563, 2.910, and 1.632, respectively, indicating that these factors influenced the groundwater system to various extents, with the demand factor being the primary one.

1. Introduction

Beijing has been known for its great dependence on groundwater. Interannual variation of groundwater depth/level is of great significance to water resources management in Beijing. Although high temporal resolution monitoring networks have been established in many areas, it is not easy to obtain these data in many parts of China. Moreover, the interannual variation of groundwater depth could provide long-term information of the territorial water crisis for urban planning compared to seasonal and monthly data [1]. For the practical reason, most cities or basins record yearly data of groundwater depth/level in China, which is necessary for interannual analysis. Additionally, interannual fluctuation of groundwater depth/level is adaptable to reflect the large temporal scale dry/wet conditions [1–3].

A sharp decline has been witnessed in the groundwater level in Beijing Plain in the early 21st century. This megacity relies upon groundwater resources heavily in the past. Groundwater supply is made up of more than 70% of the total water supply at the beginning of 21st century. According to the *Beijing Water Resources Bulletin 2013*, Beijing has a water supply of 3.64 billion m^3, which is 50 million m^3 larger than that of 2012. The water supply derives from surface water of 0.48 billion m^3 (13%), groundwater of 2.01 billion m^3 (55%), reclaimed water of 0.8 billion m^3 (22%), and water from the *South-to-North Water Diversion* of 0.35 billion m^3 (10%). To release the depletion of traditional water resources, Beijing has developed reclaimed water and transferring water in the last decade. Since the *South-to-North Water Diversion Project (Middle Route)* was completed in 2014, Beijing gained

gradually added transferred water (1.05 billion m^3 per year) from the Yangtze River Basin. It seemed likely that the water scarcity in Beijing would be alleviated to some extent; however, groundwater resources still consisted of more than 50% of the total amount in 2013 [4].

Though it has been well understood that the groundwater experienced a severe depletion in the past years, the spatial variation of groundwater remains still insufficiently studied, which is of great importance in groundwater management. For instance, the Beijing Plain, one of the largest urban areas in the world, showed great inner spatial difference in urban development. This indicates that the Plain cannot be treated as a whole. Wang et al. [5] and Song et al. [6] divided Beijing into four and six subunits, respectively, considering the effects of topography and urban span. Rapid urbanization is enlarging the gap between metropolitan areas and suburban areas. Zheng et al. [7] have confirmed that the groundwater renewability varied across the Beijing Plain. Therefore, the spatial variation of groundwater level is a necessity in Beijing Plain as well as other urban areas globally.

Given that a number of researches of spatiotemporal variation of groundwater level in Beijing Plain have been initiated [8–10], it is of great importance to seek the possible causes to the variation. Recent researches showed that the groundwater depletion could be attributed to decreasing precipitation, increasing water demand, water extravagancy, poor utility ratio, and other unpredicted problems [11–15]. Numerical models have been proven to be an effective way to investigate the relationship between groundwater level and environmental-social factors [16, 17]. For example, Terrie et al. have explored the long-term balance of precipitation and groundwater exchange in the peninsular lake district. Results showed that net groundwater exchange with the lake was positive on average but too small to balance the net precipitation deficit, while some recent studies illustrated that rainfall is influencing the groundwater depths in quick and slow pattern [18, 19]. Evapotranspiration was also linked to groundwater at high water table region [20]. However, when the groundwater depth is over a threshold, this linkage is no longer strong enough to influence the water table [21]. Then, the groundwater evapotranspiration (*ETg*) is eliminated from the actual evapotranspiration (*ETa*).

Studies also indicated that net groundwater imbalance could be widened by groundwater pumping and surface water withdrawals [22]. For instance, Eshtawi et al. (2015) have studied the potential impacts of urban expansion, related to water supply and groundwater recharge, on groundwater depth via the combination of surface water model and MODFLOW-USG [15]. Local water management practices could significantly alter the groundwater quantity in the territorial system [23]. It has been reported that total groundwater consumption accounted for 43% of the total irrigation water use globally [13]. Increasing water supply demand has been reported resulting from rapid increase in population, urbanization, and industrialization [24]. This trend would bring larger stress on local water crisis and groundwater sustainability.

Most previous studies relied on only a few scattered groundwater monitoring stations and did not reveal the spatial difference of groundwater level within the Plain [8]. Consequently, the important role of urban span, which should be discussed by detailed subunits, played in the distribution of groundwater level could not be well analyzed. In this study, an evenly distributed and high-resolution groundwater level database was used to remedy this shortcoming. By dividing the Beijing Plain into three subareas, the spatial characteristics of groundwater variation could be detected, which could benefit future physically based studies.

Even fewer of them have witnessed the driving forces of groundwater level in the perspective of water balance. Previous studies were often data-driven, which made the detection less effective. Therefore, we have proposed a factor analysis method, combined with correlation analysis, based on a regional water balance model, to identify the major factors that contribute to the variation. For the purpose of water resources management and strategy-making, this variable-fair method could be more valuable and cost-effective than pure mathematical models and be applied to other groundwater-fed urban areas.

2. Study Area

Beijing Plain has a geographic location of 115°40′–117°24′E and 39°26′–40°27′N with a total coverage of 116,512 km^2, located mainly in the center and southeast part of Beijing. The elevations range from 10 to 500 m, with the northwest being relatively high and the southeast being low generally.

Beijing, the capital of China, located in the northwest of North China Plain, is a megacity directly controlled by the central government and also the political and economic center. Within the 16 districts of entire Beijing, 9 districts were covered by the study area in whole or in part [25]. Five natural rivers, Juma river, Yongding river, Beiyun river, Chaobai river, and Linyun river, with 85 reservoirs are located in the Beijing Municipality, while the Miyun reservoir and Guanting reservoir consist of 90.5% of the surface water resources [4].

As one of the largest cities in the world, Beijing is facing severe water shortage problems. This city has an annual average precipitation of 595 mm, which is about 9.9 billion m^3 each year. However, 37.78% of the precipitation transforms to available water resources (3.74 billion m^3) due to 60.6% (6 billion m^3) of the high evapotranspiration. Beijing owns a growing population of 21, 516, 000 in 2014, which generates a huge amount of water demand each year. While more than 50% of water resources derive from groundwater, the continuous declining of groundwater level has become a key constraint factor to the social development. The paradox between increasing water demand and limiting water resources keeps sustainable development of living challenging. Beijing has always kept water scarcity as one of the priorities in China, which deserves cost-effective strategies in dealing with water problems. Beijing is confronted with the fact that water resources per capita were 117 m^3 in 2013, which is 12.5% of China and 3.33% of the world [4].

Table 1: Variables selected from the Beijing Water System.

Number	Variables	Unit	Symbols	Data series
1	Inflow	$10E08\ m^3$	Qin	2001–2010
2	Outflow	$10E08\ m^3$	Qout	2001–2010
3	Surface water resources	$10E08\ m^3$	SWR	2001–2010
4	Groundwater resources	$10E08\ m^3$	GWR	2001–2010
5	Precipitation	$10E08\ m^3$	Pa	2001–2010
6	Agricultural water use	$10E08\ m^3$	AWU	2001–2010
7	Industrial water use	$10E08\ m^3$	IWU	2001–2010
8	Domestic water use	$10E08\ m^3$	DWU	2001–2010
9	Environmental water use	$10E08\ m^3$	EWU	2001–2010
10	Groundwater depth/level	m	GWD	2001–2010

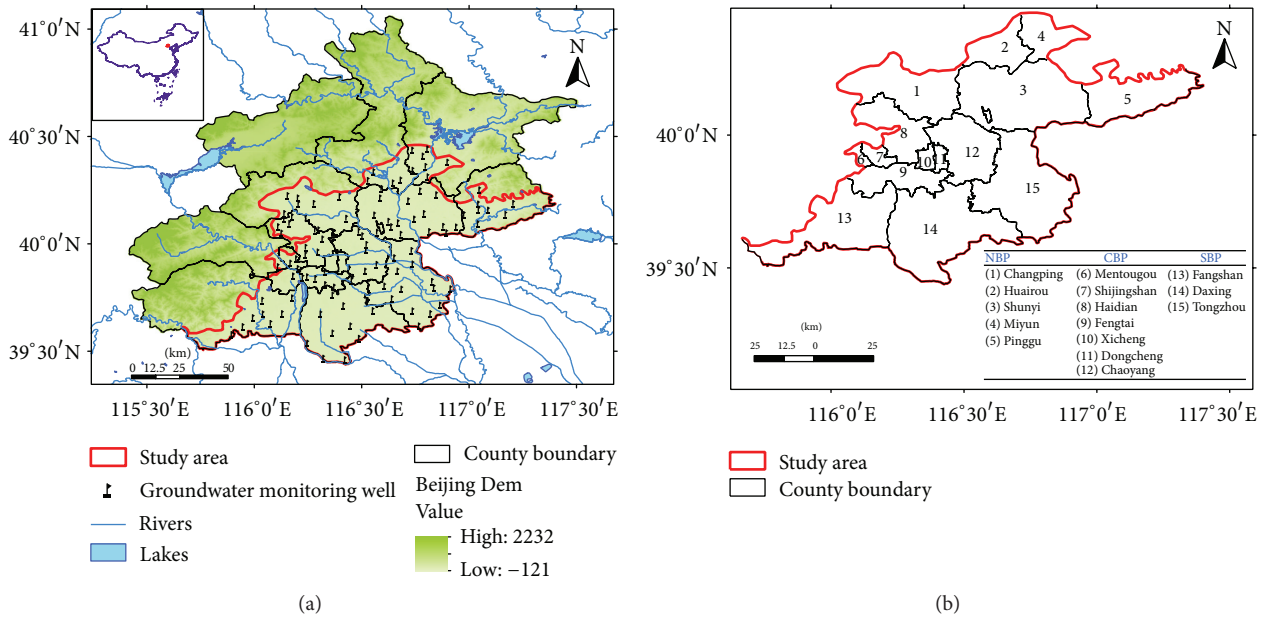

Figure 1: (a) Location of the study area and the 106 groundwater monitoring wells in Beijing Plain. Red solid lines denoted the boundary of study area, namely, Beijing Plain. (b) Subareas division of Beijing Plain.

3. Materials and Methods

3.1. Data Sources. Temporal data of inflow (Qin) and outflow (Qout), surface water and groundwater storage (SWR and GWR), precipitation amount (Pa), and water use by sectors were derived from Beijing Water Bulletin (2001 to 2010) and published references [4]. The basic information of the temporal dataset is shown in Table 1.

Distributed groundwater monitoring data from 2001 to 2010 were collected from the field groundwater monitoring wells. We selected 106 groundwater monitoring sites in Beijing Plain to obtain the spatial characteristics of groundwater depth/level. These monitoring wells were evenly distributed in the study area, which could demonstrate the spatial variation reasonably. Afterwards, Beijing Plain has been divided into three subareas according to the geographical feature: NBP, CBP, and SBP, respectively. These three subareas represented the north, central, and south part of the Plain (Figure 1). The NBP contains Changping, Shunyi, and Pinggu districts, the CBP contains Haidian, Mentougou, Shijingshan, Fengtai, Xicheng, Dongcheng, and Chaoyang districts, and SBP contains Fangshan, Daxing, and Tongzhou districts. Generally, the north and west part are relatively higher than the south and east part. These three subareas differ from each other in terms of social and economic status. The NBP comprises the majority of the irrigated land in Beijing Plain, and the CBP represents the economic and population center, while the SBP is less developed compared with the other two subareas due to its location [26, 27].

3.2. Trend Analysis. The methods of linear regression were used to analyze the temporal trends of the groundwater depth in this study [28]. Linear regression is a parametric method used to obtain the trend of groundwater depth/level variables over time [5, 8]. The linear regression equation can be represented as

$$y = a + bx + \varepsilon. \quad (1)$$

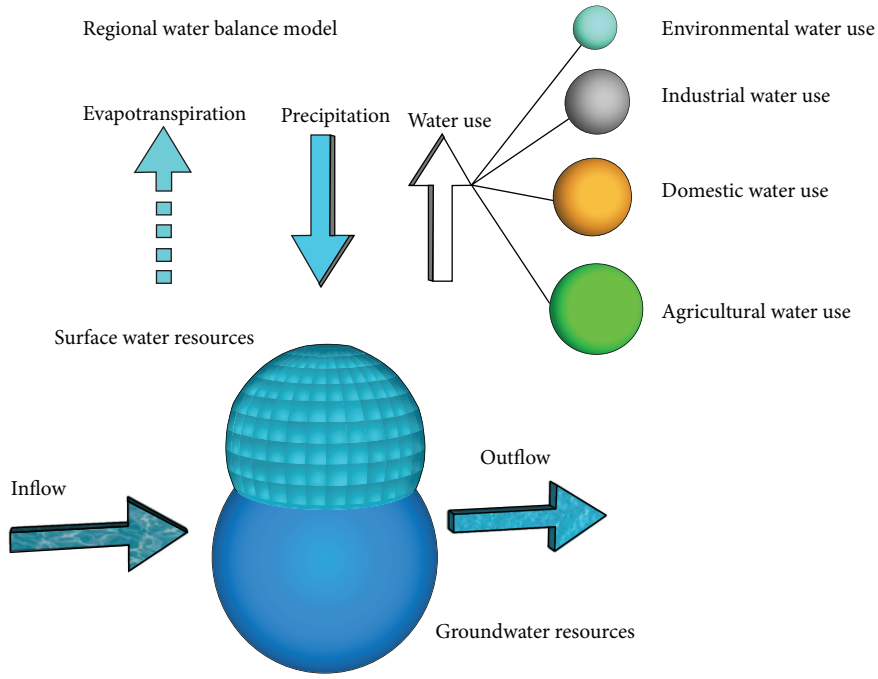

Figure 2: Theoretical water balance model of Beijing Water System.

The slope b can be used as an indicator of trend and is calculated as

$$b = \frac{n\sum_{i=1}^{n} x_i y_i - \sum_{i=1}^{n} x_i \sum_{i=1}^{n} y_i}{n\sum_{i=1}^{n} x_i^2 - \left(\sum_{i=1}^{n} x_i\right)^2}, \quad (2)$$

where y_i is the groundwater depth/level, x_i is the time, and n is the length of time sequence. Statistically significant b indicates the slope of a linear trend. Additionally, smooth regression lines have been used to demonstrate the long-term trend of the groundwater depth/level [29, 30].

3.3. Mann-Kendall Test. We examined the general trend and the abrupt changing point using Mann-Kendall test for the groundwater level time series [31, 32]. The Mann-Kendall test is widely used for nonlinear trend and turning point test. The indexes of the Mann-Kendall test were calculated as follows:

$$\mathrm{UF}_k = \frac{s_k - E(s_k)}{\sqrt{\mathrm{Var}(s_k)}}, \quad k = 1, 2, \ldots, n,$$

$$s_k = \sum_{i=1}^{k} r_i, \quad r_i = \begin{cases} 1 & (x_i > x_j) \\ 0 & (\text{else}), \end{cases} \quad j = 1, 2, \ldots, i, \quad (3)$$

$$E(s_k) = \frac{n(n-1)}{4},$$

$$\mathrm{Var}(s_k) = \frac{n(n-1)(2n+5)}{72}.$$

For a time series $\vec{x} = (x_1, x_2, \ldots, x_n)$, n stands for the length of the time series. UF_k and UB_k are the two statistical indices of the Mann-Kendall test, s_k stands for an accumulative value of r_i, $E(s_k)$ stands for the mean value of s_k, and $\mathrm{Var}(s_k)$ stands for the variance of s_k. Then, invert the time series sequence to form a new one $\tilde{x} = (x_n, x_{n-1}, \ldots, x_1)$, and calculate the indexes above once more and UB_k for the new time series $\tilde{x} = (x_n, x_{n-1}, \ldots, x_1)$. Apparently, the values of UF_k and UB_k are time series as well. Two critical values were set for significance measurement as $U_{0.05} = \pm 1.96$. Finally, the sequence curve of UF_k, UB_k and two horizontal lines indicating the critical values were drawn in the same plot. A significant increasing or decreasing trend could be detected when the curve of UF_k crosses the $U_{0.05} = \pm 1.96$ line. Additionally, statistical results including Kendall's tau, S and p value (two-tailed) have been calculated to identify the trend [28].

3.4. Spatial Interpolation. Spatial interpolation has been widely used for detecting groundwater level distribution from monitoring sites. There exist many methods including polynomial, nearest-neighbor, Inverse Distance Weighted, and Kriging to detect the changing pattern of groundwater level. The ordinary Kriging method was selected in this study, which contains the highest correlation coefficient calculated from the cross-validation test [5]. It also produced the closest representation of the real values, which was in the form of the lowest difference between the observed and predicted values of known data points [5]. Thus, we used the Kriging to obtain the spatial pattern of groundwater depth/level in the study area.

3.5. Driving Force Detection in the Perspective of Regional Water Balance Model. In this paper, 9 variables were introduced to investigate the driving force and major causes of the groundwater variation, particularly, precipitation, inflow, outflow, water storage, and water uses (Figure 2).

Table 2: Results of Mann-Kendall test of groundwater depth/level.

	Kendall's tau	S	p value (two-tailed)	α
Groundwater depth	1	45	$8.31e-05$	0.05
Groundwater level	−1	−45	$8.30e-05$	0.05

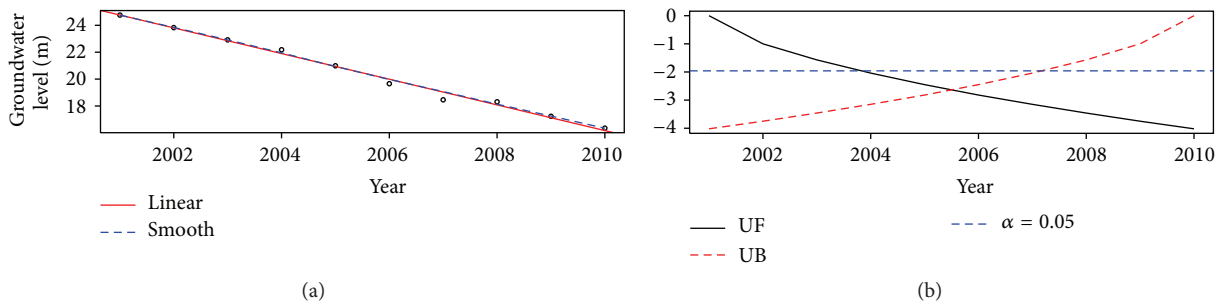

Figure 3: (a) Groundwater level variation during the period 2001 to 2010. (b) Mann-Kendall test results for groundwater level.

These variables were defined as follows. (i) Precipitation amount was averaged to the entire Beijing district based on the observed data of national individual rain gauge stations. (ii) Evapotranspiration was connected with surface water evapotranspiration and groundwater evaporation. Generally, the groundwater evaporation, which often resulted from the upward capillary flux from the underlying aquifer, was rare when the water table was 4 m or more below the ground [33]. It depends on whether the ends of the plant roots are able to reach the water table in this region [34]. Thus, we assumed that the groundwater evaporation was eliminated. (iii) In this study, inflow stands for the overland flow that is produced in the upper reaches of Beijing which flows into the boundary of Beijing and the diverted water from the *South-to-North Water Diversion Project*, while outflow means the drainage which is emitted from the urban drainage system. (iv) Surface water resources and groundwater resources stand for the water storage in Beijing. In this paper, the surface water storage mainly includes the reservoir storage and the stream flow, while the groundwater storage is the sum of crevice water, cavern water, porous confined water, and unconfined water. (v) We categorized water use in four classes: agricultural water use (AWU), industrial water use (IWU), domestic water use (DWU), and environmental water use (EWU).

In the present study, Pearson test was conducted to understand the correlation among these variables. Based on the Pearson test results, factor analysis was implemented to these variables to test whether these variables act in groups and how they work. Maximum Likelihood Estimation (MLE) method was selected as the exact means of factor analysis in this study for dimension reducing analysis [35–37]. Then, major factors were drawn from the factor analysis results, since the variables were picked out from the water balance model, which means the factor analysis is variable-fair. This method could be spread to other groundwater-fed urban areas globally. All the statistical work was conducted by using R programming.

4. Results

4.1. Temporal Analysis of Groundwater Depth/Level in Beijing Plain. Though the groundwater level has been reported to drop for 14.17 m from 1986 to 2013 [4], the mean annual groundwater depth from 2001 to 2010 varies from 17.34 m to 24.94 m with a monotone enlarging trend during the period. The mean annual groundwater level also showed the same variation, which slid from 24.76 m to 16.35 m in Beijing Plain. The linear regression results indicated that the groundwater level experienced a significant falling during the period with a linear variation of −0.954 m each year averagely.

Similar conclusion was drawn from the Mann-Kendall test results of both groundwater depth and groundwater level. There is a clearly declining trend in groundwater level, as Kendall's tau equals −1 with the p value being less than 0.05 (Table 2). The trend is also shown by the black (UF) and red (UB) lines, respectively, and the horizontal dashed lines correspond to the confidence limits at the significance level of $\alpha = 0.05$. Figure 3 shows that a statistically significant trend of decreasing groundwater level which is indicated as the black line crosses over the dashed line since 2004.

4.2. Spatial Characteristics of Groundwater Level in Beijing Plain. Groundwater depth/level records were collected from 106 wells over the period of 2001 to 2010. The data were used to analyze the interannual spatial variations in groundwater conditions (Figure 4). Generally, the north part of Beijing Plain showed a larger groundwater depth than the south part. In 2001 and 2005 (Figures 4(a) and 4(b)), the deepest groundwater depth is spotted in the northeast of the Plain, including partial NBP and CBP, while the largest value moved to the northeast part of the Plain in 2010. It could be deduced that the groundwater depletion was getting worse in the NBP in the period.

In terms of groundwater level, it showed precipitous decreasing gradient from northwest to southeast. While the

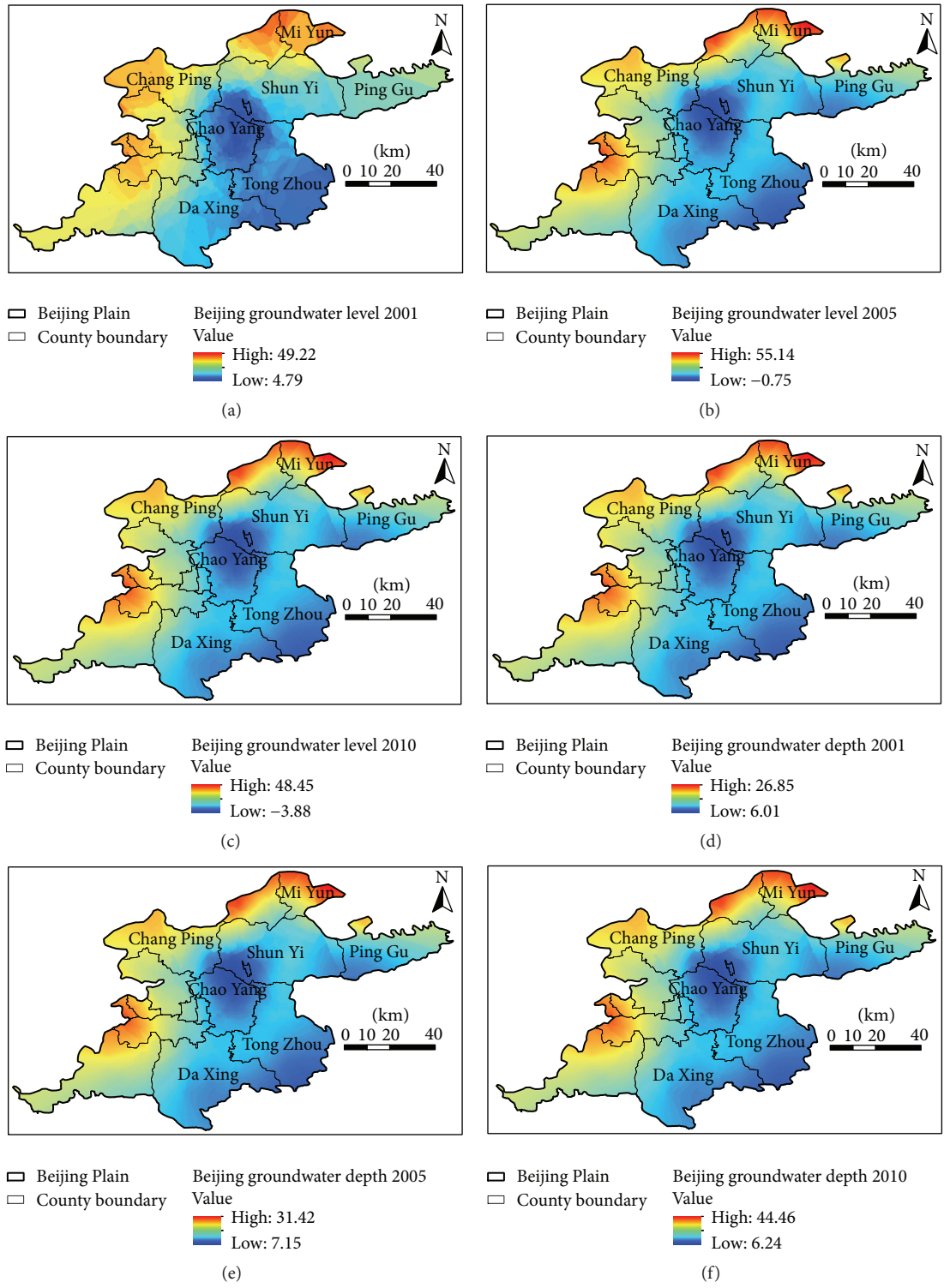

Figure 4: Distribution of groundwater depth/level (m) in Beijing Plain: (a) groundwater depth in 2001, (b) groundwater depth in 2005, (c) groundwater depth in 2010, (d) groundwater level in 2001, (e) groundwater level in 2005, and (f) groundwater level in 2010.

elevation of the Beijing Plain declines from the northwest to southeast gradually (Figure 1), it should be noted that the center of the study area (the CBP area) had the lowest groundwater level in 2001, 2005. Similar phenomenon could be detected from Figure 4(f) that the NBP got lower groundwater level in 2010 than the previous years. This difference between the variation of the geomorphological characteristics of Beijing Plain and that of the groundwater level

Table 3: Variation of groundwater level at monitoring station.

Threshold	Difference level	Number of stations	Percentage
<0	L_0	16	15.24%
0~5	L_1	31	29.52%
5~10	L_2	18	17.14%
10~15	L_3	20	19.05%
15~20	L_4	5	4.76%
20~25	L_5	6	5.71%
25~30	L_6	9	8.57%

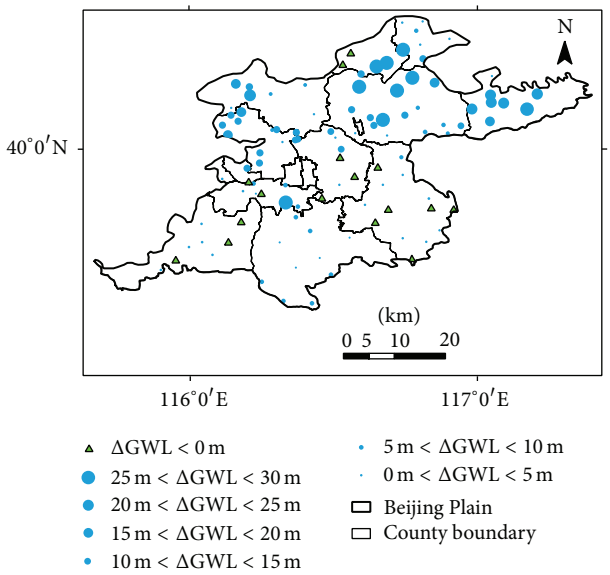

Figure 5: Bubble plot of groundwater level decreasing in Beijing Plain between 2001 and 2010.

indicates that local impacts severely influenced the groundwater level.

The groundwater depth/level data were further divided into seven categories: L_0~L_6 (Table 3). The monitoring sites where the groundwater level increased from 2001 to 2010 were defined as L_0. Those sites where the groundwater level was decreasing from 2001 to 2010 were classified into L_1~L_6 with an interval of 5 m.

Spatial variation showed that the groundwater level has different changing pattern in the research period. Among the monitoring data, 29.52% of them changed in 5 m, which accounted for most of the stations. Those 17.14% of the sites witnessed a groundwater level decreasing in the threshold of 5 to 10 m and 19.05% of them in the threshold of 10 to 15 m. Those points in which the groundwater level decreased at more than 15 meters comprised only 19.04% of the total groundwater monitoring data. Figure 5 indicated that large groundwater depletion was detected in the north part of Beijing Plain, while the majority of sites where the groundwater level slightly decreased or revived located in the south Beijing Plain.

4.3. Correlation Analysis. The results showed that the groundwater depth had significantly high correlation coefficient with agricultural water use, industrial water use, domestic water use, and environmental use (correlation efficient > 0.8 and p value < 0.05). Particularly, among the four highly related predictors, the groundwater depth was positively correlated with agricultural and industrial water use, while the other two showed negative relationship (Table 4). These predictors were highly correlated with each other ($p > 0.6$). For instance, the four water sectors were highly interrelated. The precipitation was positively related with inflow, outflow, surface water resources, and groundwater resources. Obviously, the fluctuation of groundwater depth was affected by the coefforts of these variables. Therefore, the multifactor analysis was used to study the co-contribution of these predictors to the variation of groundwater depth. The correlation coefficients and the significant level were displayed in Table 4.

4.4. Factor Analysis. It is difficult to make predictions on groundwater depth using the raw data of the predictors. Therefore, factor analysis was conducted to the 9 predictors of the groundwater depth by using the Maximum Likelihood Dimensionality Reduction method. Factors without multicollinearity were generated, based on the raw variables after the reducing dimensionality. Absolute loading of each variable which is over 0.7 is categorized as a factor.

Results showed that three factors have been selected (Table 5). Factor 1 was composed of agricultural water use, industrial water use, domestic water use, and environmental use. All the variables in factor 1 have shown highly relevant relationships with groundwater depth. These variables are highly connected with social water demand. Thus, factor 1 was named as "demand factor." Factor 2 included surface water storage, groundwater storage, and precipitation amount, which was concluded as "supply factor." Factor 3 consisted of the outflow of the region, which was nominated as "loss factor." The eigenvalues of the factors were 3.563, 2.910, and 1.632, respectively. The values indicate that the first factor contributes the largest explanatory importance to the variables, followed by the remaining two in sequence. The proportion variance of these factors shows the same results, which are 0.396, 0.323, and 0.181, respectively. The accumulative variance is of 90.5%.

5. Discussion

5.1. The Great Drop Period Deserves Concentration. Results showed that a sharp decline has been witnessed from 2001 to 2010. Actually, the groundwater depth in Beijing was normally less than 10 m in the early 1980s [9]. However, the decreasing speed of the groundwater level had been accelerated from 0.3 m/year in 1980s to 0.5 m/year in 1990s and then to 1.2 m/year in 2000s. The groundwater depth reached 24.94 m in 2010 [9]. The last period was named as "the great drop" for its largest decreasing extent. Reports have also pointed out that the North China Plain, where Beijing is located, has experienced an overpumped period since 1970s and many groundwater depression cones were formed [38].

Table 4: Correlation coefficient of groundwater depth and its predictors.

	Qin	Qout	SWR	GWR	Pa	AWU	IWU	DWU	EWU
Qin	1								
Qout	**0.92***	1							
SWR	**0.84***	**0.79***	1						
GWR	0.41*	0.50*	0.58*	1					
Pa	**0.67***	**0.64***	**0.86***	**0.82***	1				
AWU	0.47*	0.32	0.51*	−0.30	0.17	1			
IWU	0.49*	0.44*	0.34	−0.34	0.05	**0.83***	1		
DWU	−0.45*	−0.27	−0.56*	0.22	−0.23	**−0.92***	**−0.64***	1	
EWU	−0.23	−0.13	−0.21	0.43*	0.05	**−0.84***	**−0.82***	**0.74***	1
GWD	0.56	0.42	0.55	−0.26	0.23	***0.97****	***0.87****	***−0.90****	***−0.81****

*$\alpha = 0.05$.

Table 5: Loadings of variables to each factor.

	Factor 1	Factor 2	Factor 3
Qin	0.301	0.574	0.686
Qout	0.131	0.526	**0.837**
SWR	0.36	**0.86**	0.351
GWR	−0.434	**0.782**	0.175
Pa		**0.905**	0.192
AWU	**0.978**	0.128	0.149
IWU	**0.788**	−0.124	0.482
DWU	**−0.901**	−0.27	
EWU	**−0.864**	0.163	−0.122
Eigenvalue	3.563	2.910	1.632
Proportion variance	0.396	0.323	0.181
Cumulative variance	0.396	0.719	0.901

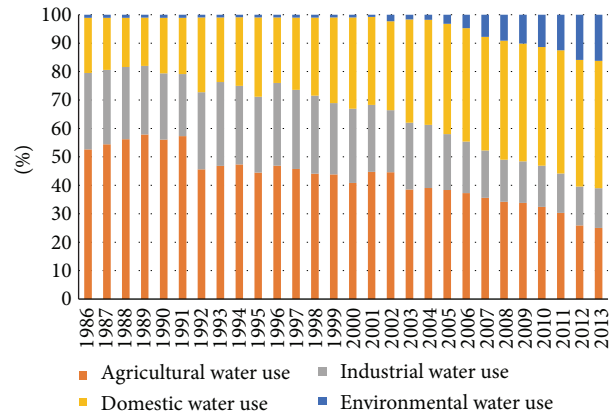

Figure 6: Water consumption composition in Beijing from 1980 to 2013.

This has caused severe water shortage, especially for the irrigated land which relies on groundwater, and derived ecoenvironmental problems relating to low groundwater level [39, 40].

Factor analysis and correlation analysis indicated that the groundwater depth showed high linear correlation with water usage in four social sectors but exerted less correlation with inflow, water storage, precipitation, and outflow. These predictors in the regional water balance model could be categorized as three classes: (i) demand factor, including water uses; (ii) supply factor, including water storage and precipitation; and (iii) loss factor, including regional outflow. The contributions to the total variance were 39.6%, 32.3%, and 18.1%, respectively. Therefore, it can be inferred that the water usage should be the major influencing factor to the variation of groundwater depth, followed by the water supply. The water loss from the regional water system has less influence.

Water usage becomes the main contribution to the variance of groundwater level because it switched its dependence from surface fresh water to groundwater since the 1980s. Miyun and Guanting reservoir lose the ability to supply enough water gradually because their water amount has reduced to 10 percent of the original storage capacities. Moreover, Guanting reservoir was too polluted to supply water [41]. A new water usage policy has therefore been initiated to cut back water supply to irrigation from Miyun and Guanting reservoir in order to guarantee domestic water supply since 1980s [41]. This triggered the urgent need of groundwater as an alternative water source for irrigation [41].

Agriculture took 64% of the water consumption in Beijing in the 1980s. This ratio decreased to 25% in 2013 gradually. We found out that the groundwater level was declining, while the agricultural water use was also decreasing. Though many researchers believed the groundwater variation was highly linked to irrigation water use, groundwater depth in Beijing Plain may exert converse answers [13, 42, 43]. The water consumption from ongoing urbanization would gradually cut off agricultural water use, which will account for less proportion in the future.

However, the domestic and environmental water demands were correlated with the population increasing and extending of human need. Therefore, we proposed that the depletion of groundwater should be attributed partially to the expanding of population growth. The domestic water use, originated from 8% of the total in the 1980s, has reached 45% in 2013 (Figure 6). This drastic change indicated the variation of the water use composition and implied the transformation

of the social structure in the past three decades. This may be attributed to the population booming in Beijing. The resident population has been increasing from 13.64 million in 2000 to 20.19 million in 2011, with an increasing rate of 4.365% per year. In addition, with more floating population, the population on water resources is more severe than the previous years.

5.2. Spatial Variation of Groundwater Level in Beijing Plain Exerts More Information. Though a general sharp decreasing of groundwater level happened in the great drop period, not all the regions in Beijing Plain showed the same trend. The NBP had a similar trend, while the south part did not. The most severe groundwater depletion was identified in the CBP and partial NBP. The lowest groundwater level was detected in the CBP, near lower reaches of the Miyun reservoir. The majority of irrigated land is distributed in this region, which depends on groundwater totally [41]. Zhu et al. (2015) also pointed out that the groundwater withdrawal had triggered the continuous increasing of land subsidence in the NBP from 2003 to 2010 [43].

It should be noted that only 8.57% of the monitoring sites suffered from the largest decreasing. And 19.04% sites endured a decreasing extent of more than 15 m. Most of the areas faced the fact of the decreasing of the groundwater level being less than 15 m. That means that the depletion in NBP may be majorly responsible for the groundwater deterioration, which deserves more focus in future groundwater management.

However, a reviving trend was recognized in some monitoring sites in the great drop period, especially in Fangshan and Tongzhou districts. It can be explained by less irrigated land in the SBP than NBP and less population in the SBP than CBP, which indicates a lower abstraction rate than the recharge rate of groundwater. Therefore, the groundwater level in SBP did not decrease as in the NBP and CBP. Yang et al. (2009) also have confirmed that the SBP area showed less groundwater overdraft than the NBP and CBP areas [44]. This illustrates the effect of local impact factor on shaping the groundwater system.

6. Conclusion

The spatiotemporal variation of groundwater level is essential to water resources management in Beijing, as groundwater will still comprise the majority of water source in the next decade. The following conclusions could be drawn through this study:

(1) During the period of 2001 to 2010, the groundwater level fell from 24.76 m to 16.35 m, with an annual changing rate of −0.841 m per year. This trend is statistically significant according to the Mann-Kendall test results.

(2) There exists large spatial difference of groundwater level within Beijing Plain. Groundwater depth in north part of Beijing Plain was larger than the south part. A northwest to southeast dropping gradient of groundwater level was noted from the spatial variation plots. Among the sampling sites, 19.04% of the total were confronted with groundwater level decline of more than 15 m, while the other 29.52% shared the decreasing of groundwater level within 5 m. Most of the sites were located in the NBP. Due to the enormous amount of irrigated groundwater demand, the downstream of Miyun reservoir, located in NBP and CBP partially, faced most severe groundwater depletion. Many areas in the SBP (15.24% of the total samplings) presented a recovery phenomenon of groundwater level during the period of 2001 to 2010. It is assumed that the low development in this region placed less pressure on groundwater than its north counterpart. Therefore, we deduce that the local impact factor may play a more important role in the process.

(3) Water usage of four sectors was highly related to groundwater level. The precipitation, inflow, outflow, and water storage were not corresponding to the groundwater level. The variables in the model were categorized in three classes based on factor analysis: (i) "demand factor" (including water use of the four sectors), (ii) "supply factor" (including surface water storage, groundwater storage, and precipitation), and (iii) "loss factor" (including outflow). The contributions of the three factors to total variance were 39.6%, 32.3%, and 18.1%, respectively. The domestic and environmental water usage is steadily increasing which will be majorly responsible for the groundwater depletion.

(4) Nevertheless, this study has some limitations to be addressed in the future work. Firstly, more data should be filled within the database. Seasonal or monthly data would be a help in determining more details of the variation. Although the factor analysis was conducted to detect the shared characteristics, the contribution of each variable in the three factors was not clear yet. Future studies may fix this by focusing on the groundwater depth/level and each of these variables. Secondly, further studies should be conducted in spatial analysis to explain the differences within Beijing Plain by collecting more spatial data of the driving factors. For instance, the distributed water consumption data of each district could offer better understanding of the spatial variation of groundwater level.

Conflict of Interests

The authors declare no conflict of interests.

Acknowledgment

This research was supported by a grant from The General Key Program of National Natural Science Foundation of China (40830637).

References

[1] A. Lutz, S. Minyila, B. Saga, S. Diarra, B. Apambire, and J. Thomas, "Fluctuation of groundwater levels and recharge patterns in Northern Ghana," *Climate*, vol. 3, no. 1, pp. 1–15, 2015.

[2] S. Chaudhuri and S. Ale, "Long-term (1930–2010) trends in groundwater levels in Texas: influences of soils, landcover and water use," *Science of the Total Environment*, vol. 490, pp. 379–390, 2014.

[3] A. J. M. Kuss and J. J. Gurdak, "Groundwater level response in U.S. principal aquifers to ENSO, NAO, PDO, and AMO," *Journal of Hydrology*, vol. 519, pp. 1939–1952, 2014.

[4] Beijing Water Authority, *Beijing Water Bulletin*, Beijing Water Authority, Beijing, China, 2010–2013.

[5] J. Wang, R. Zhang, and Y. Wang, "Areal differences in diurnal variations in summer precipitation over Beijing metropolitan region," *Theoretical and Applied Climatology*, vol. 110, no. 3, pp. 395–408, 2012.

[6] X. Song, J. Zhang, A. AghaKouchak et al., "Rapid urbanization and changes in spatiotemporal characteristics of precipitation in Beijing metropolitan area," *Journal of Geophysical Research: Atmospheres*, vol. 119, no. 19, pp. 11,250–11,271, 2014.

[7] J. Zheng, Y. Teng, J. Wang, and L. Hu, "Assessment of the groundwater renewability in Beijing plain area," in *Proceedings of the 5th International Conference on Bioinformatics and Biomedical Engineering (iCBBE '11)*, pp. 1–4, IEEE, Wuhan, China, May 2011.

[8] Y. Zhou, D. Dong, J. Liu, and W. Li, "Upgrading a regional groundwater level monitoring network for Beijing Plain, China," *Geoscience Frontiers*, vol. 4, no. 1, pp. 127–138, 2013.

[9] L. Yu, C. Yu, S. Ying et al., "Sustainable utilization measures of groundwater resources in Beijing," *Journal of Groundwater Science and Engineering*, vol. 2, no. 4, pp. 60–66, 2014.

[10] Y. Lu, X. Du, Y. Yang et al., "Compatibility assessment of recharge water with native groundwater using reactive hydrogeochemical modeling in Pinggu, Beijing," *CLEAN—Soil, Air, Water*, vol. 42, no. 6, pp. 722–730, 2014.

[11] I. Vitola, V. Vircavs, K. Abramenko, D. Lauva, and A. Veinbergs, "Precipitation and air temperature impact on seasonal variations of groundwater levels," *Environmental and Climate Technologies*, vol. 10, no. 1, pp. 25–33, 2012.

[12] Y. Choi, Y. Choi, T.-H. Le, S. Shin, and D. Kwon, "Groundwater levels estimation and forecasting by integrating precipitation-based period-dividing algorithm and response surface methodology," *Desalination and Water Treatment*, vol. 54, no. 4-5, pp. 1270–1280, 2014.

[13] S. Siebert, J. Burke, J. M. Faures et al., "Groundwater use for irrigation—a global inventory," *Hydrology and Earth System Sciences*, vol. 14, no. 10, pp. 1863–1880, 2010.

[14] T. Eshtawi, M. Evers, and B. Tischbein, "Quantifying the impact of urban area expansion on groundwater recharge and surface runoff," *Hydrological Sciences Journal*, 2015.

[15] T. Eshtawi, M. Evers, and B. Tischbein, "Potential impacts of urban area expansion on groundwater level in the Gaza Strip: a spatial-temporal assessment," *Arabian Journal of Geosciences*, vol. 8, no. 12, pp. 10565–10584, 2015.

[16] M. E. Soylu, E. Istanbulluoglu, J. D. Lenters, and T. Wang, "Quantifying the impact of groundwater depth on evapotranspiration in a semi-arid grassland region," *Hydrology and Earth System Sciences*, vol. 15, no. 3, pp. 787–806, 2011.

[17] X. Li, G. Li, and Y. Zhang, "Identifying major factors affecting groundwater change in the North China plain with grey relational analysis," *Water*, vol. 6, no. 6, pp. 1581–1600, 2014.

[18] C.-D. Jan, T.-H. Chen, and H.-M. Huang, "Analysis of rainfall-induced quick groundwater-level response by using a Kernel function," *Paddy and Water Environment*, vol. 11, no. 1–4, pp. 135–144, 2013.

[19] M. G. Abdullahi and I. Garba, "Effect of rainfall on groundwater level fluctuation in Terengganu, Malaysia," *Journal of Geophysics & Remote Sensing*, vol. 4, no. 2, pp. 142–146, 2015.

[20] P. Wang and S. P. Pozdniakov, "A statistical approach to estimating evapotranspiration from diurnal groundwater level fluctuations," *Water Resources Research*, vol. 50, no. 3, pp. 2276–2292, 2014.

[21] A. Lam, D. Karssenberg, B. J. J. M. van den Hurk, and M. F. P. Bierkens, "Spatial and temporal connections in groundwater contribution to evaporation," *Hydrology and Earth System Sciences*, vol. 15, no. 8, pp. 2621–2630, 2011.

[22] T. M. Lee, L. A. Sacks, and A. Swancar, "Exploring the long-term balance between net precipitation and net groundwater exchange in Florida seepage lakes," *Journal of Hydrology*, vol. 519, pp. 3054–3068, 2014.

[23] G. Leng, M. Huang, Q. Tang, H. Gao, and L. R. Leung, "Modeling the effects of groundwater-fed irrigation on terrestrial hydrology over the conterminous United States," *Journal of Hydrometeorology*, vol. 15, no. 3, pp. 957–972, 2014.

[24] K. Mahmood, A. D. Rana, S. Tariq et al., "Groundwater levels susceptibility to degradation in Lahore Metropolitan," *Science International (Lahore)*, vol. 25, no. 1, pp. 123–126, 2013.

[25] L. Wang and Q. He, "The evaluation of groundwater resources value of Beijing based on emergy theory," *Advances in Materials Science and Engineering*, vol. 2015, Article ID 743136, 9 pages, 2015.

[26] C. He, N. Okada, Q. Zhang, P. Shi, and J. Zhang, "Modeling urban expansion scenarios by coupling cellular automata model and system dynamic model in Beijing, China," *Applied Geography*, vol. 26, no. 3-4, pp. 323–345, 2006.

[27] X. H. Yuan, X. Ji, H. Chen, B. Chen, and G. Q. Chen, "Urban dynamics and multiple-objective programming: a case study of Beijing," *Communications in Nonlinear Science and Numerical Simulation*, vol. 13, no. 9, pp. 1998–2017, 2008.

[28] Y. Yin, H. Liu, X. Yi, and W. Liu, "Spatiotemporal variation and abrupt change analysis of temperature from 1960 to 2012 in the Huang-Huai-Hai Plain, China," *Advances in Meteorology*, vol. 2015, Article ID 643493, 11 pages, 2015.

[29] R. M. Hirsch, J. R. Slack, and R. A. Smith, "Techniques of trend analysis for monthly water quality data," *Water Resources Research*, vol. 18, no. 1, pp. 107–121, 1982.

[30] O. P. Lamigueiro, *Displaying Time Series, Spatial, and Space-Time Data with R*, CRC Press, ETSIDI-UPM, Madrid, Spain, 2014.

[31] P. D. Valz and A. I. McLeod, "A simplified derivation of the variance of Kendall's tau," *The American Statistician*, vol. 44, article 2, 1990.

[32] K. W. Hipel and A. I. McLeod, *Time Series Modelling of Water Resources and Environmental Systems*, Elsevier, Amsterdam, The Netherlands, 1994.

[33] P. J.-F. Yeh and J. S. Famiglietti, "Regional groundwater evapotranspiration in Illinois," *Journal of Hydrometeorology*, vol. 10, no. 2, pp. 464–478, 2009.

[34] X. Chen and Q. Hu, "Groundwater influences on soil moisture and surface evaporation," *Journal of Hydrology*, vol. 297, no. 1–4, pp. 285–300, 2004.

[35] R. Cudeck and L. L. O'Dell, "Applications of standard error estimates in unrestricted factor analysis: significance tests for factor loadings and correlations," *Psychological Bulletin*, vol. 115, no. 3, pp. 475–487, 1994.

[36] A. B. Costello and J. W. Osborne, "Best practices in exploratory factor analysis: four recommendations for getting the most from your analysis," *Practical Assessment, Research & Evaluation*, vol. 10, no. 7, pp. 1–9, 2005.

[37] M. Muca, L. Puka, K. Bani, and E. Shahu, "Principal components and the maximum likelihood methods as tools to analyze large data with a psychological testing example," *European Scientific Journal*, vol. 9, no. 20, pp. 176–185, 2013.

[38] R. Yuan, X. Song, D. Han, L. Zhang, and S. Wang, "Upward recharge through groundwater depression cone in piedmont plain of North China Plain," *Journal of Hydrology*, vol. 500, pp. 1–11, 2013.

[39] X. Deng, H. Xu, M. Ye, B. Li, J. Fu, and Z. Yang, "Impact of long-term zero-flow and ecological water conveyance on the radial increment of *Populus euphratica* in the lower reaches of the Tarim River, Xinjiang, China," *Regional Environmental Change*, vol. 15, no. 1, pp. 13–23, 2015.

[40] R. Dupas, G. Gruau, S. Gu, G. Humbert, A. Jaffrézic, and C. Gascuel-Odoux, "Groundwater control of biogeochemical processes causing phosphorus release from riparian wetlands," *Water Research*, vol. 84, pp. 307–314, 2015.

[41] Probe International, *Beijing Water Crisis: 1949–2008*, Probe International, Toronto, Canada, 2008.

[42] Q. Hao, J. Shao, Y. Cui, and Z. Xie, "Applicability of artificial recharge of groundwater in the Yongding River alluvial fan in Beijing through numerical simulation," *Journal of Earth Science*, vol. 25, no. 3, pp. 575–586, 2014.

[43] L. Zhu, H. Gong, X. Li et al., "Land subsidence due to groundwater withdrawal in the northern Beijing plain, China," *Engineering Geology*, vol. 193, pp. 243–255, 2015.

[44] M. Yang, Y. Kang, and Q. Zhang, "Decline of groundwater table in Beijing and recognition of seismic precursory information," *Earthquake Science*, vol. 22, no. 3, pp. 301–306, 2009.